



UNIVERSITA' DEGLI STUDI DI TORINO

SCUOLA DI DOTTORATO IN SCIENZE DELLA VITA E DELLA SALUTE
DOTTORATO DI RICERCA IN FISIOPATOLOGIA MEDICA

Ciclo XXXIII
ANNI ACCADEMICI: 2017-2020

TESI DI DOTTORATO

A novel glomerular millifluidic device as platform for kidney disease studies and investigation of EV therapeutic potential

Tutor

Prof.Ssa Benedetta Bussolati

PhD Student

Dott.Ssa Linda Bellucci

Index

Abstract	1
1. The physiology of the glomerular filtration barrier	3
2. The structure of GFB	4
3. Organ-on-a-chip technology	16
4. <i>Introduction to review</i> : Therapeutic potential of extracellular vesicles derived from mesenchymal stem cells.....	33
<i>Review</i> : Potential applications of extracellular vesicles in solid organ transplantation	34
5. <i>The PhD project</i> : Protecting effect of mesenchymal stem cell-derived extracellular vesicles in a milli-fluidic advanced in vitro model of glomerular filtration after doxorubicin damage.....	47
6. Application of millifluidic device in renal disease models.....	80
6.1 <i>Article</i> : Molecular and functional characterization of urine-derived podocyte from patients with Alport syndrome.....	81
6.2 <i>Article</i> : Novel podocyte cell model from human apol1 high risk genotype	94
Conclusions and directions for future research.....	120
Acknowledgments.....	122

Abstract

Animal experimentation is the fundamental step that precedes the transfer to the clinic. Despite this, it involves a number of disadvantages, including ethical, economic and translational issues. In fact, animal-to-human translational success is not always guaranteed, and results in a phenomenon called “translational failure”. For these reasons, in recent years a new branch has developed in the field of preclinical studies, which is placed between the traditional 2D *in vitro* cultures and animal models: the experimentation in three dimensional (3D) dynamic models. The fluidic device technology usually consists of a small bioreactor that contains cells of human origin, and of a system that allows the continuous perfusion of fluid, for example a peristaltic pump, thus mimicking blood circulation. Through fluid flow control, viability, differentiation, orientation and cell function can be enhanced, while microscopic and molecular analysis allows monitoring and evaluation of cellular layers over time. The goal of this technology is not the faithful reproduction of the organ, but the construction of a minimally functional unit, which can recapitulate the function of the organ itself. For example, cells cultured on membranes can recreate interfaces between different tissues, such as alveolar-capillary interface, blood-brain barrier and, in case of kidney, the glomerular or tubular blood-epithelial interfaces. Drug-induced nephrotoxicity has been identified as a leading cause of severe acute renal failure in critically ill patients, and in the middle time, it is one of the leading factors in drug development failure, wasting tremendous money and time in pharmaceutical industry. For this reason, especially in the field of nephrology, it is urgently needed to correlate the *in vitro* nephrotoxicity assays to the *in vivo* animal testing and clinical trial, to better analyse drug metabolism, renal excretion or cell metabolic functions.

In the present study, I developed a multilayer millifluidic model to simulate the glomerulus, the filtration unit of the kidney nephron. Based on the physiological structure of the glomerular filtration barrier, the glomerulus consists in three layers: a layer of immortalized human glomerular endothelial cells (h-GECs), a porous membrane coated with type IV collagen and a layer of

immortalized human podocytes (h-POD-SV 40). A permeability test that measures the passage of serum albumin through the tri-layer, was used to assess the functional barrier integrity.

In summary, in my PhD work I characterized different glomerular pathological models on a dynamic *in vitro* device, using stabilized human cell lines, with particular attention to the podocyte damage.

In detail, the millifluidic model was applied to the following projects:

1. A model mimicking the Alport syndrome, a genetic disease characterized by an impairment of the glomerular basement membrane was achieved, by plating inside the bioreactor immortalized podocytes isolated from patients, in the absence of the coating with type IV collagen.
2. A study on the role of the APOL1 high-risk genotype (HRG) as predisposing factor of various nondiabetic kidney diseases in African population was conducted, using a mutated podocyteline for the APOL1 gene isolated from urine of a human donor carrying The data obtained are presented in an article proof format in the text.
3. Lastly, I investigated the pathophysiology of drug-induced acute kidney injury (AKI) with doxorubicin as model drug. In this project, the use of MSC-EVs as therapeutics was proposed. The results obtained so far have confirmed not only their ability of MSC-EVs to be internalized by cells, but also to revert the podocyte damage induced by doxorubicin.

I also participated to the production of a review which lays the foundations for the use of EVs for therapeutic purposes, supported by our results of improvement of cell viability in the dynamic model, in agreement with what it has been observed in animal models.

Introduction

1. The physiology of the glomerular filtration barrier

The glomerulus, the filtering unit of kidney, is a tangle of capillaries surrounded by the Bowman's capsule (Figure 1a), into which urine is filtered. Glomeruli filter approximately 180 litres of blood per day into the tubules, where 99% of the primary filtrate is reabsorbed and the remaining 1–2 litres of waste are excreted [1]. A glomerulus is composed by three major components: a fenestrated endothelium, a complex mesh of proteins composing the glomerular basement membrane (GBM) and a layer of specialized visceral epithelial cells, called podocytes, that form the slit diaphragms between interdigitating foot processes (Figure 1b) [2].

These structures, together, represent the glomerular filtration barrier (GFB). The GFB ensures the continuous ultrafiltration of plasma, retaining plasma proteins and permitting the formation of the primary glomerular filtrate, that enters a space delimited by the visceral and parietal epithelial cells before modification during transit through the tubule [3]. Since all components of the glomerular membrane are important for its function, proteinuria will occur regardless of which layer is affected by disease.

Figure 1

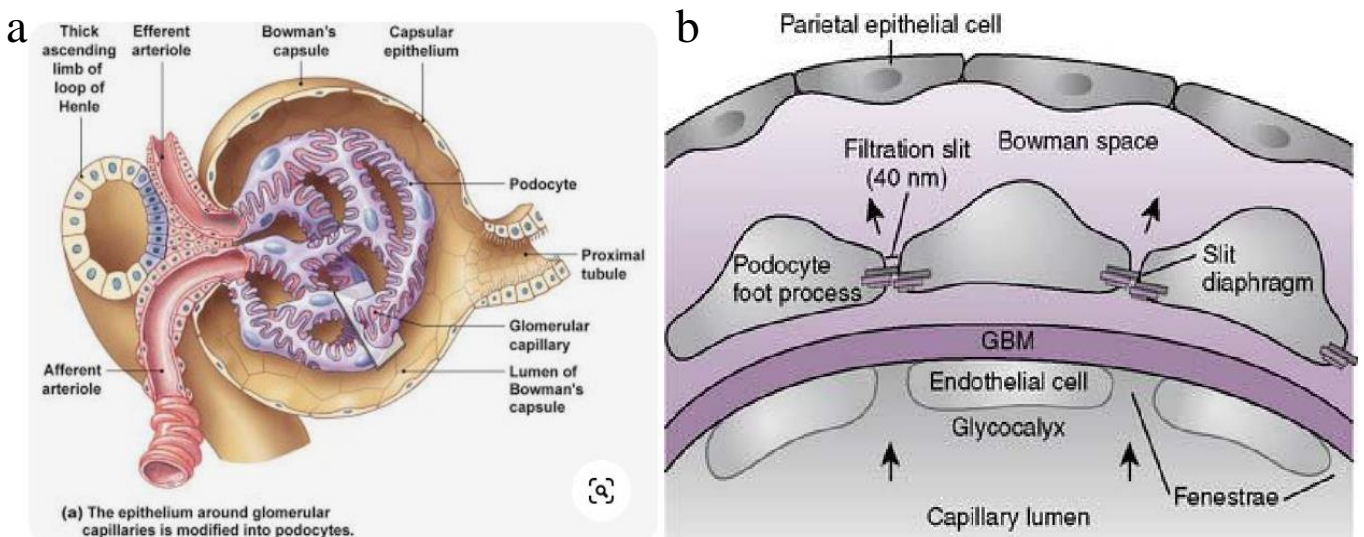


Figure 1. a) A section of the glomerulus. b) The glomerular filtration barrier

2. The structure of GFB

2.1 Endothelium

Following the blood flow, then proceeding from the vascular side to the luminal side, it is possible to recognize firstly the layer made up of Glomerular endothelial cells (GEnC), cells uniquely adapted for selective permeability and filtration. There are many properties that make these cells difficult to analyze, including the position within the glomerulus, and for the experimental purposes, the fact that they are difficult to maintain in culture without altering their phenotype [4]. GEnC are unusually flattened, with a height around the capillary loops of ~50–150 nm. Although capillaries with continuous endothelium are the most common type in skeletal muscle, cardiac muscle, and skin, the glomerular capillaries have endothelial cells with a large fenestrated area, appearing as trans-cytoplasmic holes, constituting 20–50% of the entire endothelial surface [5]. GEnC fenestrations are thus localized in the region of cytoplasm that is opposite to podocytes foot processes and filtration slit across the basement membrane [6].

The fenestrations

The most used model to analyze glomerulus formation is rodents, since it is completed within two weeks. The first cuboidal, fenestrated GEnC arise from the mesenchyme, and subsequently migrate into the developing glomerulus cleft [7]. During the capillary loop stage, endothelial cells proliferate and undergo various morphological changes, including evident thinning and the formation of fenestrations [8]. at the same time, the podocytes already present on the opposite side of the membrane, also developing, show poorly formed foot processes. Therefore, the formation of fenestrations and the maturation of the podocytic foot processes are two events that occur hand in hand: the fenestrations of immature GEnC initially present structures similar to diaphragms, which

then give way to podocytic ones [9]. *In vitro* and *in vivo* studies have led to the hypothesis that the vascular-endothelial growth factor (VEGF) plays an important role in the induction of endothelial fenestrations, not only in the glomerulus, activating signaling pathways effecting migration, proliferation, and permeability. VEGFs (VEGF-A to -E) comprise a family of growth factors that act through VEGF receptors (VEGFR) 1–3. Podocytes have been shown to begin expressing VEGF in the s-shaped phase, that is when immature GEnC are migrating into the cleft. GEnC express VEGFR2 from this stage and maintain the expression through to maturity, while podocytes will continue to produce VEGF at high levels, suggesting the importance of the signaling role of this factor in the functioning of the glomerulus [10,11]. Using the transgenic technique, the production of VEGF by podocytes was manipulated, confirming that, during the development of GEnC, a deprivation of VEGF leads to the thickening of endothelial cells, and to the loss of fenestrae [12]. Conversely, overexpression causes the capillary loops to collapse. VEGF antibody blockade in adult animals also causes damage to the GEnC with thickening, detachment from the basement membrane and regression of fenestrations [13,14].

The unusually high density of fenestrae is thought to allow high permeability to water and small solutes in the glomerulus. In fact, the fenestrae are ~60 nm in diameter, and albumin, which is restricted by the glomerular wall, has a diameter of only 3.6 nm. This evidence has been used in the past to suggest that endothelial cells do not contribute to the permselectivity of the glomerular barrier. However, endothelial cells possess a charge-selective coating with an active barrier role. Rostgaard and Qvortrup [15] described a high density of fibers in the windows, probably consisting of negatively charged proteoglycans. Other studies support a permselective layer at the endothelium [16-18]. These studies, which include both morphological and functional data, contribute to the notion that glomerular endothelial cells and their cell lining must be considered when evaluating the permselective properties of the glomerular barrier.

The endothelial glycocalyx

More recently, it has been recognized that a thin meshwork of glycosaminoglycans covers the entire luminal glomerular endothelial layer, even bridging the fenestrations [19]. The recognition of the endothelial glycocalyx required special fixation and staining techniques, including the use of specific lectins for visualizing the glycocalyx, that are not routinely performed on kidney biopsies [20]. By using these tools, the contribution of the endothelial glycocalyx to the permeability properties of the GFB is now well established, as are alterations in its components as contributors to albuminuria in various glomerular diseases. Thus, the endothelial glycocalyx is now considered the initial, coarse barrier for macromolecular exclusion from ultrafiltration.

Figure 2

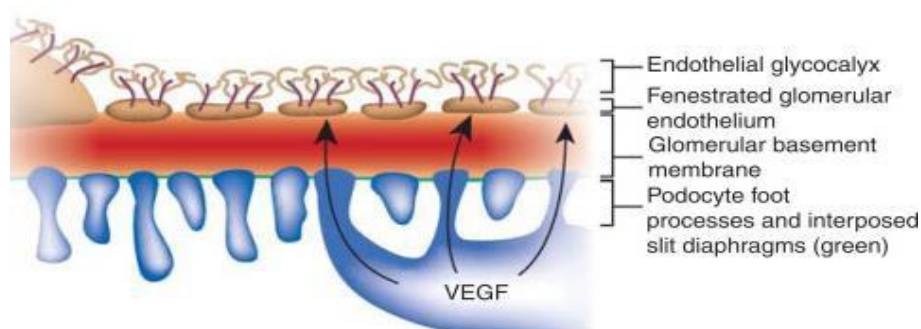


Figure 2: The glomerular endothelium. The endothelium is covered by a layer of glycocalyx: a mesh of cell-surface-anchored proteoglycans (core proteins and carbohydrate side chains, predominantly heparan sulfate and chondroitin sulfate) and adsorbed plasma proteins and glycosaminoglycans. Vascular endothelial growth factor (VEGF) is produced by podocytes and acts to maintain the adjacent glomerular endothelium [21].

So far many constituents of the endothelial glycocalyx have been recognized, including cell surface, anchored components such as proteoglycans (PGs) and sialoproteins, and adsorbed components such as albumin, orosomucoid and lumican 9 [22,23]. PGs consist of two parts: a central protein, such as glypican or syndecan, and glycosaminoglycan (GAG)-side chains; for example, heparan sulphate and chondroitin sulphate GAGs are very present and largely responsible for the anionic charge. Hyaluronate, on the other hand, is a non-sulphate GAG which may be anchored to the cell surface by various receptors and interacting proteins or simply adsorbed onto the cell surface-anchored components [24]. Sialoproteins, possessing several neuraminic acid residues, are also prominent.

Adsorbed components of the endothelial glycocalyx are essential for normal function of the layer. Estimates of glycocalyx thickness vary greatly, but it appears that the layer extends up to 1 μm from the endothelial cell membrane and varies in composition and appearance between different blood vessels and vascular beds [25,26]. Many mechanisms on the regulation of the glycocalyx composition have not yet been elucidated, but it is likely that this is determined by the balance between the stimuli that increase the biosynthesis of the glycocalyx (e.g. shear stress [27]) and those that lead to its degradation (e.g. inflammation [28]).

2.2 Glomerular basement membrane

Glomerular basement membrane (GBM) (Figure 3), that separates podocytes and endothelium is one of most studied basement membranes. Its role is not only structural, but actively participates in the selectivity of the filtration barrier, allowing water and small solutes to pass into the urinary space, but by holding back the passage of macromolecules and cells; in fact, proteinuria and hematuria are indicators of the malfunctioning of the barrier [1]. Structural and biochemical analyses in the past have succeeded in highlighting the 3-layer structure of the GFB, but not identifying exactly the components of the GBM. More recently, proteomic data based on mass spectrometry has shown how the basement membrane located in the glomerulus is unique for multiple characteristics, for example the prominent presence of collagen type IV. Other important components are laminins, nidogens, heparansulphate, proteoglycans (HSPGs), agrin, perlecan and collagen XVIII, as well as a series of structures with reservoir function for growth factors. Aspects of the cell important for cellular tissue homeostasis such as proliferation, polarity, migration, signaling, differentiations, are regulated by this adhesive layer sheet.

Figure 3

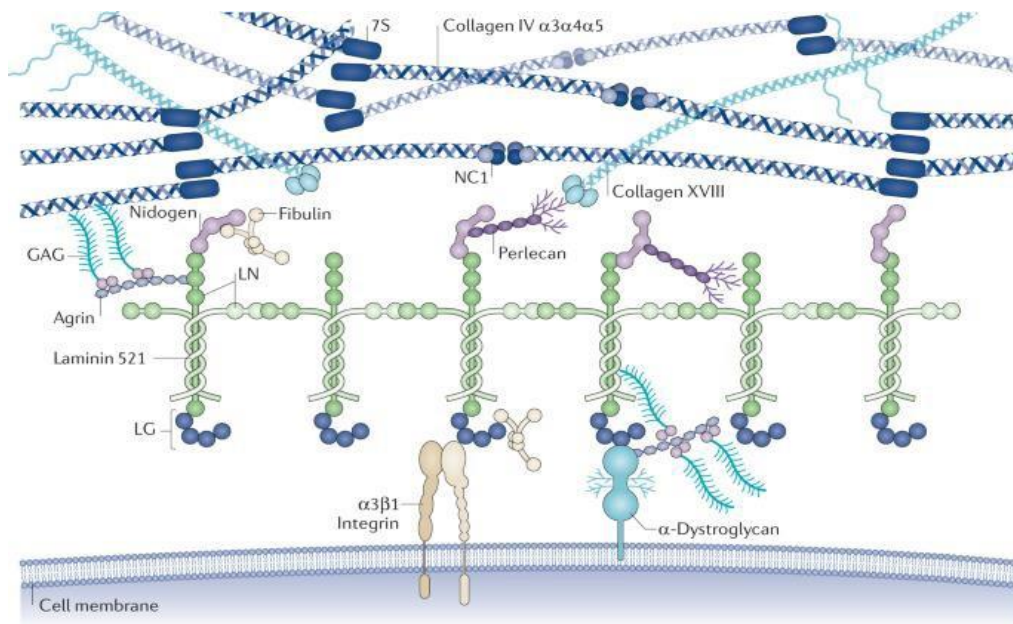


Figure 3. The major components of all basement membranes include laminins, collagen IV, nidogens and the heparan sulfate proteoglycans agrin, perlecan and collagen XVIII. The GBM is enriched in the $\alpha3\alpha4\alpha5$ isoform of collagen IV as well as in laminin 521, which interacts with cell-surface receptors $\alpha3\beta1$ integrin and α -dystroglycan on podocytes and endothelial cells. Minor components such as fibulin 1 are also present in the GBM. 7S, collagen IV 7S domain; GAG, glycosaminoglycan; LG, laminin G-like domain G; LN, laminin N-terminal domain; NC1, non-collagenous domain [1].

GBM assembly

The formation of the mature GBM involves the fusion of two reticulates, produced in parallel by podocytes and endothelial cells during glomerulogenesis [29].

In vitro analyzes of the embryoid bodies have shown that the assembly of the GBM occurs according to a hierarchical order. This hierarchical assembly is evident from protein localization analysis, for example by time-lapse imaging of endogenous GFP-tagged basement membrane proteins in *Drosophila* during development, and the observation of embryonic lethality with the loss of basement membrane components. The first event consists in the secretion by the endodermal cells of the extracellular space of laminin heterodimers, which generate an immature basement membrane. This primordial reticulate binds to specific cell surface receptors, for example integrins, discoid domain receptors (DDR), α -dystroglycan and syndecan [30]. Follows the deposition and polymerization of type IV collagen which establishes a lattice mesh on the laminin sheet. With the union of the two

basal layers, GBM consists of two laminin sheets on either side of a thick, central collagenous network. Hence, GBM is much thicker than any other basement membrane, reaching approximately 330-460 nm in the human glomerulus [31] and 50-300nm in rodents [32]. The third step involves the deposition of the HSPGs perlecan and agrin, that connects laminin and collagen IV polymers via nidogen [33]. The thickness of the animal membranes is due to the incorporation of water molecules by the side chains of GAG, which in turn bind to agrin and other proteoglycans. According to the studies on *Drosophila*, the early *drosophila* embryo is capable of the laminin- α and laminin- β subunits [34]. the sequence of events occurring in this organism exactly matches the dynamic expression profiles of basement membrane orthologs in *Caenorhabditis elegans* embryos, as well as our understanding of basement membrane development from knockout studies in vertebrate models [35]. Studies on mice confirm the assembly hierarchy and the importance of the different basal components. In fact, it emerged that both a laminin and type IV collagen deficiency prevent the assembly of the basement membrane causing death in the embryonic state, earlier in the first case, late in the second. The lack of laminin prevents the membrane from being assembled [36], and the lack of collagen IV, causes instead an irregular morphology and rupture of the basement membranes throughout the embryo [37].

Complexity of type IV collagens

Type IV collagen is encoded by six genes (COL4A1–6) in vertebrates, which form three triple helix trimers, $\alpha 1\alpha 1\alpha 2$, $\alpha 3\alpha 4\alpha 5$ and $\alpha 5\alpha 5\alpha 6$. The chains are large proteins that consist of a short, N-terminal ~ 25 amino acid 7S domain, a long ~ 1,400 amino acid collagenous domain and a C- terminal ~ 230 amino acid NC domain. Collagen IV is the element of GBM that confers flexibility and resistance to traction and compression, probably thanks to the central collagenous domain (which contains the Gly-X-Y sequences that permit triple helix formation) also contains about 20 short NC (or interruption)

domains [38]. Once secreted by the cell, the collagen chains assemble to form a polymer adjacent to the laminin sheet. the collagen IV network is characterized by the binding of the interprotomer via homophilic covalent crosslinking or between four adjacent 7S N-terminal domains or between two NC domains adjacent to the C terminal. The assembly of polymers, in particular the oligomerization of the NC domains, it occurs only outside the cells as this process depends on chloride ions, which are more abundant in the extracellular space [39]. Lysyl oxidase-like 2 (LOXL2) mediates covalent crosslinking at the 7S domains, creating the characteristic dodecamer of the collagen IV reticulum [40].

The GBM in glomerular filtration

Although much is known about its components and assembly mechanisms, the contribution of GBM in glomerular filtration has yet to be clarified. The fact that GBM has a gel-like structure [41] has led to suppose that its permeability follows the principle of gel-permeation formalized by Ogston in 1958 [42]. This principle, which relates the permeation to the molecular size, would suggest the passage of water and ions under the force of hydraulic pressure; the fenestrated endothelium and the podocyte slit diaphragms wouldn't act by size selectivity, but only would offer resistance to capillary flow.

Among the experimental evidences supporting this theory, there is a 2017 study based on the microscopic tracking of gold nanoparticles injected into the superior mesenteric artery of mice. These different sized nanoparticles were negatively charged or stable oligoclusters. It showed that permeation in the dense lamina of GBM is size-sensitive: nanoparticles comparable in size to IgG dimers do not penetrate it, particles the size of an IgG monomer permeate to some extent, finally albumin-sized particles permeate widely. in the dense lamina. Particles passing through the dense lamina tend to accumulate upstream of the podocytic glycocalyx which crosses the fissure, but none are observed upstream of the fissure diaphragm. Furthermore, the researchers found that albumin-sized nanoparticles could be completely absorbed in this proximal tubule in small concentrations.

However, if the concentration is high, the reabsorption capacity of the tubule is saturated, producing albuminuria [43]

In maintaining the selectivity function, the compression and tension of the GBM is also very important, which partly depends on the correct expression of the diaphragm proteins. For example, it has been demonstrated that the absence of podocyte nephrin precludes the formation of the slit diaphragm and causes massive proteinuria [44,45]. In the “gel compression model” the fluid flow of glomerular filtration compresses the GBM against the restraining foot processes, likely in an increasing gradient from the lumen to the podocyte [46] and the compressed GBM hinders transport of macromolecules but allows water and small solutes to pass freely. The effacement of podocytic foot processes would reduce the compression of the GBM, leading to an increase in the size of the pores and a physiologically significant increase in the passage of larger molecules. In fact, genetic models of kidney disease, such as *Lamb2*^{-/-} or *Col4a3*^{-/-} mice, show podocyte foot process effacement and GBM thickening, which is consistent with a requirement for interdigitating podocyte foot processes in the maintenance of GBM compression.

As already shown, the anionic charge of the GBM and the glycocalyx have been held responsible for the repulsion of negatively charged proteins, such as albumin, but the question is actually more complex. Several studies have in fact contested this theory, citing as proof the fact that the depletion of HSPGs in the glomerulus does not affect glomerular function. A research conducted on mice has for example shown that the deletion of both agrin and perlecan, as well as the removal of heparan sulphate side chains by glomerular overexpression of heparinase, reduced the net negative charge of GFB but did not induce proteinuria [47]. The conflicting evidence on the role of charge selectivity suggests how much this phenomenon has not yet been fully understood.

2.3 Podocytes

Podocytes, glomerular epithelial cells, are highly specialized and differentiated cells found on the outer surface of the glomerular capillary. Their complex structural architecture is characterized by a bulky cell body and important processes extending outward from their cell body, forming interdigitated foot processes (FP) that envelop the glomerular capillaries. Additionally, FP Podocytes comprise a slit diaphragm (SD) functioning in the middle, a lattice of proteins that actively participate in podocyte signaling. FPs also possess a negatively charged coating, a glycocalyx, which actively participates in the selection of solutes filtered at the barrier. If the podocytes are damaged or lost, as happens in pathological conditions, the GBM is physically altered. This results in a process called "foot process effacement", at the base of many kidney proteinuric diseases [48].

Cytoskeletal actin contributes to both morphology and cell function. The peculiar organizations of longitudinal microfilaments in the foot process and microtubules in the primary process have several functions which include providing structural support to the cell, the ability to contract and expand cells, anchoring themselves to intracellular molecules, to mediate cell signaling.

Figure 4

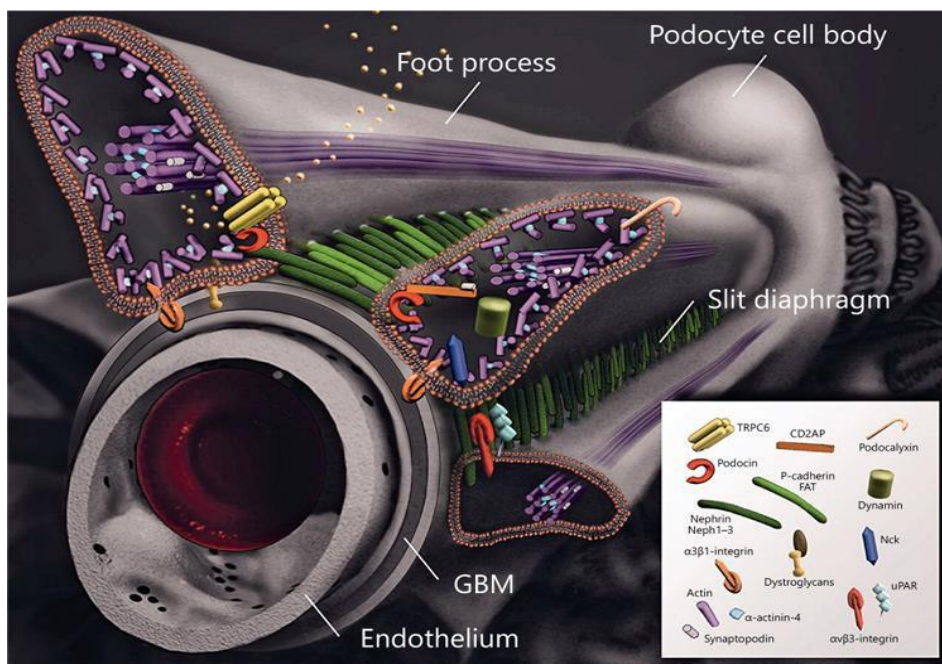


Figure 4. A 3D reconstruction of GBM, with particular attention for podocytes morphology and structure [49].

Slit-diaphragm and transmembrane proteins

The slit-diaphragm is a bridge that extracellularly connects a podocyte to the adjacent one. The podocyte component of maintaining the permselectivity function of the barrier is mainly due to the presence of particular proteins, such as nephrin, NEPH1, podocin, zona occludens-1 (ZO-1), CD2 adapter protein (CD2AP), FAT and P-cadherin; these proteins together form a signaling network that connects the diaphragm with the cytoskeleton of the cell body [50]. Moreover, genetic mutations causing malfunction or inactivation of these proteins have been reported to lead to massive proteinuria and kidney failure [51]. Some examples of proteins essential for the podocyte function will be described below.

Nephrin, a central component for glomerular ultrafiltration, possesses a small intracellular domain that has been shown to associate with the actin cytoskeleton and linked to adapter proteins, a transmembrane domain and an extracellular domain with eight distal IgG-like motifs and a similar motif to proximal type III fibronectin. Nephrin molecules from adjacent foot processes are believed to interact trans to form the basic structure of the slit diaphragm, thus forming a porous molecular sieve. Recent research shows that the phosphorylation of nephrin and tyrosine regulates the morphology of podocyte cells via Nck adapter proteins. The super family of Nck adapter proteins has two members; Nck1 and Nck2 and both are associated with the regulation of actin dynamics [52].

CD2-associated protein (CD2AP) is another intracellular protein that can interact with the C-terminal domain of nephrin. Indeed, it appears that CD2AP may act as a linker between cell membrane receptors and actin-modifying proteins. The N-terminal domain of CD2AP binds to an intermediate protein, p85 and facilitates nephrin-induced AKT signaling that protects podocytes from apoptosis [53]. Phosphorylation of tyrosine in the cytoplasmic tail of nephrin by the Src family kinase initiates a signaling cascade that promotes antiapoptotic signals.

Structurally similar to nephrin, Neph1 is a transmembrane protein belonging to the Neph family, which includes 3 components (Neph1, Neph2, and Neph3). Neph1 and Neph2, located in the slit-diaphragms, can bind to nephrine forming heterodimers, but they cannot interact with each other. Especially Neph1, very similar to nephrine, is studied for its enormous importance for its role in cell signaling: mice deficient in Neph1 were shown to develop proteinuria and renal failure but the functional significance of Neph2 and Neph3 are not clear [54].

The large transmembrane proteins FAT1 and FAT2, located in the slit-diaphragms, contain 34 tandem cadherin-like repeats. Pre-clinical research conducted in mice shows that alterations in these proteins cause proteinuria, but their role has not yet been elucidated [55].

Podocin, located in the slit diaphragm in podocytes, is a 42 kDa hairpin-like integral membrane protein. It is encoded by the NPHS2 gene and is similar to nephrin and Neph1. However, unlike nephrin and Neph1, its N and C-terminal ends are directed in the intracellular space to the cell membrane of the podocytes. It has been proposed to serve as a scaffolding protein and contributes to the structural organization of the slit diaphragm. Podocin interacts with the intracellular domains of nephrin and Neph1 and CD2AP [56]. Podocin knockout mice die shortly after birth due to severe proteinuria [57].

2.4 Relevance of shear stress

The flow of glomerular filtrate depends on the difference in hydrostatic pressure across the filtration barrier and consists of outflow from the glomerular capillaries, through the glomerular basement membrane (GBM) and into the Bowman's space [58].

The way in which the podocytes are connected in the glomerulus, through the slit diaphragmatic bridges, is a unique but at the same time very delicate system. While the outflow pushes the

endothelium towards the GBM, the inflow into the Bowman's space through the filtration slots tends to detach the podocytes from the GBM, which can end up in the urine. The fact that the podocytes detach depends on the reorganization of their cytoskeleton, which in turn depends on both tensile and shear forces. It now seems quite clear that the tensile forces are counteracted by the wall formed by the GBM [4], on the contrary the forces that oppose the shear stress need to be debated. Shear stress depends on both the flow rate and the geometry of the channel: A narrow channel or a higher flow rate corresponds to a higher shear stress. Filter flow exerts shear stress at 2 sites within the glomerulus: on the lateral walls of the foot processes within the filtration slits and on the podocyte cell bodies within Bowman's space. For example, in rats it has been calculated a shear stress of about 8 Pascal (Pa) acting on the side walls of the foot processes, while much lower values, about 0.05 Pa, has been found to act on the cell bodies of podocytes by filtrate flow through Bowman's space [60]. From a physical analysis of the forces acting on the glomerulus, the hypothesis would arise that it is the podocytic slit diaphragm that counteract shear stress, and this would be compatible with the function of size-selective filter. This theory would also explain the podocyte detachment mechanism. In short, the pressure increase causes a distension of the GBM which in turn will cause the expansion of the endothelial network and foot processes, increasing the filtrate flow per unit filtration surface area. If the pressure increases again, the GBM reaches a limit where it can no longer expand, and the filtration surface will no longer increase. From this point onward, increasing intracapillary pressures will drive increasing flows through a filtration barrier with a fixed area, increasing the flow-per-unit slit area. This wears out the podocytes, which seem to resist only as long as the connections are not irreversibly compromised.

Evidence collected so far shows that podocytes are protected by the partial extension of GBM, but the increased flow causes the shear stress to increase. It is important to note that the heterogeneous distribution of fluxes and shear stresses may contribute to the heterogeneous pattern of early glomerular disease. this could, for example, explain the protective action of angiotensin blockade in

conditions of reduced renal mass, leading to reduced filtrate flows along the entire length of the glomerular capillaries [61].

3. Organ-on-a-chip technology

The purpose of pre-clinical *in vitro* studies is to mimic what happens *in vivo*. The cost of drug discovery is steadily increasing due to the limited predictability of 2D cell culture and animal models [62]. The simultaneous evolution of fluidics applied to biotechnology and tissue engineering has given rise to organ-on-a-chip technologies, which offer an alternative to conventional preclinical models for understanding pathophysiological processes. Organ-on-a-chip devices can replicate the basic structure of the functional units of an organ or a part of it, they can recreate a tissue barrier functionality, they can even simplify a multi-organ connection, they can be used for studying drug delivery systems. They can also use human cells directly and optimize (or possibly eliminate where possible) animal testing. Although there are still limitations regarding the materials used, detection, scaling, validation, cellular fidelity, organ-on-a-chip today represent the future of pre-clinical *in vitro* studies. Figure 1a shows the evolution of three-dimensional *in vitro* culture models, highlighting their pros and cons.

Organ-on-a-chip is a fluidic cell culture device that is a more physiologically relevant *in vitro* model than cells grown in traditional media. Generally, this technology is composed of 3 fundamental factors: living cells possibly of human origin, a bioreactor within which they are seeded and a continuous perfusion system of fluid [63]. Normally pre-clinical *in vitro* studies, which represent the first stage of pre-clinical studies consist of growing living cells in a dish, and the absence of a flow makes the culture conditions very different from the real ones. Animal experimentation is also often not very predictive of the human response, as mouse cells often have different specific functions. For example, Kidney toxicity is a major cause of drug abandonment and failure. Only 2% of drug development failures are evaluated in the preclinical phase, and serious adverse effects in 420% of new drugs are discovered only after the clinical phases [64]. Micro- or milli- devices (depending on the volume of fluid flowing) may be a good solution. The ideal systems will therefore use human cell lines, they will not be two-dimensional, but will mimic the three-dimensional architecture and flow

conditions, and will ensure constant perfusion to the bioreactor. Furthermore, the reduced dimensions allow to use little material, with considerable savings in time and costs (Figure 1b).

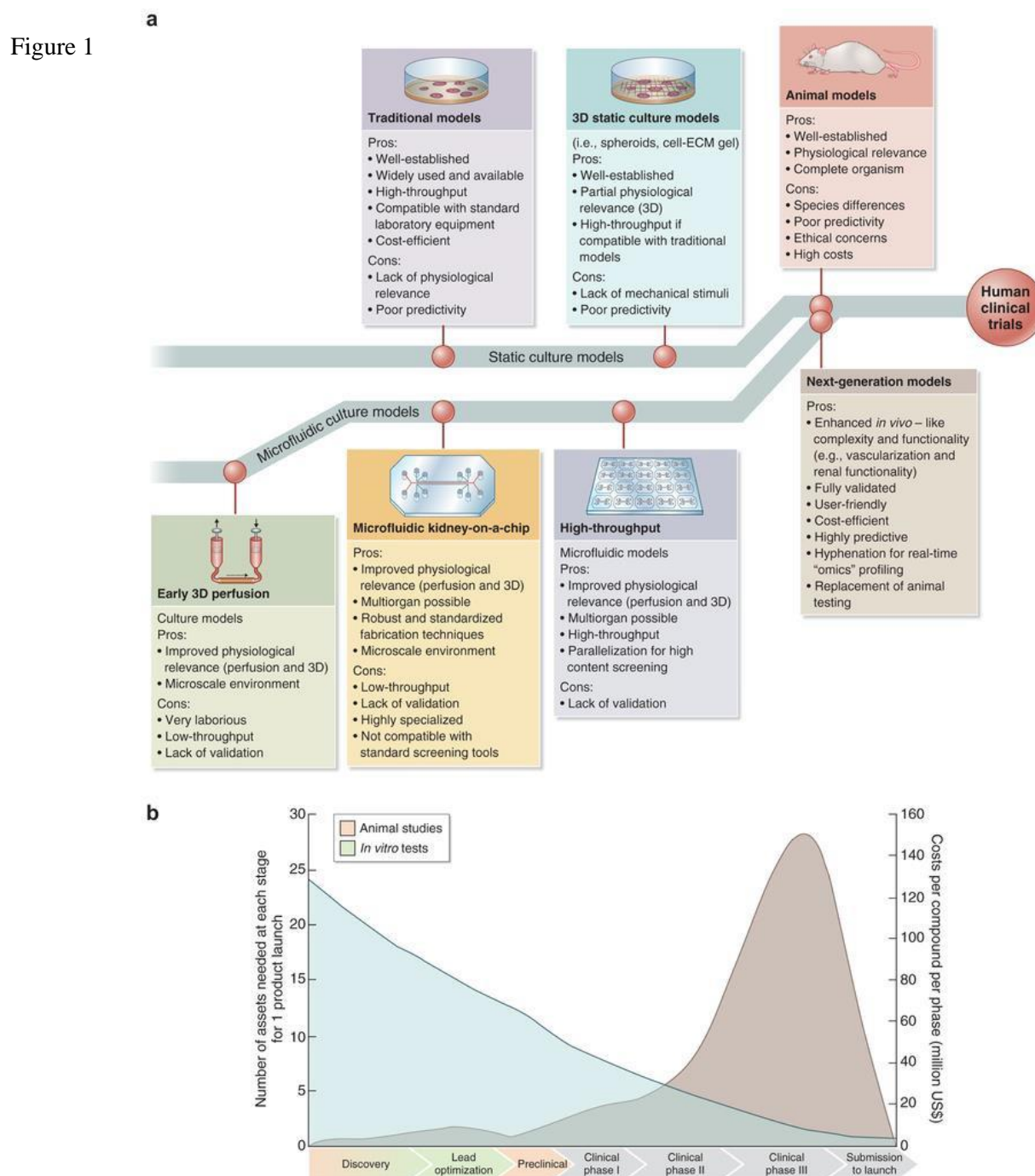


Figure 1. Future of drug testing. (a) Evolution of 3-dimensional (3D) physiologically relevant microfluidic models for nephrotoxicity screening. ECM, extracellular matrix. Adapted with permission from Wilmer MJ, Ng CP, Lanz HL, et al. Kidney-on-a-chip technology for drug-induced nephrotoxicity screening. *Trends Biotechnol.* 2016;34:156–170.8 (b) Drug testing challenge and dilemma. Reproduced from Dehne EM, Hasenberg T, Marx U. The ascendance of microphysiological systems to solve the drug testing dilemma [65].

3.1 Cells used in dynamic kidney models

The cells used for fluidic systems are diverse, including canine cells [66], porcine tubular epithelial [67], opossum tubular epithelial cells [68]. The use of cells of different species can easily lead to errors in response assessment in human disease models and in therapeutic screening. To overcome this problem, human proximal tubule cells (hPTEC) [69] were also used. The disadvantage, however, consists in obtaining sufficient numbers of primary PT cells that have a limited number of population doublings (a maximum of ~12 doublings) [70]. Using antisense nucleotides or RNA interference (small interfering RNA transfected to tumor suppressor p53 or cyclin-dependent kinase inhibitor p16INK4a), doubling of human PT cells can be increased 3 to 5-fold. When seeded into hollow fibers, these small RNA-transfected interfering cells formed a confluent layer of cells that covered the inner surface of the hollow fibers within 1 week and well-developed microvilli were visible on the apical side of these cells.

Promising, but not yet validated, is the use of HPTEC-like cells derived from embryonic stem cells [69]. More recently, induced pluripotent stem cells (iPSCs) have been explored as a continuous source of primary cells. CRISPR33 mutant renal organoids have also shown promise in disease models and drug development studies [71].

3.2 Materials used for design

3D printer technology is often applied to the production of materials for innovative fluidic culture systems. The main characteristics of these materials must be: long life, biocompatibility, haemocompatibility, gas permeability, transparency, possibility of sterilization. Polydimethylsiloxane (PDMS) is therefore often used [72], which has these characteristics, although it tends to absorb hydrophobic compounds, which could preclude its use for some pharmacological

tests [73]. Thermoplastics composed of polycarbonate, polystyrene and poly (methyl methacrylate), all of which have low absorption of hydrophobic compounds, are therefore often preferred in fluid systems [74].

These systems can then be implemented by hydrogel-based materials or natural polymers capable of mimicking physiological scaffolds. For example, Ng et al. showed hPTECs proliferated mostly in hollow fibers covered with a layer of fibrin and hydrogel. important for the determination of the system conditions are the biosensors. They have often been incorporated into bioengineered scaffolds to assess cellular behaviour in response to changes in the microenvironment. Ferrel et al. developed a microfluidic bioreactor from polycarbonate membranes coated with type IV collagen and seeded with human kidney epithelial cells and MDCK cells [75]. These bioreactors contained integrated electrodes for measuring transepithelial electrical resistance, kidney epithelial cell growth, and tight junction integrity.

3.3 Drug development and testing

An obligatory stage for the marketing of a new drug is animal testing, with all the disadvantages that this entails. Animal studies are expensive and slow, nephrotoxic responses are often species-specific. The use of human cells *in vitro*, in addition to avoiding ethical problems, could more accurately predict the response of the drug in clinical trials [76]. The cells of the proximal tubule are frequently targeted by drugs [77], as they have high capacity for reabsorption and transport of molecules, for this reason they are therefore particularly interesting to test in advanced models. For example, many models based on these cells have been useful in discovering the nephrotoxicity of cisplatin [78] and the recovery of this damage by cimetidine [79].

However, in order to correctly predict the response to a drug, one cannot ignore the presence of a fluid flow that mimics the passage of blood. 3D fluidic models are therefore the most suitable models. Drugs that disrupt renal blood flow have traditionally proved challenging for *in vitro* nephrotoxicity

screenings. Vasoconstrictors such as catecholamines and calcineurin inhibitors reduce the supply of oxygen, causing damage to the renal cord [80]. Recently developed blood vessel-on-chip devices have shown that vasoconstrictive behaviours can be evaluated in organ-on-chip models, raising the possibility that soon on-chip models may be available to model vasoconstrictive nephrotoxicity [81].

Integrated systems of multiple organ-on-a-chips could be even more interesting in the study of nephrotoxicity, as they could help evaluate the systemic and secondary toxicities of the new drug.

In 2017 Verneti et al. combined on-chip systems representing uptake (human jejunal enteroids), metabolism (primary human hepatocytes) and clearance (primary human proximal tubular epithelial cells) with skeletal muscle (human primary myocytes) and neurovascular (human neurons and astrocytes derived from iPSC), in which media were sequentially transferred from one organ to another [82]. Maschmeyer et al also developed a multi-organ on-chip model (Figure 3) that includes intestine (primary human small intestine epithelial cells), liver (primary human hepatic stellate cells combined with immortalized HepaRG cells), skin (human biopsy tissue), and cell line Human renal PT (RPTEC/TERT1) were similarly developed to evaluate drug absorption, distribution, metabolism and excretion, as well as multi-organ toxicity [83].

In conclusion, current data suggest that fluidic devices are the most reliable tools in predicting nephrotoxicity. Drugs for some pathologies vasoconstrictive nephropathy can already be successfully tested on vascular systems, or on multi-organ systems, however much progress still needs to be made to make data on other more complex pathologies replicable.

3.4 Kidney dynamic models

In 2009, Kyung-Jin Jang and Kahp-Yang Suh released the first model that replicates a portion of the kidney on the chip [84]. The design foresees the presence of two compartments, an upper channel that simulates the urinary lumen and has a flow of fluid and a lower part filled with soil that mimics the interstitial space (Figure 2). Kidney cells are subjected to much less frictional stress than endothelial or lung cells; this device uses rat distal tubular cells, which have a shear stress ~ 1 dyn/cm. In short, Primary Rat Inner Medullary Collecting Duct (IMCD) cells are cultured within the canal. To generate an environment similar to that present in the tubule *in vivo*, a fluidic shear stress of ~ 1 dyn/cm is applied for 5 hours. This condition is considered optimal for the reproduction of the tubular environment, as evidenced by the polarization, cytoskeletal organization and molecular transport analyzed.

Figure 2

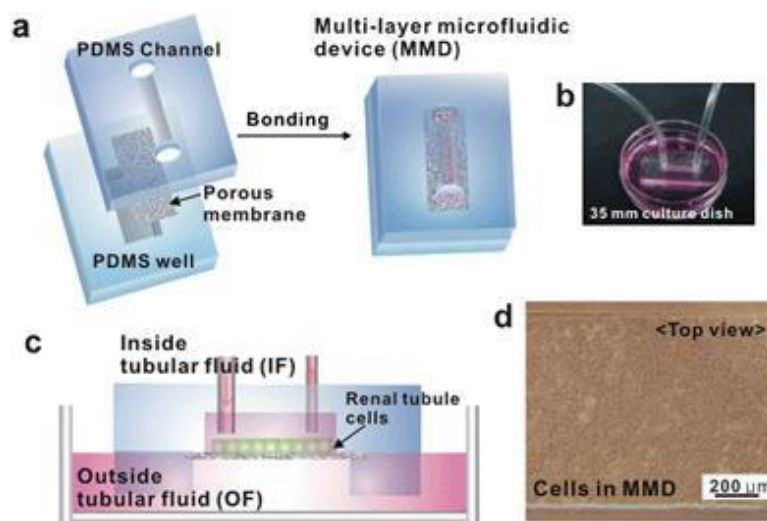


Figure 2. Fabrication and operation of a the multi-layer microfluidic device (MMD) of Kyung-Jin Jang and Kahp-Yang Suh . (a) The MMD is a sandwich assembly of polydimethyl siloxane (PDMS) channel, polyester membrane, and PDMS reservoir bonded with plasma treatment. (b) Photograph showing the operation of MMD that is connected to a syringe pump with silicone tubes. The MMD is placed on a culture dish containing an outside tubular fluid (OF). (c) Schematic of the device on a culture dish. (d) Microscope image of IMCD cells within the MMD. Cells are grown confluent after seeding 3 days. This image shows complete isolation of cells in the channel without any leakage.

Later, Jang et al. present a second article in which the design of the device remains essentially unchanged, but human proximal tubular cells are used. In this model, the author tries to

reproduce the nephrotoxicity induced by cisplatin [79]. Primary kidney epithelial cells are isolated from the proximal tubule and cultured on the upper side of a porous polyester membrane, which divides the main channel of the device into two adjacent channels, thereby creating a luminal apical canal and an interstitial basal space. Exposure of the epithelial monolayer to an apical stress (0.2 dyne/cm²) which mimics the presence of live renal tubules, leads to greater polarization of epithelial cells and the formation of primary cilia, which is different from traditional culture systems in transwell.

Worthy of note is a work published in 2015 by a group of German researchers [83], in which a microphysiological system was developed that is able to maintain, for 28 days of co-culture, the functionality of 4 organs (intestine, liver, skin and kidney), reproduced in proportion in a miniaturized system. The pre-formed models of the human intestine and skin were integrated into a four-organs-chip on standard inserts for cell culture, with a size 100,000 times smaller than the human organ. A three-dimensional based spheroid, equivalent to 10 liver lobules, mimics renal function, while a barrier, which separates the flow of medium flowing through the organs from the fluids excreted by the kidney, was generated by a polymeric membrane covered by a single layer of human proximal tubular epithelial cells. This approach represents the first attempt to create an *in vitro* multi-organ microfluidic system, which could be very useful for drug testing.

Figure 3

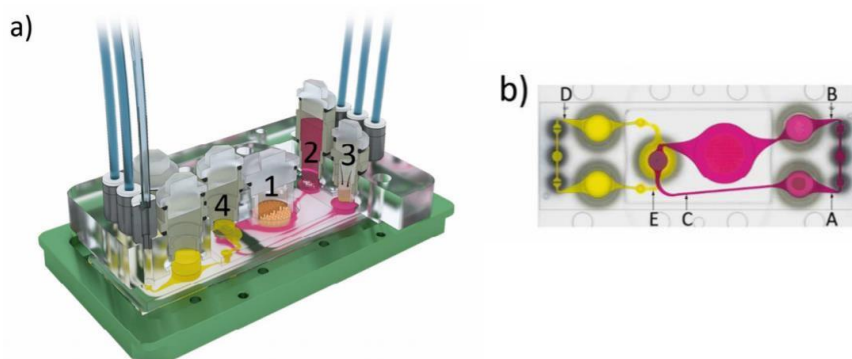


Figure 3. The microfluidic four-organ-chip device of Maschmeyer. a) 3D view of the device comprising two polycarbonate cover-plates, the PDMS-glass chip accommodating a surrogate blood flow circuit (pink) and an excretory flow circuit (yellow). Numbers represent the four tissue culture compartments for intestine (1), liver (2), skin (3), and kidney (4) tissue. A central cross-section of each tissue culture compartment aligned along the interconnecting microchannel is depicted. b) Evaluation of fluid dynamics in the 4OC using μ PIV. Top view of the four-organ-chip layout illustrating the positions of three measuring spots (A, B and C) in the surrogate blood circuit and two spots (D, E) in the excretory circuit.

In the last 5 years, as evidence of the rapid evolution of this technology, two research works have been presented that propose two different models of glomerulus-on-a-chip. In 2016, Zhou et al. show the possibility of mimicking hypertensive nephropathy by means of a microfluidic device that reproduces the functionality of the glomerulus and performs filtration in a physiological microenvironment with complex hydrodynamic factors [85]. This glomerulus-on-a-chip consists of 4 units: each contains 4 interconnected cell culture chambers, to simulate the glomerular capillary network. The size of the inlet channels is greater than the size of the sample outlet channels, since the diameter of the afferent arterioles is greater than that of the efferent arterioles. Each unit has been designed to connect to a common inlet from which a syringe pump applies a certain flow rate of the culture medium (Figure 4).

Figure 4

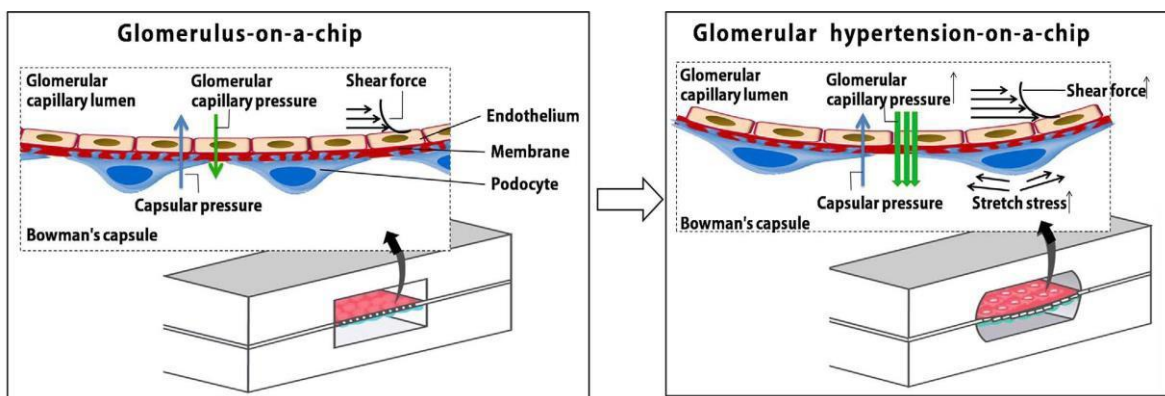


Figure 4. Glomerulus-on-a-chip (GC) microdevice of Zhou group. The effective filtration pressure depends on glomerular capillary pressure, capsular pressure and shear force. The microfabricated glomerulus mimic device uses compartmentalized PDMS microchannels to form a GFB on a membrane coated with ECM. (B1) The device recreated the physiological glomerular filtration function by supplying perfusion flow in the upper microchannel and causing mechanical forces (e.g., glomerular capillary pressure, shear force, and stretch stress) to act on the GFB membrane; (B2) a pathological glomerular microenvironment was established by perfusion flow regulating mechanical forces.

In short, a porous membrane is coated with a basement membrane extract; subsequently, murine endothelial glomerular cells (GEnC) and murine podocytes (MPC-5) are seeded on opposite sides of the membrane. When the cells come to confluence, the culture medium is introduced into the endothelial compartment at a rate of 5 $\mu\text{l}/\text{min}$, which is then recovered from the podocyte

compartment, i.e. after passing through the filtration barrier. To simulate hypertensive nephropathy the flow rate was increased to 10-15 $\mu\text{l}/\text{min}$. Under these conditions, it has been proven that as the flow rate increases, the shear stress increases in a directly proportional manner. Of particular importance was the method adopted to verify the functionality of GFB: fluorescein-isothiocyanate (FITC) conjugated to inulin, FITC-fetal bovine serum (BSA) and FITC IgG were used to approximate small, medium and large molecules, respectively. From the analyzes carried out, it emerges that the permeability of GFBco-culture is considerably lower than the single monolayers of endothelial cells and podocytes.

Glomerulus-on-a-chip models are far less represented, partly due to the difficulty of culturing human glomerular cells. One research published on the subject is from April 2017 also proposed a model of damage induced by diabetic nephropathy [86]. To reproduce the human glomerular microenvironment, a two-layer compartmentalized device was designed, formed by parallel channels, in which primary glomerular micro-tissues subject to microflow were grown. The capillary canal was infused with glomerular microtissues under low flow, to reproduce the luminal capillary side of the glomerulus. The central canal was injected with Matrigel, which forms a 3D structure suitable for the adhesion and development of isolated glomeruli. Finally, a third channel was used to collect the filtrate of the capillary channel, thus representing the capsular side of the glomerulus. This device has been used to reproduce glucose-induced critical pathological responses in diabetic nephropathy as observed in humans. The results showed that hyperglycemia plays a crucial role in the development of increased permeability of the albumin barrier and glomerular dysfunction, factors that lead to proteinuria.

The development of a functional glomerulus-on-a-chip was stymied by a lack of functional podocytes until the recent work by Musah et al. [87], who obtained terminally differentiated podocytes from human iPSCs. These podocytes were cocultured with endothelial cells on opposite sides of a laminin-coated membrane in a system with separate microfluidic channels mimicking urinary and blood flow. Production of basement membrane collagen and a tissue-tissue interface were observed

as was a physiological differential clearance of albumin and inulin. Adriamycin caused podocyte disruption, loss of function, and cell death in this system mimicking the toxicity of Adriamycin *in vivo* were observed.

Figure 5

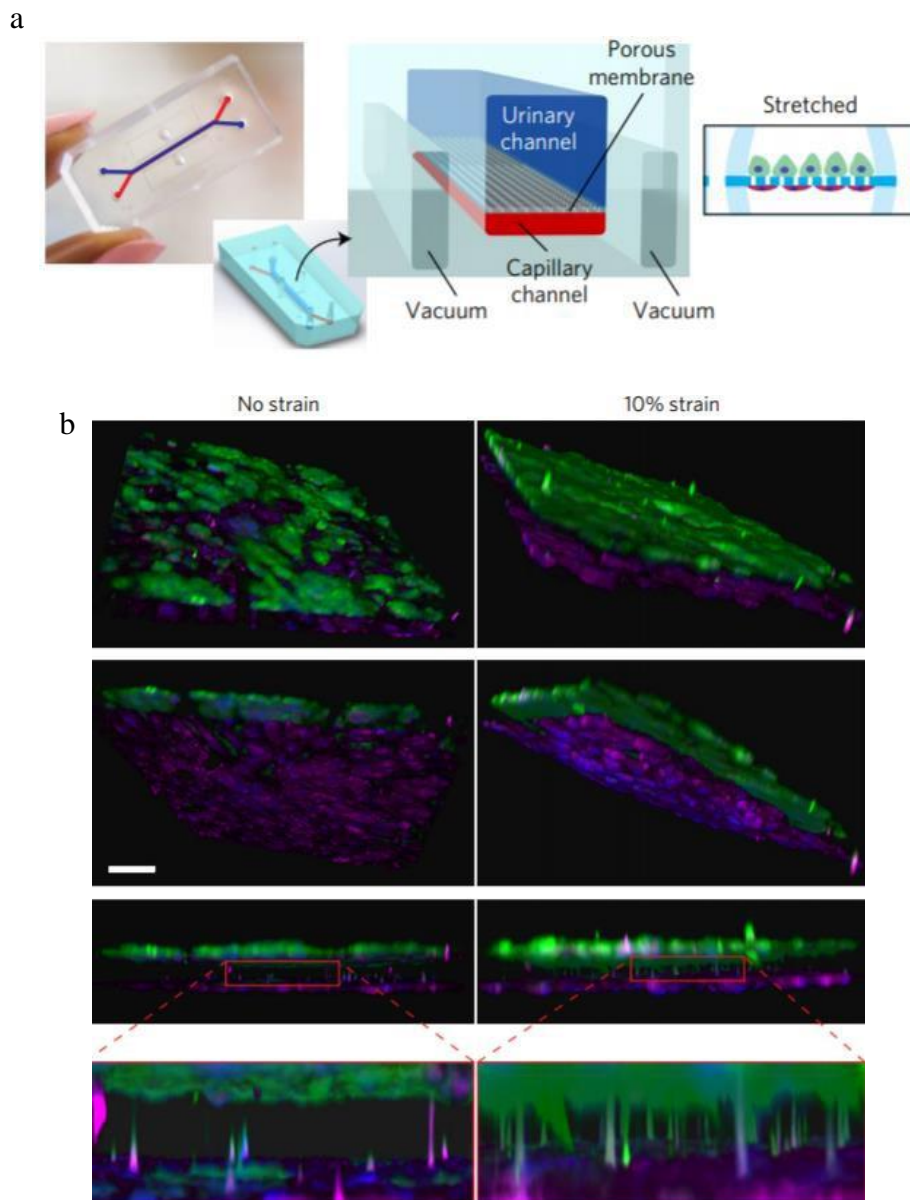


Figure 5. Model of Musah et al. a) Schematic representation of glomerular capillary wall with podocytes and endothelial cells separated by the GBM. Arrow shows directional flow of molecules from the capillary lumen to urinary space. b) Three-dimensional reconstructed views of the tissue-tissue interface formed by hiPS-cell-derived podocytes (top, green) and human glomerular endothelial cells (bottom, magenta) showing that cyclic application of 10% strain enhanced the extension of podocyte cell processes through the pores of the flexible ECM-coated PDMS membrane so that they insert into the abluminal surface of the underlying glomerular endothelium (insets).

References

1. Naylor, R.W.; Morais, M.R.P.T.; Lennon, R. Complexities of the glomerular basement membrane. *Nat. Rev. Nephrol.* **2020**.
2. Pollak, M.R.; Quaggin, S.E.; Hoenig, M.P.; Dworkin, L.D. The glomerulus: The sphere of influence. *Clin. J. Am. Soc. Nephrol.* **2014**, *9*, 1461–1469.
3. Arif, E.; Nihalani, D. Glomerular Filtration Barrier Assembly: An insight. *Postdoc J.* **2013**, *1*, 33.
4. Haraldsson, B.; Nyström, J.; Deen, W.M. Properties of the Glomerular Barrier and Mechanisms of Proteinuria. *Physiol. Rev.* **2008**, *88*.
5. Bulger, R.E.; Eknoyan, G.; Purcell, D.J.; Dobyan, D.C. Endothelial characteristics of glomerular capillaries in normal, mercuric chloride-induced, and gentamicin-induced acute renal failure in the rat. *J. Clin. Invest.* **1983**, *72*, 128–141.
6. Satchell, S.C.; Braet, F. Glomerular endothelial cell fenestrations: An integral component of the glomerular filtration barrier. *Am. J. Physiol. - Ren. Physiol.* **2009**, *296*.
7. Ichimura, K.; Stan, R. V.; Kurihara, H.; Sakai, T. Glomerular endothelial cells form diaphragms during development and pathologic conditions. *J. Am. Soc. Nephrol.* **2008**, *19*, 1463–1471.
8. Reeves, W.H.; Kanwar, Y.S.; Farquhar, M.G. Assembly of the glomerular filtration surface: Differentiation of anionic sites in glomerular capillaries of newborn rat kidney. *J. Cell Biol.* **1980**, *85*, 735–753.
9. Quaggin, S.E.; Kreidberg, J.A. Development of the renal glomerulus: Good neighbors and good fences. *Development* **2008**, *135*, 609–620.
10. Brown, L.F.; Berse, B.; Tognazzi, K.; Manseau, E.J.; Van De Water, L.; Senger, D.R.; Dvorak, H.F.; Rosen, S. Vascular permeability factor mRNA and protein expression in human kidney. *Kidney Int.* **1992**, *42*, 1457–1461.
11. Satchell, S.C.; Harper, S.J.; Tooke, J.E.; Kerjaschki, D.; Saleem, M.A.; Mathieson, P.W. Human Podocytes Express Angiopoietin 1, a Potential Regulator of Glomerular Vascular Endothelial Growth Factor. *J. Am. Soc. Nephrol.* **2002**, *13*.
12. Eremina, V.; Baelde, H.J.; Quaggin, S.E. Role of the VEGF--a signaling pathway in the glomerulus: evidence for crosstalk between components of the glomerular filtration barrier. *Nephron. Physiol.* **2007**, *106*, p32-7.
13. Kamba, T.; Tam, B.Y.Y.; Hashizume, H.; Haskell, A.; Sennino, B.; Mancuso, M.R.; Norberg, S.M.; O'Brien, S.M.; Davis, R.B.; Gowen, L.C.; et al. VEGF-dependent plasticity of fenestrated capillaries in the normal adult microvasculature. *Am. J. Physiol. - Hear. Circ. Physiol.* **2006**, *290*.
14. Sugimoto, H.; Hamanog, Y.; Charytan, D.; Cosgrove, D.; Kieran, M.; Sudhakar, A.; Kalluri, R. Neutralization of circulating vascular endothelial growth factor (VEGF) by anti-VEGF antibodies and soluble VEGF receptor 1 (sFlt-1) induces proteinuria. *J. Biol. Chem.* **2003**, *278*, 12605–12608.

15. Rostgaard, J.; Qvortrup, K. Sieve plugs in fenestrae of glomerular capillaries--site of the filtration barrier? *Cells. Tissues. Organs* **2002**, *170*, 132–8.
16. Ciarimboli, G.; Hjalmarsson, C.; Bökenkamp, A.; Schurek, H.J.; Haraldsson, B. Dynamic alterations of glomerular charge density in fixed rat kidneys suggest involvement of endothelial cell coat. *Am. J. Physiol. - Ren. Physiol.* **2003**, *285*.
17. Deen, W.M. What determines glomerular capillary permeability? *J. Clin. Invest.* 2004, *114*, 1412–1414.
18. Avasthi, P.S.; Koshy, V. The anionic matrix at the rat glomerular endothelial surface. *Anat. Rec.* **1988**, *220*, 258–266.
19. Salmon, A.H.; Satchell, S.C. Endothelial glycocalyx dysfunction in disease: Albuminuria and increased microvascular permeability. *J. Pathol.* 2012, *226*, 562–574.
20. Schlöndorff, D.; Wyatt, C.M.; Campbell, K.N. Revisiting the determinants of the glomerular filtration barrier: what goes round must come round. *Kidney Int.* 2017, *92*, 533–536.
21. Satchell, S.C. The glomerular endothelium emerges as a key player in diabetic nephropathy. *Kidney Int.* 2012, *82*, 949–951.
22. Weinbaum, S.; Tarbell, J.M.; Damiano, E.R. The Structure and Function of the Endothelial Glycocalyx Layer. *Annu. Rev. Biomed. Eng.* **2007**, *9*, 121–167.
23. Haraldsson, B.; Nyström, J.; Deen, W.M. Properties of the glomerular barrier and mechanisms of proteinuria. *Physiol. Rev.* 2008, *88*, 451–487.
24. Fridén, V.; Oveland, E.; Tenstad, O.; Ebefors, K.; Nyström, J.; Nilsson, U.A.; Haraldsson, B. The glomerular endothelial cell coat is essential for glomerular filtration. *Kidney Int.* **2011**, *79*, 1322–1330.
25. Reitsma, S.; Slaaf, D.W.; Vink, H.; Van Zandvoort, M.A.M.J.; Oude Egbrink, M.G.A. The endothelial glycocalyx: Composition, functions, and visualization. *Pflugers Arch. Eur. J. Physiol.* 2007, *454*, 345–359.
26. Ebong, E.E.; MacAluso, F.P.; Spray, D.C.; Tarbell, J.M. Imaging the endothelial glycocalyx *in vitro* by rapid freezing/freeze substitution transmission electron microscopy. *Arterioscler. Thromb. Vasc. Biol.* **2011**, *31*, 1908–1915.
27. Arisaka, T.; Mitsumata, M.; Kawasumi, M.; Tohjima, T.; Hirose, S.; Yoshida, Y. Effects of shear stress on glycosaminoglycan synthesis in vascular endothelial cells. In Proceedings of the Annals of the New York Academy of Sciences; Blackwell Publishing Inc., 1994; Vol. 748, pp. 543–554.
28. Mulivor, A.W.; Lipowsky, H.H. Inflammation- and ischemia-induced shedding of venular glycocalyx. *Am. J. Physiol. - Hear. Circ. Physiol.* **2004**, *286*.
29. Abrahamson, D.R. Origin of the glomerular basement membrane visualized after *in vivo* labeling of laminin in newborn rat kidneys. *J. Cell Biol.* **1985**, *100*, 1988–2000.
30. Li, S.; Edgar, D.; Fässler, R.; Wadsworth, W.; Yurchenco, P.D. The role of laminin in embryonic cell polarization and tissue organization. *Dev. Cell* 2003, *4*, 613–624.

31. Mandache, E.; Gherghiceanu, M. Ultrastructural defects of the glomerular basement membranes associated with primary glomerular nephropathies. *Ultrastruct. Pathol.* **2004**, *28*, 103–108.
32. Randles, M.J.; Collinson, S.; Starborg, T.; Mironov, A.; Krendel, M.; Königshausen, E.; Sellin, L.; Roberts, I.S.D.; Kadler, K.E.; Miner, J.H.; et al. Three-dimensional electron microscopy reveals the evolution of glomerular barrier injury. *Sci. Rep.* **2016**, *6*, 1–13.
33. Fox, J.W.; Mayer, U.; Nischt, R.; Aumailley, M.; Reinhardt, D.; Wiedemann, H.; Mann, K.; Timpl, R.; Krieg, T.; Engel, J.; et al. Recombinant nidogen consists of three globular domains and mediates binding of laminin to collagen type IV. *EMBO J.* **1991**, *10*, 3137–46.
34. Matsubayashi, Y.; Louani, A.; Dragu, A.; Sánchez-Sánchez, B.J.; Serna-Morales, E.; Yolland, L.; Gyoergy, A.; Vizcay, G.; Fleck, R.A.; Heddleston, J.M.; et al. A Moving Source of Matrix Components Is Essential for De Novo Basement Membrane Formation. *Curr. Biol.* **2017**, *27*, 3526-3534.e4.
35. Graham, P.L.; Johnson, J.J.; Wang, S.; Sibley, M.H.; Gupta, M.C.; Kramer, J.M. Type IV collagen is detectable in most, but not all, basement membranes of *Caenorhabditis elegans* and assembles on tissues that do not express it. *J. Cell Biol.* **1997**, *137*, 1171–1183.
36. Smyth, N.; Vatansever, S.H.; Murray, P.; Meyer, M.; Frie, C.; Paulsson, M.; Edgar, D. Absence of basement membranes after targeting the LAMC1 gene results in embryonic lethality due to failure of endoderm differentiation. *J. Cell Biol.* **1999**, *144*, 151–160.
37. Pöschl, E.; Schlötzer-Schrehardt, U.; Brachvogel, B.; Saito, K.; Ninomiya, Y.; Mayer, U. Collagen IV is essential for basement membrane stability but dispensable for initiation of its assembly during early development. *Development* **2004**, *131*, 1619–1628.
38. Xu, T.; Zhou, C.Z.; Xiao, J.; Liu, J. Unique Conformation in a Natural Interruption Sequence of Type XIX Collagen Revealed by Its High-Resolution Crystal Structure. *Biochemistry* **2018**, *57*, 1087–1095.
39. Cummings, C.F.; Pedchenko, V.; Brown, K.L.; Colon, S.; Rafi, M.; Jones-Paris, C.; Pokydeshaeva, E.; Liu, M.; Pastor-Pareja, J.C.; Stothers, C.; et al. Extracellular chloride signals collagen IV network assembly during basement membrane formation. *J. Cell Biol.* **2016**, *213*, 479–494.
40. Añazco, C.; López-Jiménez, A.J.; Rafi, M.; Vega-Montoto, L.; Zhang, M.Z.; Hudson, B.G.; Vanacore, R.M. Lysyl oxidase-like-2 cross-links collagen IV of glomerular basement membrane. *J. Biol. Chem.* **2016**, *291*, 25999–26012.
41. Smithies, O. Why the kidney glomerulus does not clog: A gel permeation/diffusion hypothesis of renal function. *Proc. Natl. Acad. Sci. U. S. A.* **2003**, *100*, 4108–4113.
42. Ogston, A.G. The spaces in a uniform random suspension of fibres. *Trans. Faraday Soc.* **1958**, *54*, 1754–1757.
43. Lawrence, M.G.; Altenburg, M.K.; Sanford, R.; Willett, J.D.; Bleasdale, B.; Ballou, B.; Wilder, J.; Li, F.; Miner, J.H.; Berg, U.B.; et al. Permeation of macromolecules into the renal glomerular basement membrane and capture by the tubules. *Proc. Natl. Acad. Sci. U. S. A.* **2017**, *114*, 2958–2963.

44. Kestilä, M.; Lenkkeri, U.; Männikkö, M.; Lamerdin, J.; McCready, P.; Putaala, H.; Ruotsalainen, V.; Morita, T.; Nissinen, M.; Herva, R.; et al. Positionally cloned gene for a novel glomerular protein--nephrin--is mutated in congenital nephrotic syndrome. *Mol. Cell* **1998**, *1*, 575–82.
45. Putaala, H.; Soininen, R.; Kilpeläinen, P.; Wartiovaara, J.; Tryggvason, K. The murine nephrin gene is specifically expressed in kidney, brain and pancreas: Inactivation of the gene leads to massive proteinuria and neonatal death. *Hum. Mol. Genet.* **2001**, *10*, 1–8.
46. Fissell, W.H.; Miner, J.H. What is the glomerular ultrafiltration barrier? *J. Am. Soc. Nephrol.* **2018**, *29*, 2262–2264.
47. Khalil, R.; Lalai, R.A.; Wiweger, M.I.; Avramut, C.M.; Koster, A.J.; Spaink, H.P.; Bruijn, J.A.; Hogendoorn, P.C.W.; Baelde, H.J. Glomerular permeability is not affected by heparan sulfate glycosaminoglycan deficiency in zebrafish embryos. *Am. J. Physiol. - Ren. Physiol.* **2019**, *317*, F1211–F1216.
48. Reiser, J.; Altintas, M.M. Podocytes. *F1000Research* **2016**, *5*.
49. Grahammer, F.; Schell, C.; Huber, T.B. The podocyte slit diaphragm - From a thin grey line to a complex signalling hub. *Nat. Rev. Nephrol.* **2013**, *9*, 587–598.
50. Tryggvason, K.; Pikkarainen, T.; Patrakka, J. Nck Links Nephrin to Actin in Kidney Podocytes. *Cell* **2006**, *125*, 221–224.
51. Pavenstädt, H.; Kriz, W.; Kretzler, M. Cell Biology of the Glomerular Podocyte. *Physiol. Rev.* **2003**, *83*.
52. Jones, N.; Blasutig, I.M.; Eremina, V.; Ruston, J.M.; Bladt, F.; Li, H.; Huang, M.; Larose, L.; Li, S.S.C.; Takano, T.; et al. Nck adaptor proteins link nephrin to the actin cytoskeleton of kidney podocytes. *Nature* **2006**, *440*, 818–823.
53. Huber, T.B.; Hartleben, B.; Kim, J.; Schmidts, M.; Schermer, B.; Keil, A.; Egger, L.; Lecha, R.L.; Borner, C.; Pavenstädt, H.; et al. Nephrin and CD2AP Associate with Phosphoinositide 3-OH Kinase and Stimulate AKT-Dependent Signaling. *Mol. Cell. Biol.* **2003**, *23*, 4917–4928.
54. Donoviel, D.B.; Freed, D.D.; Vogel, H.; Potter, D.G.; Hawkins, E.; Barrish, J.P.; Mathur, B.N.; Turner, C.A.; Geske, R.; Montgomery, C.A.; et al. Proteinuria and Perinatal Lethality in Mice Lacking NEPH1, a Novel Protein with Homology to NEPHRIN. *Mol. Cell. Biol.* **2001**, *21*, 4829–4836.
55. Tryggvason, K.; Patrakka, J.; Wartiovaara, J. Hereditary Proteinuria Syndromes and Mechanisms of Proteinuria. *N. Engl. J. Med.* **2006**, *354*, 1387–1401.
56. Sellin, L.; Huber, T.B.; Gerke, P.; Quack, I.; Pavenstädt, H.; Walz, G. NEPH1 defines a novel family of podocin interacting proteins. *FASEB J.* **2003**, *17*, 115–117.
57. Boute, N.; Gribouval, O.; Roselli, S.; Benessy, F.; Lee, H.; Fuchshuber, A.; Dahan, K.; Gubler, M.C.; Niaudet, P.; Antignac, C. NPHS2, encoding the glomerular protein podocin, is mutated in autosomal recessive steroid-resistant nephrotic syndrome. *Nat. Genet.* **2000**, *24*, 349–354.

58. Kriz, W.; Lemley, K. V. Potential relevance of shear stress for slit diaphragm and podocyte function. *Kidney Int.* 2017, *91*, 1283–1286.
59. Haraldsson, B.; Nyström, J.; Deen, W.M. Properties of the glomerular barrier and mechanisms of proteinuria. *Physiol. Rev.* 2008, *88*, 451–487.
60. Endlich, N.; Endlich, K. The Challenge and Response of Podocytes to Glomerular Hypertension. *Semin. Nephrol.* **2012**, *32*, 327–341.
61. Lemley, K. V. Glomerular pathology and the progression of chronic kidney disease. *Am. J. Physiol. Physiol.* **2016**, *310*, F1385–F1388.
62. Zhang, B.; Korolj, A.; Lai, B.F.L.; Radisic, M. Advances in organ-on-a-chip engineering. *Nat. Rev. Mater.* 2018, *3*, 257–278.
63. Kim, S.; Takayama, S. Organ-on-a-chip and the kidney. *Kidney Res. Clin. Pract.* **2015**, *34*, 165–9.
64. Lavery, H.G.; Benson, C.; Cartwright, E.J.; Cross, M.J.; Garland, C.; Hammond, T.; Holloway, C.; McMahon, N.; Milligan, J.; Park, B.K.; et al. How can we improve our understanding of cardiovascular safety liabilities to develop safer medicines? *Br. J. Pharmacol.* 2011, *163*, 675–693.
65. Ashammakhi, N.; Wesseling-Perry, K.; Hasan, A.; Elkhammas, E.; Zhang, Y.S. Kidney-on-a-chip: untapped opportunities. *Kidney Int.* 2018, *94*, 1073–1086.
66. Mu, X.; Zheng, W.; Xiao, L.; Zhang, W.; Jiang, X. Engineering a 3D vascular network in hydrogel for mimicking a nephron. *Lab Chip* **2013**, *13*, 1612–1618.
67. Kim, S.; Lesherperez, S.C. a.; Kim, B.C. hou. C.; Yamanishi, C.; Labuz, J.M.; Leung, B.; Takayama, S. Pharmacokinetic profile that reduces nephrotoxicity of gentamicin in a perfused kidney-on-a-chip. *Biofabrication* **2016**, *8*, 015021.
68. Ferrell, N.; Ricci, K.B.; Groszek, J.; Marmorstein, J.T.; Fissell, W.H. Albumin handling by renal tubular epithelial cells in a microfluidic bioreactor. *Biotechnol. Bioeng.* **2012**, *109*, 797–803.
69. Narayanan, K.; Schumacher, K.M.; Tasnim, F.; Kandasamy, K.; Schumacher, A.; Ni, M.; Gao, S.; Gopalan, B.; Zink, D.; Ying, J.Y. Human embryonic stem cells differentiate into functional renal proximal tubular-like cells. *Kidney Int.* **2013**, *83*, 593–603.
70. Sanechika, N.; Sawada, K.; Usui, Y.; Hanai, K.; Kakuta, T.; Suzuki, H.; Kanai, G.; Fujimura, S.; Yokoyama, T.A.; Fukagawa, M.; et al. Development of bioartificial renal tubule devices with lifespan-extended human renal proximal tubular epithelial cells. *Nephrol. Dial. Transplant.* **2011**, *26*, 2761–2769.
71. Freedman, B.S.; Brooks, C.R.; Lam, A.Q.; Fu, H.; Morizane, R.; Agrawal, V.; Saad, A.F.; Li, M.K.; Hughes, M.R.; Werff, R. Vander; et al. Modelling kidney disease with CRISPR-mutant kidney organoids derived from human pluripotent epiblast spheroids. *Nat. Commun.* **2015**, *6*.
72. Mata, A.; Fleischman, A.J.; Roy, S. Characterization of Polydimethylsiloxane (PDMS) Properties for Biomedical Micro/Nanosystems. *Biomed. Microdevices* **2005**, *7*, 281–293.

73. Toepke, M.W.; Beebe, D.J. PDMS absorption of small molecules and consequences in microfluidic applications. *Lab Chip* **2006**, *6*, 1484–6.
74. Nge, P.N.; Rogers, C.I.; Woolley, A.T. Advances in microfluidic materials, functions, integration, and applications. *Chem. Rev.* **2013**, *113*, 2550–2583.
75. Ferrell, N.; Desai, R.R.; Fleischman, A.J.; Roy, S.; Humes, H.D.; Fissell, W.H. A microfluidic bioreactor with integrated transepithelial electrical resistance (TEER) measurement electrodes for evaluation of renal epithelial cells. *Biotechnol. Bioeng.* **2010**, *107*, 707–716.
76. Drug-induced nephrotoxicity - PubMed Available online: <https://pubmed.ncbi.nlm.nih.gov/18819242/> (accessed on Jan 10, 2021).
77. Tiong, H.Y.; Huang, P.; Xiong, S.; Li, Y.; Vathsala, A.; Zink, D. Drug-induced nephrotoxicity: Clinical impact and preclinical *in vitro* models. *Mol. Pharm.* **2014**, *11*, 1933–1948.
78. Schetz, M.; Dasta, J.; Goldstein, S.; Golper, T. Drug-induced acute kidney injury. *Curr. Opin. Crit. Care* **2005**, *11*, 555–565.
79. Jang, K.-J.; Mehr, A.P.; Hamilton, G.A.; McPartlin, L.A.; Chung, S.; Suh, K.-Y.; Ingber, D.E. Human kidney proximal tubule-on-a-chip for drug transport and nephrotoxicity assessment. *Integr. Biol. (Camb)*. **2013**, *5*, 1119–29.
80. Hansell, P.; Welch, W.J.; Blantz, R.C.; Palm, F. Determinants of kidney oxygen consumption and their relationship to tissue oxygen tension in diabetes and hypertension. *Clin. Exp. Pharmacol. Physiol.* **2013**, *40*, 123–137.
81. Yasotharan, S.; Pinto, S.; Sled, J.G.; Bolz, S.S.; Günther, A. Artery-on-a-chip platform for automated, multimodal assessment of cerebral blood vessel structure and function. *Lab Chip* **2015**, *15*, 2660–2669.
82. Verneti, L.; Gough, A.; Baetz, N.; Blutt, S.; Broughman, J.R.; Brown, J.A.; Foulke-Abel, J.; Hasan, N.; In, J.; Kelly, E.; et al. Functional Coupling of Human Microphysiology Systems: Intestine, Liver, Kidney Proximal Tubule, Blood-Brain Barrier and Skeletal Muscle. *Sci. Rep.* **2017**, *7*.
83. Maschmeyer, I.; Lorenz, A.K.; Schimek, K.; Hasenberg, T.; Ramme, A.P.; Hübner, J.; Lindner, M.; Drewell, C.; Bauer, S.; Thomas, A.; et al. A four-organ-chip for interconnected long-term co-culture of human intestine, liver, skin and kidney equivalents. *Lab Chip* **2015**, *15*, 2688–2699.
84. Jang, K.-J.; Suh, K.-Y. A multi-layer microfluidic device for efficient culture and analysis of renal tubular cells. *Lab Chip* **2010**, *10*, 36–42.
85. Zhou, M.; Zhang, X.; Wen, X.; Wu, T.; Wang, W.; Yang, M.; Wang, J.; Fang, M.; Lin, B.; Lin, H. Development of a Functional Glomerulus at the Organ Level on a Chip to Mimic Hypertensive Nephropathy. *Sci. Rep.* **2016**, *6*, 31771.
86. Wang, L.; Tao, T.; Su, W.; Yu, H.; Yu, Y.; Qin, J. A disease model of diabetic nephropathy in a glomerulus-on-a-chip microdevice. *Lab Chip* **2017**, *17*, 1749–1760.

87. Musah, S.; Mammoto, A.; Ferrante, T.C.; Jeanty, S.S.F.; Hirano-Kobayashi, M.; Mammoto, T.; Roberts, K.; Chung, S.; Novak, R.; Ingram, M.; et al. Mature induced-pluripotent-stem-cell-derived human podocytes reconstitute kidney glomerular-capillary-wall function on a chip. *Nat. Biomed. Eng.* **2017**, *1*.

4. Therapeutic potential of extracellular vesicles derived from mesenchymal stem cells.

In the last decade, the therapeutic potential of extracellular vesicles derived from mesenchymal stromal cells (MSC-EVs) is gaining increasing interest. To introduce the topic, fundamental for my thesis project, here is a review that aims to explore the therapeutic effects of MSC-EVs in the field of solid organ transplantations. The notions provided by the text, from biogenesis, to classification, to their immunosuppressive and regenerative role, lay the foundations for the testing of MSC-EVs as therapeutic molecules against acute renal damage in the dynamic glomerulus *in vitro*, as will be explained later in this thesis work.

Review

Potential Applications of Extracellular Vesicles in Solid Organ Transplantation

Cristina Grange ¹, Linda Bellucci ², Benedetta Bussolati ^{2,*} and Andrea Ranghino ^{1,3}

¹ Department of Medical Sciences, University of Turin, 10126 Turin, Italy; cristina.grange@unito.it (C.G.); andrea.ranghino@unito.it (A.R.)

² Department of Molecular Biotechnology and Health Sciences, University of Turin; 10126 Turin, Italy; linda.bellucci@unito.it

³ SOD Nefrologia, Dialisi e Trapianto Rene, AOU Ospedali Riuniti, 60126 Ancona, Italy

* Correspondence: benedetta.bussolati@unito.it; Tel.: +39-011-6706453; Fax: +39-011-6631184

Received: 17 December 2019; Accepted: 5 February 2020; Published: 5 February 2020



Abstract: Extracellular vesicles (EVs) play an important role in cell-to-cell communication by delivering coding and non-coding RNA species and proteins to target cells. Recently, the therapeutic potential of EVs has been shown to extend to the field of solid organ transplantations. Mesenchymal stromal cell-derived EVs (MSC-EVs) in particular have been proposed as a new tool to improve graft survival, thanks to the modulation of tolerance toward the graft, and to their anti-fibrotic and pro-angiogenic effects. Moreover, MSC-EVs may reduce ischemia reperfusion injury, improving the recovery from acute damage. In addition, EVs currently considered helpful tools for preserving donor organs when administered before transplant in the context of hypothermic or normothermic perfusion machines. The addition of EVs to the perfusion solution, recently proposed for kidney, lung, and liver grafts, resulted in the amelioration of donor organ viability and functionality. EVs may therefore be of therapeutic interest in different aspects of the transplantation process for increasing the number of available organs and improving their long-term survival.

Keywords: exosomes; regenerative medicine; machinery perfusion; transplant; preconditioning

1. Introduction

Solid organ transplantation represents the gold standard treatment for patients with end-stage organ failure. Specifically, kidney transplantation has become a routine procedure because of its beneficial effects on patient survival and quality of life, together with its economic aspects [1]. Although the global observatory on donation and transplantation reported a total of 139,024 solid organ transplants worldwide with 90,306 kidneys in 2017, this met less than 10% of the global need [2]. Data from Eurotransplant [3], NHS-UK [4], and US registries [5] show that 141,568 patients are waiting for a transplant, 82% of which are kidney transplants. Therefore, the gap existing between the need for transplants and organ availability represents a major challenge to be addressed by scientific community [6]. To reduce this gap, novel strategies have to be explored. The main option being explored at present is the increase of the pool of deceased donors, including donors after circulatory death (DCDs), which actually represent about 20% of the deceased donors worldwide, and older donors with comorbidities such as hypertension, mild renal impairment, and death from cerebrovascular events (extended criteria donors, ECDs) [7]. Nevertheless, organs from DCDs and ECDs are more prone to developing an ischemic-reperfusion injury (IRI) compared to standard donors, and consequently represent an increased risk of primary non-function and delayed graft function (DGF) [8]. In addition, long-term graft survival is still a critical factor that needs to be improved.

Among the different strategies in regenerative medicine, EVs have been recently recognized as a promising and innovative tool with which to accelerate tissue recovery after organ damage. EVs are a heterogeneous group of membranous vesicles that possess a central role in the mechanisms of cell-to-cell communication [9,10]. In the last decade, interest and knowledge in the field of EVs has increased enormously, and it is now well established that EVs may influence the function of target cells by transferring bioactive molecules and genetic materials, inducing epigenetic changes in recipient cells [11–13].

In this review, we present the current literature regarding the potential application of stem-cell-derived EVs, dissecting their possible application as an innovative therapeutic tool to precondition grafts before transplant as well as to prevent ischemic/reperfusion damage (Figure 1). In particular, we describe their use in pre-transplant solid organ preservation in association with normothermic and hypothermic perfusion machines. In addition, their role in the limitation of IRI is highlighted for kidney, liver, lung, and heart. Finally, we present their immunomodulatory properties in bone marrow transplantation.

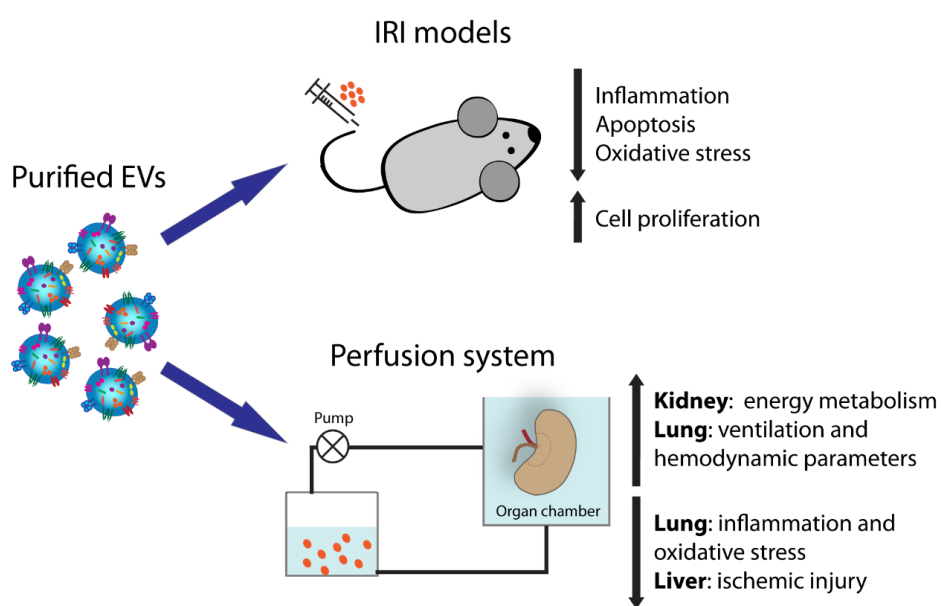


Figure 1. Extracellular vesicle (EV) activities in solid organ transplantation.

2. Stem-Cell-Derived EVs and Regenerative Medicine

EVs released by healthy cells are very heterogeneous in size and composition, and they can be classified based on their origin and dimension into two main categories: small EVs, ranging between 30 and 100 nm, and large EVs, ranging between 50 and 1000 nm [14].

Among small EVs, exosomes are the most characterized vesicles, considered to originate from multivesicular bodies after their fusion with the cell membrane [15]. However, other subtypes of small EVs different from the multivesicular-body-derived exosomes have been identified, for instance after plasma membrane budding [14].

Large EVs, also called microvesicles/ectosomes, comprise different populations of vesicles originating from the budding of the plasma membrane [16]. The different EV populations express common and specific surface markers. For instance, tetraspanins such as CD9, CD81, and CD63 are mainly expressed by small EVs [14]. In addition, small EVs are characterized by the presence of molecules of the endosomal sorting complex required for transport (ESCRT), heat shock proteins (HSP70 and HSP90), and auxiliary proteins (ALIX, TSG101, and VPS4). In terms of variance, large EVs are specifically characterized by expression of the CD40 ligand [17,18]. The detailed composition of EV cargo has been deeply dissected and several databases collecting these results are now available, such as EVpedia [19], Exocarta [20],

and Vesiclepedia [21]. EVs can be isolated from the majority of body fluids such as plasma and serum, amniotic and seminal fluids, saliva, urine, or nasal and bronchial lavage fluids [9,22].

It is important to take into consideration that a limitation to consistent EV characterization is the variability in EV isolation protocols. Depending on the size of EVs and on the fluids of origin, different techniques can be utilized, including ultra-high-speed centrifugation, polymer precipitation, immunoaffinity capture, or microfluidics-based techniques, among others [23]. Rigor criteria for EV isolation and characterization were recently proposed by the International Society for Extracellular Vesicles (ISEV) [14].

Stem-cell-derived EVs possess many characteristics in common with the originating cells; for instance, they carry some transcription factors classically expressed by stem cells, such as Nanog and Oct-4, as well as stem (CD133 and c-Kit) and mesenchymal markers (CD105, CD29, and CD73) [24]. It has been clearly demonstrated that stem-cell-derived EVs recapitulate the pro-regenerative capacity of the cells of origin and, in particular, those derived from mesenchymal stromal cells (MSCs) appear the ideal candidates to favor tissue regeneration. MSC-EVs may be isolated from MSCs derived from different adult tissues such as bone marrow, peripheral and cord blood, adipose tissue, or neonatal birth-associated tissues including placenta and umbilical cord [25]. Several studies have shown that MSC-EVs possess strong pro-regenerative properties using preclinical models of renal, lung, liver, and heart injuries, mimicking the beneficial effect of the cells themselves [14,26,27]. The activity of EVs mainly results in the reduction of apoptosis, oxidative stress, and inflammation and in increase of cell proliferation [24,28,29].

3. Normothermic and Hypothermic Perfusion Machines

In order to increase the number of successful transplants, the use of machine perfusion is currently proposed to ameliorate the function of organs from marginal donors such as DCDs and ECDs. Dynamic perfusion of organs appears a useful strategy to evaluate pretransplant graft function, limiting the discard rate [30–32]. Moreover, this approach reduces the incidence of DGF in recipients receiving organs from ECDs and DCDs.

At present, dynamic machine perfusion can be done in hypothermic (HMP) or in normothermic (NMP) conditions with or without oxygen. Several studies have demonstrated that both HPM and NPM are useful in the assessment of organ viability prior to transplantation [32–34]. Specifically, HMP is able to reduce DGF and to increase the graft survival of organs harvested from ECDs, but conflicting results have been reported on the beneficial effects of HMP on grafts from DCDs [35–40]. Another beneficial effect of HMP is the removal of inflammatory mediators that may have detrimental effects on graft function. The delivery of oxygen added to the hypothermic perfusate may help to restore adenosine triphosphate (ATP) content [41–44]. Because of the unknown effects of this oxygenated perfusion on transplanted patients, a large international randomized controlled trial has been planned to investigate the beneficial effects of oxygenated short-term perfusion of kidneys from ECDs (Consortium for Organ Preservation in Europe COPE Trials) [45].

As oxygenated machine perfusion, NMP may protect organs from IRI by restoring ATP levels [46,47]. In particular, *ex vivo* normothermic perfusion, consisting of circulation through the harvested organs of warm oxygenated red-cell-based solution, is able to restore the metabolism and function of the graft prior to transplantation [48–50]. NMP could offer a better evaluation of organ viability compared to HMP, especially in kidney and liver grafts because of urine or bile production, together with a better preservation of graft function [51].

Both HMP and NMP allow the delivery of targeted therapies to organs prior to transplantation. In particular, these approaches offer the potential to explore the effects of several therapeutic strategies, such as gene-silencing, nanoparticles, and cell therapies, in a fully functioning graft [52–57].

4. EVs for Kidney Transplant

An innovative EV-based application for organ preservation is the use of EVs in the perfusion solution. A first report in the literature recently demonstrated that EVs released by MSCs, delivered in the perfusate during organ cold perfusion (4 h), preserve and protect kidney function. Histological and genetic analyses on EV-treated kidneys revealed upregulation of enzymes involved in energy metabolism and reduction of global ischemic damage. In addition, the analysis of lactate, LDH, and glucose in the effluent fluid confirmed a greater use of energy substrates by EV-treated kidneys, supporting the report of improved functionality (Table 1) [58].

Moreover, an extensive number of publications have highlighted the beneficial effect of EVs in preclinical models of IRI, further implying their possible application to limit organ damage [9]. In particular, EVs isolated from different MSC sources [59–62] have been shown to accelerate renal recovery after damage, promoting cell proliferation and blocking inflammation and apoptosis when intravenously injected after IR damage [63]. The mechanisms of action reported appear different between the EV sources: MSC-EVs obtained from Wharton’s jelly stimulate tubular proliferation and reduce inflammation and apoptosis via mitochondrial protection [61,62], while those from cord blood promote tubular dedifferentiation and proliferation by the transfer of human HGF [60]. Moreover, EVs isolated from bone marrow MSCs were protective mainly by suppressing inflammation when injected under the renal capsule [64]. In addition, EVs obtained from MSCs isolated from glomeruli have also been demonstrated to be capable of reducing ischemic damage [65].

Moreover, a recent publication demonstrated that EVs isolated from the venal perfusate of rats subjected to remote ischemia preconditioning ameliorated renal function when injected into another animal with IRI. To explore the underlying mechanism, authors tested *in vivo*, in the same IRI model, the effect of EVs released by human proximal tubular cells cultured in hypoxia, supporting the thesis that remote ischemia precondition activates a repairing program into tubular cells by the release of pro-regenerative EVs [66].

Whereas all the studies mentioned above evaluated classical ischemic damage in models of renal artery clamping, Wu and co-workers tested for the first time the effect of EVs in a rat model of IRI after DCD renal transplantation [67]. The authors confirmed that Wharton’s jelly MSC-EVs, intravenously injected after renal transplantation, mitigated renal damage, improving survival and function. In particular, MSC-EVs were shown to reduce cell apoptosis and inflammation, to stimulate HGF production, and subsequently to alleviate fibrosis [67].

Table 1. List of EV applications for organ preconditioning. Abbreviations: bone marrow (BM), human liver stem cells (HLSCs).

Organs	EV Sources	Type of Perfusion	Time of Preconditioning	Results	References
Kidney	BM-MSCs	Hypothermic	4 h	Preservation and protection	Gregorini et al. [58]
Lung	BM-MSCs	Normothermic	6 h	Improvement of ventilation and hemodynamic parameters	Gennai et al. [68]
Lung	BM-MSCs	Normothermic	6 h	Restoring permeability and reduction of inflammation	Park et al. [69]
Lung	BM-MSCs	Normothermic	1 h	Attenuation of IR dysfunction and immunomodulation	Stone et al. [70]
Lung	BM-MSCs	Normothermic	3 h	Reduction of inflammation and oxidative stress	Lonati et al. [71]
Liver	HLSCs	Normothermic	4 h	Limitation of the progression of ischemic injury	Rigo et al. [72]

5. EVs for Lung Transplantation

Adult lung transplantation is considered the most effective strategy for end-stage pulmonary disease, although the reported 5-year survival rate is only 50% [73]. Infections, immunomodulation, and IRI are in fact some of the aspects involved in lung transplant failure [74]. Through *ex vivo* lung perfusion, donor lungs can be evaluated and reconditioned, while organs are perfused and ventilated [75].

The use of MSC-EVs has been proposed as a valid alternative for the rehabilitation of marginal human lungs [68]. Upon administering MSC-EVs in the perfusion fluid, a dose-dependent increase of alveolar fluid clearance, a decrease of lung weight gain, and an improvement of airway and hemodynamic parameters were observed as compared to perfusion alone (Table 2). Moreover, the study showed that CD44 was involved in the EV uptake mechanism, as the efficacy of MSC-EVs decreased with the administration of anti-CD44 antibody.

A significant improvement of inflammatory conditions has also been ascribed to the EV effect on lung bacterial infections. For example, MSC-EVs have been demonstrated to be effective in restoring lung protein permeability and reducing inflammation in *Escherichia-coli*-endotoxin-induced acute lung injury in mice. In particular, MSC-EV treatment restored protein permeability and reduced inflammation, extravascular lung water, and total protein levels in the bronchoalveolar lavage fluid, demonstrating a reduction in pulmonary edema [76]. On this path, in a recent work, the effects of MSC-EVs were investigated in an ex vivo perfused human lung model, injured with severe *E. coli* pneumonia [69]. The paper confirmed a significant increase of alveolar fluid clearance and decrease in protein permeability, as well as the lowering of the bacterial load and the neutrophil count in the injured alveolus (Table 2). MSC pretreatment with a toll-like-receptor 3 agonist before the isolation of EVs increased their bactericidal activity.

Moreover, Stone and colleagues demonstrated the attenuation of IR dysfunction in lungs after treatment with MSC-EVs both in vivo and in ex vivo perfusion systems [70]. In particular, they observed a decrease of pro-inflammatory cytokines and upregulation of keratinocyte growth factor, PGE2, and IL-10. Recently, in a mouse model of ex vivo lung perfusion, EV-treated organs showed decreased vascular resistance and a rise of perfusate nitric oxide metabolites. Moreover, EV treatment prevented the reduction in pulmonary ATP and increased the medium–high-molecular-weight hyaluronan in the perfusate. The genes modulated in the pulmonary tissue by EV administration were involved in anti-inflammatory and anti-oxidative stress pathways [71].

6. EVs for Liver Transplantation

The use of EVs released by stem cells as an innovative option to improve the viability of pre-transplant livers was recently assessed in a model of ex vivo rat liver NMP. HLSC-EVs (EVs isolated from human liver stem cells) were added to perfusate 15 min after the initiation of NMP and administered for 4 h within the perfusate. The results showed that HLSC-EVs limited the progression of ischemic injury, with a significant reduction of the levels of aspartate aminotransferase and alanine aminotransferase and a decrease of histological damage compared with results of NMP alone (Table 2) [72]. Moreover, the authors demonstrated that HLSC-EVs were uptaken by hepatocytes, supporting the thesis that EVs may recondition liver cells before transplantation [72].

Moreover, the potential therapeutic use of stem-cell-derived-EVs for liver regeneration, has been also clearly demonstrated in pre-clinical models of liver IRI. In fact, hepatic ischemia and related inflammation should be limited to avoid complication after liver transplantation [77]. The intravenous injection of murine MSC-EVs prior to IRI reduced the area of necrosis and apoptosis with concomitant increased liver function [77]. In addition, MSC-EVs have been shown to limit liver inflammation and oxidative stress [77]. Similar results were obtained using EVs isolated from MSCs from inducible pluripotent stem cells [78] or bone marrow [79]. Recently, Yao et al. demonstrated that human umbilical cord MSC-EVs protect hepatic apoptosis post-IRI, modulating neutrophils and reducing oxidative stress [80].

7. Stem-Cell-Derived EVs as Future Therapeutics in Heart Transplantation

EVs have been shown to be powerful allies against cardiovascular damage. Some important interconnected effects related to EVs could improve the success of a heart transplantation, including immunomodulatory properties, the improvement of heart function and vessel formation, and the amelioration of myocardial function during IRI [81].

Much evidence confirms the hypothesis that cardiac progenitor cells release pro-regenerative and anti-fibrotic EVs in response to hypoxic conditions [82,83], mainly due to their miRNA cargo [82]. Moreover, cardiac-progenitor-cell-derived EVs, released into their environment, can stimulate migration of endothelial cells [84] and inhibit both cardiac fibroblast activation and collagen synthesis [85].

In parallel, MSC-EV treatment has also been proven as a therapeutic option to limit ischemic damage in the heart. In particular, MSC-EV administration increased phosphorylated-Akt and phosphorylated-GSK-3 β , as well as ATP/NADH level, and could reduce phosphorylated-c-JNK and inflammatory response in ischemic/reperfused hearts [86].

8. EVs for Islet Transplantation

Today, there are still many factors that limit the success of pancreatic islet transplantation, including islet source limitation, sub-optimal engraftment, lack of oxygen and blood supply for transplanted islets, and immune rejection [87]. In parallel with the other described organs, MSC-EVs may also be of benefit for islet transplantation.

One of the primary reasons for apoptosis and reduced beta-cell function in transplants is hypoxic damage. Recently, EVs from human-umbilical-cord-derived MSCs were shown to have a therapeutic effect on the survival and function of neonatal porcine islets exposed to hypoxia [88]. The use of EVs, in comparison with medium alone, enhanced the yield and survival of porcine islets, and showed an improvement of the function through the amelioration of mitochondrial respiration efficiency [88].

In addition, Di Wen and colleagues showed that MSC-EV administration through delivery of small RNAs promoted islet function and inhibited immune rejection [89]. In a mouse model, they used MSC-EVs transfected with shFas and anti-miR-375 in order to silence Fas and miR-375 in human islets, observing an improvement of islet viability and function. Moreover, the authors observed the inhibition of peripheral blood mononuclear cell proliferation and the enhancement of T-cell regulatory function. Based on these works, EVs from different sources appear of interest to increase the possibility of successful islet transplantation.

9. Role of MSC-EVs in the Amelioration of Graft Versus Host Disease

EVs derived from bone marrow MSCs possess an immunosuppressive potential that can be harnessed to treat graft versus host disease (GVHD), which today represents the greatest complication after allogeneic transplantation. The majority of the literature on the subject has generically focused on the effects of the whole MSC secretome, including EVs and soluble factors. Recently, the specific role of EVs has been highlighted, showing an effect on innate and adaptive immunity (Table 2).

For example, in 2005, Aggarwal and Pittenger highlighted that the secretome, released by MSCs, be responsible for modulation of immune reaction, involved in GVHD [90]. In fact, if co-cultured with purified subpopulations of immune cells, human MSCs were able to switch an inflammatory response into a tolerant phenotype. In particular, MSCs induced mature dendritic cells type 1 and type 2 to decrease TNF- α and to increase IL-10 secretion, respectively; they also induced T helper 1 lymphocytes and natural killer cells to decrease interferon (IFN) γ secretion. In addition, they enhanced a regulatory response, causing the T helper 2 cells to increase secretion of IL-4, increasing the proportion of regulatory T cells and producing prostaglandin (PG) E₂ [90].

Moreover, soluble factors released by MSCs, such as vascular endothelial growth factor and IL-6, were shown to inhibit T-cell proliferation and to be involved in a partial inhibition of dendritic cell differentiation [91]. Selmani et al. not only confirmed the role of the MSC secretome in modulating innate immunity, but they also sustained its strong modulation of adaptive immunity [92]. Moreover, they reported that the nonclassic HLA class I molecule HLA-G is responsible for the immunomodulatory properties of MSCs [92].

In a recent work, it was shown that bone marrow MSC-EVs recapitulate the therapeutic effects of the cells against acute GVHD [93]. A systemic infusion of MSC-EVs in mice with acute GVHD was associated with the suppression of CD4⁺ and CD8⁺ T cells and with the preservation of circulating

naive T cells, possibly due to the unique microRNA profiles of MSC-EVs. The analysis on microRNA cargo in MSC-EVs identified that their target genes were involved in regulation of the cell cycle, T-cell receptor signaling, and GVHD [93]. These findings suggest that MSC-EVs could be a new potential therapeutic option to prevent GVHD, to be tested in future clinical trials.

Table 2. Immunomodulatory properties of MSC secretome/EVs.

Cell Types	Actions	Mechanisms	Effector	References
T lymphocytes	Decrease of TH1 secretion of IFN- γ [91] Increase of TH2 secretion of IL-4 [91] Increase of the proportion of T-regs [91] Suppression of T-naïve differentiation [94] Decrease in proliferation and migration [94] Decrease of CD4 ⁺ CD8 ⁺ [94]	Constitutive production of COX2 and PGE2 [91–93] Secretion of TGF- β [91] Secretion of soluble HLA-G5 [93]	Secretome [91–93] EVs [94]	S. Aggarwal et al. [91] Z.Selmani et al. [93] S. Fujii et al. [94]
DC	Reversion of maturation of DCs [92] Decrease DC1 production of TNF- α [91] Increase DC2 production of IL-10 [91]	Secretion of IL-6 [91]	Secretome [91,92]	S. Aggarwal et al. [91] F. Djouad et al. [92]
NK	Inhibition [91] Alteration of secreted cytokines [91]	Secretion of indoleamine 2,3-deoxygenase [91] Secretion of PGE2 [91] Secretion of TGF- β [91]	Secretome [91]	S. Aggarwal et al. [91]

10. Conclusions

The organ demand is continuously increasing and there is a constant need to expand the pool of donors. Increasing organ availability represents a major challenge in the field of transplantation.

Among the most recent innovative strategies, the use of EVs seems very promising. The application of EVs in the perfusion solution, recently proposed for kidney, lung, and liver grafts, results in the amelioration of donor organ viability and functionality. Moreover, consolidated results describe the beneficial effects of EV administration in several preclinical models of IRI. In particular, stem-cell-derived EVs have displayed strong pro-regenerative properties in different models of renal, lung, liver, and heart injuries. IRI is an unavoidable consequence after transplants and the severity of this phenomenon affects the graft outcome, leading to delayed graft function, graft rejection, chronic rejection, and chronic graft dysfunction. The development of strategies to limit the progression of IRI is fundamental for the success of transplants. Altogether, EVs appear the ideal candidate to target different aspects during transplantation process.

Author Contributions: Writing—original draft preparation, A.R., C.G., L.B. and B.B.; writing—review and editing, L.B., C.G. and B.B.; funding acquisition, B.B. All authors have read and agreed to the published version of the manuscript.

Funding: This research was funded by, Regione Piemonte POR FESR 2014/2020—Grant “Bando Piattaforma Tecnologica Salute e Benessere”, Project “Terapie Avanzate per Processi Fibrotici Cronici (EVER)”.

Conflicts of Interest: The authors declare no conflict of interest.

References

1. Wolfe, R.A.; Ashby, V.B.; Milford, E.L.; Ojo, A.O.; Ettenger, R.E.; Agodoa, L.Y.C.; Held, P.J.; Port, F.K. Comparison of mortality in all patients on dialysis, patients on dialysis awaiting transplantation, and recipients of a first cadaveric transplant. *N. Engl. J. Med.* **1999**, *341*, 1725–1730. [CrossRef] [PubMed]
2. 2017 Global Report—GODT. Available online: <http://www.transplant-observatory.org/download/2017-activity-data-report/> (accessed on 2 December 2019).

3. Branger, P.; Undine, S. *Eurotransplant Annual Report 2018*. 2018. Available online: <https://www.eurotransplant.org/organs/kidney/> (accessed on 5 February 2020).
4. NHS Organ Donation and Transplantation Activity Report 2018/19. 2019. Available online: <https://www.organdonation.nhs.uk/helping-you-to-decide/about-organ-donation/statistics-about-organ-donation/transplant-activity-report/> (accessed on 5 February 2020).
5. Hart, A.; Smith, J.M.; Skeans, M.A.; Gustafson, S.K.; Wilk, A.R.; Castro, S.; Robinson, A.; Wainright, J.L.; Snyder, J.J.; Kasiske, B.L.; et al. OPTN/SRTR 2017 Annual Data Report: Kidney. *Am. J. Transplant.* **2019**, *19*, 19–123. [[CrossRef](#)] [[PubMed](#)]
6. Abramowicz, D.; Oberbauer, R.; Heemann, U.; Viklicky, O.; Peruzzi, L.; Mariat, C.; Crespo, M.; Budde, K.; Oniscu, G.C. Recent advances in kidney transplantation: A viewpoint from the Descartes advisory board. *Nephrol. Dial. Transplant.* **2018**, *33*, 1699–1707. [[CrossRef](#)] [[PubMed](#)]
7. Sørensen, S.S. Rates of renal transplantations in the elderly—data from Europe and the US. *Transplant. Rev.* **2015**, *29*, 193–196. [[CrossRef](#)]
8. Nashan, B.; Abbud-Filho, M.; Citterio, F. Prediction, prevention, and management of delayed graft function: Where are we now? *Clin. Transplant.* **2016**, *30*, 1198–1208. [[CrossRef](#)]
9. Grange, C.; Skovronova, R.; Marabese, F.; Bussolati, B. Stem Cell-Derived Extracellular Vesicles and Kidney Regeneration. *Cells* **2019**, *8*, 1240. [[CrossRef](#)]
10. Quesenberry, P.J.; Aliotta, J.; Deregibus, M.C.; Camussi, G. Role of extracellular RNA-carrying vesicles in cell differentiation and reprogramming. *Stem Cell Res. Ther.* **2015**, *6*, 1–10. [[CrossRef](#)]
11. Valadi, H.; Ekström, K.; Bossios, A.; Sjöstrand, M.; Lee, J.J.; Lötvall, J.O. Exosome-mediated transfer of mRNAs and microRNAs is a novel mechanism of genetic exchange between cells. *Nat. Cell Biol.* **2007**, *9*, 654–659. [[CrossRef](#)]
12. Ratajczak, M.Z.; Ratajczak, J. Horizontal transfer of RNA and proteins between cells by extracellular microvesicles: 14 years later. *Clin. Transl. Med.* **2016**, *5*. [[CrossRef](#)]
13. Deregibus, M.C.; Cantaluppi, V.; Calogero, R.; Lo Iacono, M.; Tetta, C.; Biancone, L.; Bruno, S.; Bussolati, B.; Camussi, G. Endothelial progenitor cell—Derived microvesicles activate an angiogenic program in endothelial cells by a horizontal transfer of mRNA. *Blood* **2007**, *110*, 2440–2448. [[CrossRef](#)]
14. Théry, C.; Witwer, K.W.; Aikawa, E.; Alcaraz, M.J.; Anderson, J.D.; Andriantsitohaina, R.; Antoniou, A.; Arab, T.; Archer, F.; Atkin-Smith, G.K.; et al. Minimal information for studies of extracellular vesicles 2018 (MISEV2018): A position statement of the International Society for Extracellular Vesicles and update of the MISEV2014 guidelines. *J. Extracell. Vesicles* **2018**, *7*, 1535750. [[CrossRef](#)] [[PubMed](#)]
15. Mathivanan, S.; Ji, H.; Simpson, R.J. Exosomes: Extracellular organelles important in intercellular communication. *J. Proteomics* **2010**, *73*, 1907–1920. [[CrossRef](#)] [[PubMed](#)]
16. van der Pol, E.; Böing, A.N.; Harrison, P.; Sturk, A.; Nieuwland, R. Classification, functions, and clinical relevance of extracellular vesicles. *Pharmacol. Rev.* **2012**, *64*, 676–705. [[CrossRef](#)] [[PubMed](#)]
17. Mobarrez, F.; Sjövik, C.; Soop, A.; Hållström, L.; Frostell, C.; Pisetsky, D.S.; Wallén, H. CD40L expression in plasma of volunteers following LPS administration: A comparison between assay of CD40L on platelet microvesicles and soluble CD40L. *Platelets* **2015**, *26*, 486–490. [[CrossRef](#)] [[PubMed](#)]
18. Jeppesen, D.K.; Fenix, A.M.; Franklin, J.L.; Higginbotham, J.N.; Zhang, Q.; Zimmerman, L.J.; Liebler, D.C.; Ping, J.; Liu, Q.; Evans, R.; et al. Reassessment of Exosome Composition. *Cell* **2019**, *177*, 428–445.e18. [[CrossRef](#)] [[PubMed](#)]
19. Kim, D.K.; Kang, B.; Kim, O.Y.; Choi, D.S.; Lee, J.; Kim, S.R.; Go, G.; Yoon, Y.J.; Kim, J.H.; Jang, S.C.; et al. EVpedia: An integrated database of high-throughput data for systemic analyses of extracellular vesicles. *J. Extracell. Vesicles* **2013**, *2*, 1–7. [[CrossRef](#)]
20. Mathivanan, S.; Fahner, C.J.; Reid, G.E.; Simpson, R.J. ExoCarta 2012: Database of exosomal proteins, RNA and lipids. *Nucleic Acids Res.* **2012**, *40*, D1241–4. [[CrossRef](#)]
21. Kalra, H.; Simpson, R.J.; Ji, H.; Aikawa, E.; Altevogt, P.; Askenase, P.; Bond, V.C.; Borràs, F.E.; Breakefield, X.; Budnik, V.; et al. Vesiclepedia: A Compendium for Extracellular Vesicles with Continuous Community Annotation. *PLoS Biol.* **2012**, *10*, 8–12. [[CrossRef](#)] [[PubMed](#)]
22. Keller, S.; Ridinger, J.; Rupp, A.K.; Janssen, J.W.G.; Altevogt, P. Body fluid derived exosomes as a novel template for clinical diagnostics. *J. Transl. Med.* **2011**, *9*, 86. [[CrossRef](#)]

23. Yang, X.-X.; Sun, C.; Wang, L.; Guo, X.-L. New insight into isolation, identification techniques and medical applications of exosomes. *J. Control. Release* **2019**, *308*, 119–129. [[CrossRef](#)]
24. Bruno, S.; Chiabotto, G.; Favaro, E.; Deregibus, M.C.; Camussi, G. Role of extracellular vesicles in stem cell biology. *Am. J. Physiol. Cell Physiol.* **2019**, *317*, C303–C313. [[CrossRef](#)] [[PubMed](#)]
25. Grange, C.; Tritta, S.; Tapparo, M.; Cedrino, M.; Tetta, C.; Camussi, G.; Brizzi, M.F. Stem cell-derived extracellular vesicles inhibit and revert fibrosis progression in a mouse model of diabetic nephropathy. *Sci. Rep.* **2019**, *9*, 4468. [[CrossRef](#)] [[PubMed](#)]
26. Heldring, N.; Mäger, I.; Wood, M.J.A.; Le Blanc, K.; Andaloussi, S.E.L. Therapeutic Potential of Multipotent Mesenchymal Stromal Cells and Their Extracellular Vesicles. *Hum. Gene Ther.* **2015**, *26*, 506–517. [[CrossRef](#)]
27. Ferreira, J.R.; Teixeira, G.Q.; Santos, S.G.; Barbosa, M.A.; Almeida-Porada, G.; Gonçalves, R.M. Mesenchymal Stromal Cell Secretome: Influencing Therapeutic Potential by Cellular Pre-conditioning. *Front. Immunol.* **2018**, *9*, 2837. [[CrossRef](#)]
28. Collino, F.; Bruno, S.; Incarnato, D.; Dettori, D.; Neri, F.; Provero, P.; Pomatto, M.; Oliviero, S.; Tetta, C.; Quesenberry, P.J.; et al. AKI recovery induced by mesenchymal stromal cell-derived extracellular vesicles carrying micRNAs. *J. Am. Soc. Nephrol.* **2015**, *26*, 2349–2360. [[CrossRef](#)] [[PubMed](#)]
29. György, B.; Szabó, T.G.; Pásztói, M.; Pál, Z.; Misják, P.; Aradi, B.; László, V.; Pállinger, É.; Pap, E.; Kittel, Á.; et al. Membrane vesicles, current state-of-the-art: Emerging role of extracellular vesicles. *Cell. Mol. Life Sci.* **2011**, *68*, 2667–2688. [[CrossRef](#)]
30. Matsuno, N.; Konno, O.; Mejit, A.; Jyojima, Y.; Akashi, I.; Nakamura, Y.; Iwamoto, H.; Hama, K.; Iwahori, T.; Ashizawa, T.; et al. Application of machine perfusion preservation as a viability test for marginal kidney graft. *Transplantation* **2006**, *82*, 1425–1428. [[CrossRef](#)]
31. Bissolati, M.; Gazzetta, P.G.; Caldara, R.; Guarneri, G.; Adamenko, O.; Giannone, F.; Mazza, M.; Maggi, G.; Tomanin, D.; Rosati, R.; et al. Renal Resistance Trend during Hypothermic Machine Perfusion Is More Predictive of Postoperative Outcome Than Biopsy Score: Preliminary Experience in 35 Consecutive Kidney Transplantations. *Artif. Organs* **2018**, *42*, 714–722. [[CrossRef](#)]
32. Gelpi, R.; Paredes, D.; Rodríguez-Villar, C.; Roque, R.; Ruiz, A.; Adalia, R.; Peri-Cusí, L.; Sole, M.; Oppenheimer, F.; Diekmann, F. The development of a predictive model of graft function in uncontrolled donors after circulatory death: Validity of a pulsatile renal preservation machine cut-off value for kidney acceptance. *Nephrol. Dial. Transplant.* **2019**, *34*, 531–538. [[CrossRef](#)]
33. Hameed, A.M.; Pleass, H.C.; Wong, G.; Hawthorne, W.J. Maximizing kidneys for transplantation using machine perfusion: From the past to the future: A comprehensive systematic review and meta-analysis. *Medicine* **2016**, *95*, e5083. [[CrossRef](#)]
34. Brat, A.; Pol, R.A.; Leuvenink, H.G.D. Novel preservation methods to increase the quality of older kidneys. *Curr. Opin. Organ Transplant.* **2015**, *20*, 438–443. [[CrossRef](#)] [[PubMed](#)]
35. Gallinat, A.; Moers, C.; Smits, J.M.; Strelniece, A.; Pirenne, J.; Ploeg, R.J.; Paul, A.; Treckmann, J. Machine perfusion versus static cold storage in expanded criteria donor kidney transplantation: 3-year follow-up data. *Transpl. Int.* **2013**, *26*, 52–53. [[CrossRef](#)] [[PubMed](#)]
36. Ali, F.; Dua, A.; Cronin, D.C. Changing paradigms in organ preservation and resuscitation. *Curr. Opin. Organ Transplant.* **2015**, *20*, 152–158. [[CrossRef](#)] [[PubMed](#)]
37. Matos, A.C.C.; Requião Moura, L.R.; Borrelli, M.; Nogueira, M.; Clarizia, G.; Ongaro, P.; Durão, M.S.; Pacheco-Silva, A. Impact of machine perfusion after long static cold storage on delayed graft function incidence and duration and time to hospital discharge. *Clin. Transplant.* **2018**, *32*. [[CrossRef](#)] [[PubMed](#)]
38. Tedesco-Silva, H.; Mello Offerri, J.C.; Ayres Carneiro, V.; Ivani de Paula, M.; Neto, E.D.; Brambate Carvalhinho Lemos, F.; Requião Moura, L.R.; Pacheco e Silva Filho, A.; de Moraes Cunha, M.d.F.; Francisco da Silva, E.; et al. Randomized Trial of Machine Perfusion Versus Cold Storage in Recipients of Deceased Donor Kidney Transplants with High Incidence of Delayed Graft Function. *Transplant. Direct* **2017**, *3*, e155. [[CrossRef](#)] [[PubMed](#)]
39. Delsuc, C.; Faure, A.; Berthiller, J.; Dorez, D.; Matillon, X.; Meas-Yedid, V.; Floccard, B.; Marcotte, G.; Labeye, V.; Rabeyrin, M.; et al. Uncontrolled donation after circulatory death: Comparison of two kidney preservation protocols on graft outcomes. *BMC Nephrol.* **2018**, *19*, 1–9. [[CrossRef](#)] [[PubMed](#)]

40. Czigany, Z.; Lurje, I.; Tolba, R.H.; Neumann, U.P.; Tacke, F.; Lurje, G. Machine perfusion for liver transplantation in the era of marginal organs—New kids on the block. *Liver Int.* **2019**, *39*, 228–249. [[CrossRef](#)]
41. Kron, P.; Schlegel, A.; De Rougemont, O.; Oberkofler, C.E.; Clavien, P.A.; Dutkowsky, P. Short, cool, and well oxygenated—HOPE for kidney transplantation in a rodent model. *Ann. Surg.* **2016**, *264*, 815–822. [[CrossRef](#)]
42. Minor, T.; Paul, A. Hypothermic reconditioning in organ transplantation. *Curr. Opin. Organ Transplant.* **2013**, *18*, 161–167. [[CrossRef](#)]
43. Kathis, J.M.; Paul, A.; Robinson, L.A.; Selzner, M. Ex vivo machine perfusion for renal graft preservation. *Transplant. Rev.* **2018**, *32*, 1–9. [[CrossRef](#)]
44. Solhjoui, Z.; Athar, H.; Xu, Q.; Abdi, R. Emerging therapies targeting intra-organ inflammation in transplantation. *Am. J. Transplant.* **2015**, *15*, 305–311. [[CrossRef](#)] [[PubMed](#)]
45. COPE—Trials. Available online: <http://cope-eu.com/workprogramme/trials.html> (accessed on 2 December 2019).
46. Hessheimer, A.J.; Riquelme, F.; Fundora-Suárez, Y.; García Pérez, R.; Fondevila, C. Normothermic perfusion and outcomes after liver transplantation. *Transplant. Rev.* **2019**, *33*, 200–208. [[CrossRef](#)] [[PubMed](#)]
47. Palomo-López, N.; Martín-Sastre, S.; Martín-Villén, L.; Ruiz de Azúa-López, Z.; Solis-Clavijo, D.; Caballero-Gálvez, S.; Carballo-Caro, J.M.; Egea-Guerrero, J.J. Normothermic Regional Perfusion and Donation after Circulatory Death (Controlled and Uncontrolled): Metabolic Differences and Kidney Transplantation Evolution. *Transplant. Proc.* **2019**, *51*, 3044–3046. [[CrossRef](#)] [[PubMed](#)]
48. Hosgood, S.A.; Saeb-Parsy, K.; Wilson, C.; Callaghan, C.; Collett, D.; Nicholson, M.L. Protocol of a randomised controlled, open-label trial of ex vivo normothermic perfusion versus static cold storage in donation after circulatory death renal transplantation. *BMJ Open* **2017**, *7*, 1–7. [[CrossRef](#)] [[PubMed](#)]
49. Hosgood, S.A.; Thompson, E.; Moore, T.; Wilson, C.H.; Nicholson, M.L. Normothermic machine perfusion for the assessment and transplantation of declined human kidneys from donation after circulatory death donors. *Br. J. Surg.* **2018**, *105*, 388–394. [[CrossRef](#)]
50. Laing, R.W.; Mergental, H.; Yap, C.; Kirkham, A.; Whilku, M.; Barton, D.; Curbishley, S.; Boteon, Y.L.; Neil, D.A.; Hübscher, S.G.; et al. Viability testing and transplantation of marginal livers (VITAL) using normothermic machine perfusion: Study protocol for an open-label, non-randomised, prospective, single-arm trial. *BMJ Open* **2017**, *7*, 1–15.
51. Weissenbacher, A.; Hunter, J. Normothermic machine perfusion of the kidney. *Curr. Opin. Organ Transplant.* **2017**, *22*, 571–576. [[CrossRef](#)]
52. Brasile, L.; Stubenitsky, B.M.; Booster, M.H.; Arenada, D.; Haisch, C.; Kootstra, G. Transfection and transgene expression in a human kidney during ex vivo warm perfusion. *Transplant. Proc.* **2002**, *34*, 2624. [[CrossRef](#)]
53. Chen, J.; Braet, F.; Brodsky, S.; Weinstein, T.; Romanov, V.; Noiri, E.; Goligorsky, M.S. VEGF-induced mobilization of caveolae and increase in permeability of endothelial cells. *Am. J. Physiol. Cell Physiol.* **2002**, *282*, C1053–C1063. [[CrossRef](#)]
54. Chen, J.; Vemuri, C.; Palekar, R.U.; Gaut, J.P.; Goette, M.; Hu, L.; Cui, G.; Zhang, H.; Wickline, S.A. Antithrombin nanoparticles improve kidney reperfusion and protect kidney function after ischemia-reperfusion injury. *Am. J. Physiol. Ren. Physiol.* **2015**, *308*, F765–F773. [[CrossRef](#)]
55. DiRito, J.R.; Hosgood, S.A.; Tietjen, G.T.; Nicholson, M.L. The future of marginal kidney repair in the context of normothermic machine perfusion. *Am. J. Transplant.* **2018**, *18*, 2400–2408. [[CrossRef](#)] [[PubMed](#)]
56. Hamaoui, K.; Gowers, S.; Boutelle, M.; Cook, T.H.; Hanna, G.; Darzi, A.; Smith, R.; Dorling, A.; Papalois, V. Organ Pretreatment with Cytotoxic Endothelial Localizing Peptides to Ameliorate Microvascular Thrombosis and Perfusion Deficits in Ex Vivo Renal Hemoreperfusion Models. *Transplantation* **2016**, *100*, e128–e139. [[CrossRef](#)] [[PubMed](#)]
57. Hamaoui, K.; Aftab, A.; Gowers, S.; Boutelle, M.; Cook, T.; Rudd, D.; Dobson, G.P.; Papalois, V. An ex vivo comparison of adenosine and lidocaine solution and University of Wisconsin solution for hypothermic machine perfusion of porcine kidneys: Potential for development. *J. Surg. Res.* **2017**, *208*, 219–229. [[CrossRef](#)] [[PubMed](#)]
58. Gregorini, M.; Corradetti, V.; Francesca, E.; Rocca, C.; Milanesi, S.; Peloso, A.; Canevari, S.; Cecco, L.D.; Dugo, M.; Antonietta, M.; et al. Perfusion of isolated rat kidney with Mesenchymal Stromal Cells/Extracellular Vesicles prevents ischaemic injury MSC viability. *J. Cell Mol. Med.* **2017**, *21*, 3381–3393. [[CrossRef](#)]

59. Gatti, S.; Bruno, S.; Deregibus, M.C.; Sordi, A.; Cantaluppi, V.; Tetta, C.; Camussi, G. Microvesicles derived from human adult mesenchymal stem cells protect against ischaemia-reperfusion-induced acute and chronic kidney injury. *Nephrol. Dial. Transplant.* **2011**, *26*, 1474–1483. [[CrossRef](#)]
60. Gu, D.; Zou, X.; Ju, G.; Zhang, G.; Bao, E.; Zhu, Y. Mesenchymal Stromal Cells Derived Extracellular Vesicles Ameliorate Acute Renal Ischemia Reperfusion Injury by Inhibition of Mitochondrial Fission through MIR-30. *Stem Cells Int.* **2016**, *2016*, 2093940. [[CrossRef](#)]
61. Ju, G.Q.; Cheng, J.; Zhong, L.; Wu, S.; Zou, X.Y.; Zhang, G.Y.; Gu, D.; Miao, S.; Zhu, Y.J.; Sun, J.; et al. Microvesicles derived from human umbilical cord mesenchymal stem cells facilitate tubular epithelial cell dedifferentiation and growth via hepatocyte growth factor induction. *PLoS ONE* **2015**, *10*, e0121534. [[CrossRef](#)]
62. Zou, X.; Zhang, G.; Cheng, Z.; Yin, D.; Du, T.; Ju, G.; Miao, S.; Liu, G.; Lu, M.; Zhu, Y. Microvesicles derived from human Wharton's Jelly mesenchymal stromal cells ameliorate renal ischemia-reperfusion injury in rats by suppressing CX3CL1. *Stem Cell Res. Ther.* **2014**, *5*, 1–13. [[CrossRef](#)]
63. Grange, C.; Iampietro, C.; Bussolati, B. Stem cell extracellular vesicles and kidney injury. *Stem Cell Investig.* **2017**, *4*. [[CrossRef](#)]
64. Shen, B.; Liu, J.; Zhang, F.; Wang, Y.; Qin, Y.; Zhou, Z.; Qiu, J.; Fan, Y. CCR2 Positive Exosome Released by Mesenchymal Stem Cells Suppresses Macrophage Functions and Alleviates Ischemia/Reperfusion-Induced Renal Injury. *Stem Cells Int.* **2016**, *2016*, 1240301. [[CrossRef](#)]
65. Ranghino, A.; Bruno, S.; Bussolati, B.; Moggio, A.; Dimuccio, V.; Tapparo, M.; Biancone, L.; Gontero, P.; Frea, B.; Camussi, G. The effects of glomerular and tubular renal progenitors and derived extracellular vesicles on recovery from acute kidney injury. *Stem Cell Res. Ther.* **2017**, *8*, 1–15. [[CrossRef](#)] [[PubMed](#)]
66. Zhang, G.; Yang, Y.; Huang, Y.; Zhang, L.; Ling, Z.; Zhu, Y.; Wang, F.; Zou, X.; Chen, M. Hypoxia-induced extracellular vesicles mediate protection of remote ischemic preconditioning for renal ischemia-reperfusion injury. *Biomed. Pharmacother.* **2017**, *90*, 473–478. [[CrossRef](#)] [[PubMed](#)]
67. Wu, X.; Yan, T.; Wang, Z.; Wu, X.; Cao, G.; Zhang, C.; Tian, X.; Wang, J. Micro-vesicles derived from human Wharton's Jelly mesenchymal stromal cells mitigate renal ischemia-reperfusion injury in rats after cardiac death renal transplantation. *J. Cell. Biochem.* **2018**, *119*, 1879–1888. [[CrossRef](#)] [[PubMed](#)]
68. Gennai, S.; Monsel, A.; Hao, Q.; Park, J.; Matthay, M.A.; Lee, J.W. Microvesicles Derived from Human Mesenchymal Stem Cells Restore Alveolar Fluid Clearance in Human Lungs Rejected for Transplantation. *Am. J. Transplant.* **2015**, *15*, 2404–2412. [[CrossRef](#)] [[PubMed](#)]
69. Park, J.; Kim, S.; Lim, H.; Liu, A.; Hu, S.; Lee, J.; Zhuo, H.; Hao, Q.; Matthay, M.A.; Lee, J.-W. Therapeutic effects of human mesenchymal stem cell microvesicles in an ex vivo perfused human lung injured with severe *E. coli* pneumonia. *Thorax* **2019**, *74*, 43–50. [[CrossRef](#)] [[PubMed](#)]
70. Stone, M.L.; Zhao, Y.; Smith, J.R.; Weiss, M.L.; Kron, I.L.; Laubach, V.E.; Sharma, A.K. Mesenchymal stromal cell-derived extracellular vesicles attenuate lung ischemia-reperfusion injury and enhance reconditioning of donor lungs after circulatory death. *Respir Res.* **2017**, *18*, 212. [[CrossRef](#)]
71. Lonati, C.; Bassani, G.A.; Brambilla, D.; Leonardi, P.; Carlin, A.; Maggioni, M.; Zanella, A.; Dondossola, D.; Fonsato, V.; Grange, C.; et al. Mesenchymal stem cell-derived extracellular vesicles improve the molecular phenotype of isolated rat lungs during ischemia/reperfusion injury. *J. Heart Lung Transplant.* **2019**, *38*, 1306–1316. [[CrossRef](#)]
72. Rigo, F.; De Stefano, N.; Navarro-Tableros, V.; David, E.; Rizza, G.; Catalano, G.; Gilbo, N.; Maione, F.; Gonella, F.; Roggio, D.; et al. Extracellular Vesicles from Human Liver Stem Cells Reduce Injury in an Ex Vivo Normothermic Hypoxic Rat Liver Perfusion Model. *Transplantation* **2018**, *102*, e205–e210. [[CrossRef](#)]
73. Dipchand, A.I.; Rossano, J.W.; Edwards, L.B.; Kucheryavaya, A.Y.; Benden, C.; Goldfarb, S.; Levvey, B.J.; Lund, L.H.; Meiser, B.; Yusef, R.D.; et al. The Registry of the International Society for Heart and Lung Transplantation: Eighteenth Official Pediatric Heart Transplantation Report—2015; Focus Theme: Early Graft Failure. *J. Heart Lung Transplant.* **2015**, *34*, 1233–1243. [[CrossRef](#)]
74. Krishnam, M.S.; Suh, R.D.; Tomasian, A.; Goldin, J.G.; Lai, C.; Brown, K.; Batra, P.; Aberle, D.R. Postoperative complications of lung transplantation: Radiologic findings along a time continuum. *Radiographics* **2007**, *27*, 957–974. [[CrossRef](#)]
75. Meyer, K.C. Recent advances in lung transplantation. *F1000Research* **2018**, *7*, 1684. [[CrossRef](#)] [[PubMed](#)]

76. Zhu, Y.-G.; Feng, X.-M.; Abbott, J.; Fang, X.-H.; Hao, Q.; Monsel, A.; Qu, J.-M.; Matthay, M.A.; Lee, J.W. Human mesenchymal stem cell microvesicles for treatment of Escherichia coli endotoxin-induced acute lung injury in mice. *Stem Cells* **2014**, *32*, 116–125. [[CrossRef](#)] [[PubMed](#)]
77. Haga, H.; Yan, I.K.; Borelli, D.; Matsuda, A.; Parasramka, M.; Shukla, N.; Lee, D.D.; Patel, T. Extracellular vesicles from bone marrow-derived mesenchymal stem cells protect against murine hepatic ischemia/reperfusion injury. *Liver Transpl.* **2017**, *23*, 791–803. [[CrossRef](#)] [[PubMed](#)]
78. Du, Y.; Li, D.; Han, C.; Wu, H.; Xu, L.; Zhang, M.; Zhang, J.; Chen, X. Exosomes from Human-Induced Pluripotent Stem Cell-Derived Mesenchymal Stromal Cells (hiPSC-MSCs) Protect Liver against Hepatic Ischemia/Reperfusion Injury via Activating Sphingosine Kinase and Sphingosine-1-Phosphate Signaling Pathway. *Cell. Physiol. Biochem.* **2017**, *43*, 611–625. [[CrossRef](#)] [[PubMed](#)]
79. Anger, F.; Camara, M.; Ellinger, E.; Germer, C.T.; Schlegel, N.; Otto, C.; Klein, I. Human Mesenchymal Stromal Cell-Derived Extracellular Vesicles Improve Liver Regeneration after Ischemia Reperfusion Injury in Mice. *Stem Cells Dev.* **2019**, *28*, 1451–1462. [[CrossRef](#)]
80. Yao, J.; Zheng, J.; Cai, J.; Zeng, K.; Zhou, C.; Zhang, J.; Li, S.; Li, H.; Chen, L.; He, L.; et al. Extracellular vesicles derived from human umbilical cord mesenchymal stem cells alleviate rat hepatic ischemia-reperfusion injury by suppressing oxidative stress and neutrophil inflammatory response. *FASEB J.* **2019**, *33*, 1695–1710. [[CrossRef](#)]
81. Nawaz, M.; Fatima, F.; Vallabhaneni, K.C.; Penfornis, P.; Valadi, H.; Ekström, K.; Kholia, S.; Whitt, J.D.; Fernandes, J.D.; Pochampally, R.; et al. Extracellular Vesicles: Evolving Factors in Stem Cell Biology. *Stem Cells Int.* **2016**, *2016*, 1073140. [[CrossRef](#)]
82. Gray, W.D.; French, K.M.; Ghosh-Choudhary, S.; Maxwell, J.T.; Brown, M.E.; Platt, M.O.; Searles, C.D.; Davis, M.E. Identification of therapeutic covariant microRNA clusters in hypoxia-treated cardiac progenitor cell exosomes using systems biology. *Circ. Res.* **2015**, *116*, 255–263. [[CrossRef](#)]
83. Agarwal, U.; George, A.; Bhutani, S.; Ghosh-Choudhary, S.; Maxwell, J.T.; Brown, M.E.; Mehta, Y.; Platt, M.O.; Liang, Y.; Sahoo, S.; et al. Experimental, systems, and computational approaches to understanding the MicroRNA-mediated reparative potential of cardiac progenitor cell-derived exosomes from pediatric patients. *Circ. Res.* **2017**, *120*, 701–712. [[CrossRef](#)]
84. Vrijssen, K.R.; Sluijter, J.P.G.; Schuchardt, M.W.L.; van Balkom, B.W.M.; Noort, W.A.; Chamuleau, S.A.J.; Doevendans, P.A.F.M. Cardiomyocyte progenitor cell-derived exosomes stimulate migration of endothelial cells. *J. Cell. Mol. Med.* **2010**, *14*, 1064–1070. [[CrossRef](#)]
85. Bracco Gartner, T.C.L.; Deddens, J.C.; Mol, E.A.; Magin Ferrer, M.; van Laake, L.W.; Bouten, C.V.C.; Khademhosseini, A.; Doevendans, P.A.; Suyker, W.J.L.; Sluijter, J.P.G.; et al. Anti-fibrotic Effects of Cardiac Progenitor Cells in a 3D-Model of Human Cardiac Fibrosis. *Front. Cardiovasc. Med.* **2019**, *6*, 52. [[CrossRef](#)]
86. Arslan, F.; Lai, R.C.; Smeets, M.B.; Akeroyd, L.; Choo, A.; Aguor, E.N.E.; Timmers, L.; van Rijen, H.V.; Doevendans, P.A.; Pasterkamp, G.; et al. Mesenchymal stem cell-derived exosomes increase ATP levels, decrease oxidative stress and activate PI3K/Akt pathway to enhance myocardial viability and prevent adverse remodeling after myocardial ischemia/reperfusion injury. *Stem Cell Res.* **2013**, *10*, 301–312. [[CrossRef](#)] [[PubMed](#)]
87. Khosravi-Maharlooei, M.; Hajizadeh-Saffar, E.; Tahamtani, Y.; Basiri, M.; Montazeri, L.; Khalooghi, K.; Ashtiani, M.K.; Farrokhi, A.; Aghdami, N.; Nejad, A.S.H.; et al. THERAPY OF ENDOCRINE DISEASE: Islet transplantation for type 1 diabetes: So close and yet so far away. *Eur. J. Endocrinol.* **2015**, *173*, R165–R183. [[CrossRef](#)]
88. Nie, W.; Ma, X.; Yang, C.; Chen, Z.; Rong, P.; Wu, M.; Jiang, J.; Tan, M.; Yi, S.; Wang, W. Human mesenchymal-stem-cells-derived exosomes are important in enhancing porcine islet resistance to hypoxia. *Xenotransplantation* **2018**, *25*, e12405. [[CrossRef](#)] [[PubMed](#)]
89. Wen, D.; Peng, Y.; Liu, D.; Weizmann, Y.; Mahato, R.I.; Ph, D. Mesenchymal stem cell and derived exosome as small RNA carrier and Immunomodulator to improve islet transplantation. *J. Control. Release* **2016**, *238*, 166–175. [[CrossRef](#)]
90. Biancone, L.; Bruno, S.; Deregibus, M.C.; Tetta, C.; Camussi, G. Therapeutic potential of mesenchymal stem cell-derived microvesicles. *Nephrol. Dial. Transplant* **2012**, *27*, 3037–3042. [[CrossRef](#)] [[PubMed](#)]
91. Aggarwal, S.; Pittenger, M.F. Human mesenchymal stem cells modulate allogeneic immune cell responses. *Blood* **2005**, *105*, 1815–1822. [[CrossRef](#)]

92. Djouad, F.; Charbonnier, L.-M.; Bouffi, C.; Louis-Plence, P.; Bony, C.; Apparailly, F.; Cantos, C.; Jorgensen, C.; Noël, D. Mesenchymal stem cells inhibit the differentiation of dendritic cells through an interleukin-6-dependent mechanism. *Stem Cells* **2007**, *25*, 2025–2032. [[CrossRef](#)]
93. Selmani, Z.; Naji, A.; Zidi, I.; Favier, B.; Gaiffe, E.; Obert, L.; Borg, C.; Saas, P.; Tiberghien, P.; Rouas-Freiss, N.; et al. Human leukocyte antigen-G5 secretion by human mesenchymal stem cells is required to suppress T lymphocyte and natural killer function and to induce CD4+CD25highFOXP3+ regulatory T cells. *Stem Cells* **2008**, *26*, 212–222. [[CrossRef](#)]
94. Fujii, S.; Miura, Y.; Fujishiro, A.; Shindo, T.; Shimazu, Y.; Hirai, H.; Tahara, H.; Takaori-Kondo, A.; Ichinohe, T.; Maekawa, T. Graft-Versus-Host Disease Amelioration by Human Bone Marrow Mesenchymal Stromal/Stem Cell-Derived Extracellular Vesicles Is Associated with Peripheral Preservation of Naive T Cell Populations. *Stem Cells* **2018**, *36*, 434–445. [[CrossRef](#)]



© 2020 by the authors. Licensee MDPI, Basel, Switzerland. This article is an open access article distributed under the terms and conditions of the Creative Commons Attribution (CC BY) license (<http://creativecommons.org/licenses/by/4.0/>).

5. The PhD project:

Protecting effect of mesenchymal stem cell-derived extracellular vesicles in a milli-fluidic advanced *in vitro* model of glomerular filtration after doxorubicin damage

5.1 Main findings

Mesenchymal stem cells-derived extracellular vesicles (MSC- EVs) have been recognized as responsible for most of the beneficial effects attributed to MSCs and they contain a variety of soluble factors capable of activating downstream signaling. However, to better investigate the molecular mechanisms of pathology and regeneration, we need human organ-like devices that not only use human cells but also mimic 3D architecture and flow conditions within real human organs. The aim of this part of my thesis has been to evaluate the regenerative potential of MSC-EVs in a millifluidic *in vitro* 3D model of glomerulus, used to reproduce a pharmacological damage. To do this, I set a millifluidic *in vitro* 3D model of glomerular filtration, a three-layers structure composed by human-GECs and human-POD-SV 40 celllines, and the basement membrane in between coated with a matrix of Collagen type IV. The barrier thus formed is set up inside a bioreactor, in a closed milli-fluidic circuit in which fluid flows continuously at a certain flow rate. I obtained a standardized protocol and an adequate configuration of the milli-fluidic circuit, realizing co-cultures of human glomerular endothelial cells (h-GECs) and human podocytes (h-PODs) in bioreactors subject to continuous reperfusion. Once designed this device, I administered MSC-EVs for 24h in the endothelial part of the closed circuit of the glomerulus *in vitro*, to confirm the cellular ability to internalize the extracellular vesicles. The results obtained confirmed not only the ability of MSC-EVs to be internalized by cells, but also their therapeutic potential, improving podocyte vitality after pharmacological damage induced by doxorubicin.

5.2 Introduction

Human fluidic culture systems represent a significant challenge today. In particular, the capability of *in situ* continual monitoring of organ behaviours and their responses to therapeutic compounds is critical in understanding the dynamics of drug effects and therefore accurate prediction of human organ reactions [1]. Numerous advances have been made in applying these technologies to renal pathophysiology. Individual components of the nephron, such as proximal tubule, distal tubule/medullary collecting duct, have been successfully mimicked using fluidic devices and making a great contribution to the understanding of the molecular mechanisms underlying drug toxicity and therapies [2]. Within the glomeruli, there are unique and highly specialized cells able to establish an intense cross-talk between them, this cross-talk is the reason why the damage suffered by one of these cell types generates a response in the others as well [7]. Glomerular cells are critical to normal physiology, but they are targets of a number of damaging processes in disease, including immune, metabolic, vascular and malignant disorders. However, the information in our possession, coming mainly from *in vivo* models, does not completely clarify the mechanisms of glomerular biology and the pathogenesis of the disease [7]. It therefore appears clear that we need to progress beyond standard histopathology in order to describe glomerular diseases more effectively [8].

My PhD project is placed in this context and is based on an innovative technology that recapitulate the glomerular filtration barrier (GFB) in a bioreactor continuously crossed by culture medium. The complexity and uniqueness of this filter cannot be approximated with traditional culture systems but requires systems that better mimic its function and that allow us to test new therapeutic molecules, like extracellular vesicles (EVs). EVs are heterogeneous, naturally occurring, membrane-enclosed structures of varying sizes that are secreted by most cell types. Apart from apoptotic bodies, vesicles are distinguished on the basis of their biogenesis, cellular origin and size into 2 macroscopic categories: microvesicles and exosomes. While the microvesicles are generated by membrane lipid microducts that exit the cell membrane, allowing for retention of the mother cell membrane proteins, exosomes are a more homogeneous population, derived from GTPase-dependent fusion and internal

budding of endosomes/multivesicular bodies (MVB) [9].

Mesenchymal stem/stromal cells (MSCs) derived EVs have been proven to contain genetic and protein material that upon transferring to recipient cells can activate several repair mechanisms to ameliorate renal injury. In the literature there is a substantial number of publications supporting their role in promoting tissue repair and reduce inflammation in different pathological models, including models of acute kidney injury (AKI) [10,11] and chronic kidney injury (CKI) [12,13]. In this thesis project, we have demonstrated not only the ability of MSC-EVs to penetrate cells, but preliminarily we showed that they are capable of reverting cell damage in an *in vitro* dynamic model of AKI; this result opens the way to many future possibilities, concerning the development of new non- invasive therapies.

5.3 Materials and methods

Cell lines

Cultured podocytes

A laboratory-available podocyte line was used, obtained as described [14]. Briefly, decapsulated glomeruli were isolated by differential sieving from renal cortex fragments taken from surgically removed kidneys Caucasian patients, treated with collagenase and seeded in Dulbecco's modified Eagle's medium (DMEM) containing 20% FCS and d-valine. Primary cultures of podocytes were obtained by plating at high-density glomeruli untreated with collagenase. After a 10 day-incubation in DMEM-20% FCS, the cultures were trypsinized and the outgrowing podocytes were expanded. Phenotypic characterization was performed according to cell morphology (polyhedral cells with cobblestone-like appearance); positive staining for synaptopodin, WT-1, cytokeratins, vimentin, and laminin; negative staining for smooth muscle-type myosin, FVIIIr: Ag, and CD45; and cytotoxicity in response to 50 µg/ml of puromycin aminonucleoside. Established lines of podocytes were obtained by infection of pure primary cultures with a hybrid Adeno5/SV40 virus, as described [15]. Individual foci of immortalized cells were subcultured and cloned. Once the immortalized line was obtained, it was sometimes evaluated for podocytes proteins (Figure 1). The cells were cultured in DMEM High Glucose (Euroclone) 10% FCS, with the addition of penicillin/streptomycin, L-glutamine. The adherent monolayer was detached by trypsin treatment for 5 min at 37 °C.

Figure 1

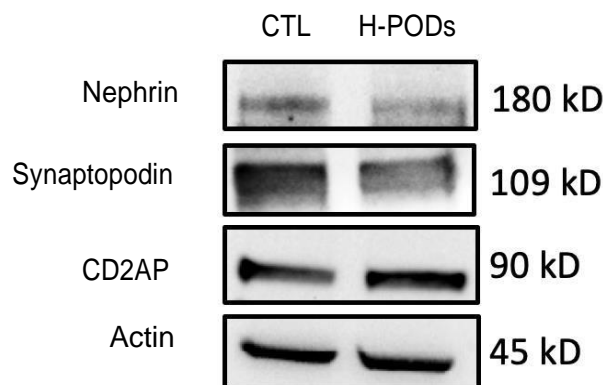


Figure 1: Expression of Podocytes markers by h-PODs used, in comparison with a validated conditionally immortalized human podocyte cell line developed by transfection with the temperature-sensitive SV40-T gene [16].

Endothelial cells

Human primary kidney glomerular endothelial cells, isolated from human kidney tissue, were acquired from Cell Biologics and subsequently immortalized. Cell line stabilization occurred at passage 2 by a retrovirus containing p-BABE-puro-hTERT plasmid (Addgene plasmid 1771), and selected using antibiotic resistance (1 $\mu\text{g}/\text{ml}$ puromycin, Gibco, Thermo Fisher). The immortalized line, used from passages 9 to 62, was constantly subjected to FACS analysis, to evaluate the maintenance of the main endothelial markers (Figure 2). Cells were expanded in flasks previously coated with attachment factor (Sigma-Aldrich) and cultured in complete EndoGRO 10% FCS, with the addition of penicillin/streptomycin and Mycozap to prevent contaminations. Cells were detached by trypsin treatment for 5-10 min at 37 °C.

Figure 2

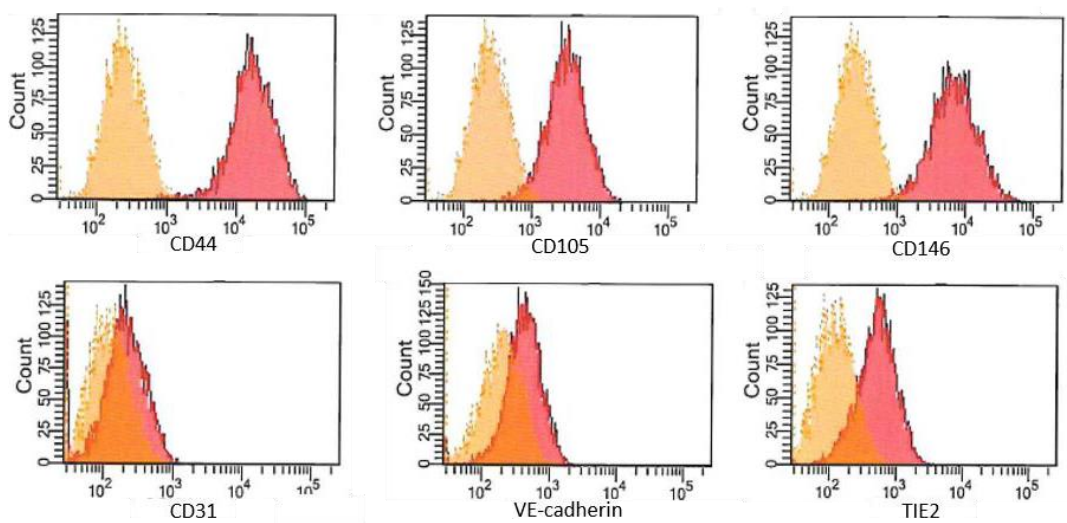


Figure 2: GEC Expression of endothelial markers.

Mesenchymal Stem Cells

Mesenchymal Stem Cells (MSCs) were obtained from Lonza, cultured and characterized as previously described [17,18]. Briefly, the MSCs were cultured in the presence of Mesenchymal Stem Cells Basal Medium

(MSCBM, Lonza). To expand the MSCs, the adherent monolayer was detached by trypsin treatment for 5 minutes at 37°C, after 15 days for the first passage and every 7 days for subsequent passages. Cells were seeded at a density of 10,000 cells/cm² and used within the passage six. At each passage, cells were counted and analyzed for immunophenotype by cytofluorimetric analysis. The following antibodies, all phycoerythrin (PE) or fluorescein isothiocyanate (FITC) conjugated were used: anti-CD105, -CD146, -CD90 (Miltenyi Biotech); -CD29, -CD44, -CD73, -CD34, -CD45, -CD80, -CD86, -CD166, HLA-I (Becton Dickinson Biosciences Pharmingen). All the cell preparations at different passages of culture expressed the typical MSC markers: CD105, CD73, CD44, CD90, CD166 and CD146. They also expressed HLA class I. MSC preparations did not express hematopoietic markers like CD45, CD14 and CD34. They also did not express the co-stimulatory molecules (CD80, CD86 and CD40). The adipogenic, osteogenic and chondrogenic differentiation ability of MSCs was determined as previously described [17].

Three-dimensional millifluidic co-culture system

Functioning of the millifluidic dynamic model

For dynamic experiments, it has been used a dynamic system fabricated by IVtech Srl (Italy). This millifluidic device allows a continuous perfusion for live cells seeded in a chamber called LiveBox

Figure 3

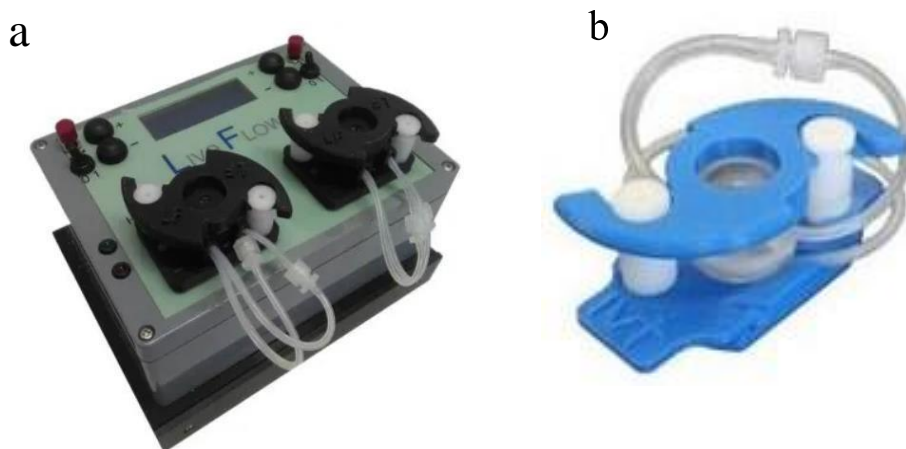


Figure 3: Ivtech millifluidic dynamic system. **a)** Live flow composed by two peristaltic pump and the flow rate control system; **b)** a bioreactor Live Box for co-cultures.

(LB) (figure 3). The main body of device, the LiveFlow (LF), is composed of two pumping heads, each one driving two independent circuit.

A circuit is in turn made up of three devices connected to each others: a peristaltic pump able to apply a specific flow-rate to the fluid in the system, LB studied to recreate an *in vitro* physiological barrier and tanks containing liquids entering and leaving the system. LB is a silicone chamber with two compartments separated by a porous membrane: one lower compartment for GECs and one upper for podocytes. In short, podocytes medium contained in one of the two inlet tanks flows up to the peristaltic pump, which gives a flow rate ranged between 50 to 500 $\mu\text{l}/\text{min}$ to the fluid that arrives in the upper part of LB, where the podocytes are present. In the same way, an endothelial culture medium is conveyed into the inferior part of the room. during the experiments conducted, two different configurations has been used. In one of these, the liquid leaving the chamber re-enters the system in a constant recirculation (Figure 4a). In the second configuration, in the lower part the liquid flows in

Figure 4

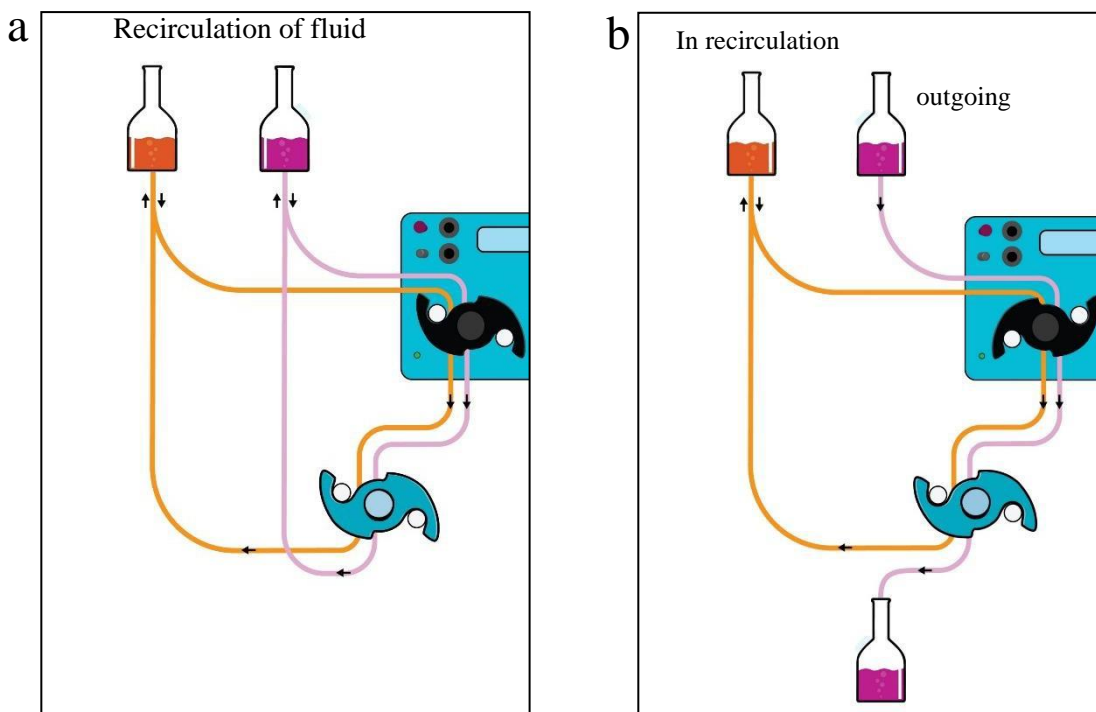


Figure 4: Different configurations of dynamic system used.

recirculation and in the upper part the culture medium enters and is collected at the exit (Figure 4b).

Preparation of co-cultures

The support on which the cells are sown is a track etched membrane (ipCELLCULTURE™, it4ip) in PET, 12 µm thick and equipped pores (Ø 0.45 µl). The membrane is initially inserted between the two plastic rings that will fit into the LB and the assembled structure is placed on a dish; the coating with type IV collagen follows. A 25% solution of type IV collagen diluted in 70% ethanol is used to completely coat the membrane, first on one side, then on the other. Then the membrane is left overnight in incubator in a poor medium. On the convex side of the membrane are seeded 100.000 h-GECs in 100-120 µl of medium. After five hours in incubator (37°C, 5% CO₂), the time deemed necessary for the cells to adhere to the support, LB is mounted so that the endothelial part is facing downwards, and bottom part is filled with endothelial medium. Subsequently, 100.000 podocytes are seeded on the part of the membrane facing upwards, in 500-600 µl of medium. The next day endothelial medium is changed completely, while about 300 µl of podocytes medium are added through top entry channel. After a day in the incubator, the chamber is attached to the circuit to allow the passage of fluid.

Damage to the GFB

Acute damage to GFB is achieved with doxorubicin (DXR) 0.5 µg/ml, directly under dynamic conditions. The reservoirs from which the fluid comes are filled with different solutions for the upper or lower part of the bioreactor: for the podocyte (upper) part DMEM HG without FBS, for the endothelial part (lower) DMEM HG with the addition of 0.5 µg/ml of DXR (Figure 5).

Figure 5

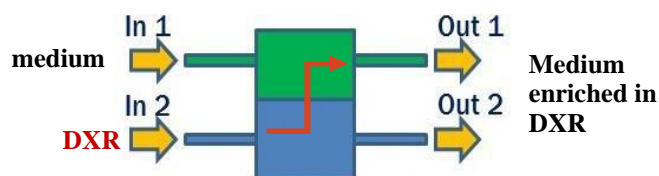


Figure 5. Bioreactor view during DXR treatment. the medium with DXR flows in the lower endothelial part, but because of the flow itself, a part permeates through the GFB, enriching the medium that is flowing in the upper part.

The medium flows for 3h in the system in the recirculation configuration (Figure 4a), at a speed of 80 μ l/min. At the end of 3h, the medium is changed, and the chambers are washed. Then, the chambers are re-connected to the circuit for 24h, in the presence of complete EndoGRO (for GECs) and DMEM HG (for h-PODs), both with 2% FBS.

Assessment of permeability

The evaluation of the barrier integrity is quantified by the passage BSA conjugated with guanidine isothiocyanate (BSA-FITC) (Sigma) [19]. A solution of DMEM HG - BSA-FITC 1 mg/ml is made to flow in the circuit, in the endothelial part, for 3h at the flow rate of 80 μ l/min. The configuration used is that in figure 4b: in recirculation for the lower part, while in the upper part normal DMEM HG enters and medium enriched in BSA-FITC comes out. The greater the damage to the filtration barrier, the greater the quantity of BSA-FITC that passes through it and reaches the outlet tank. The medium enriched in BSA-FITC and collected is then analyzed for fluorescence. in triplicate, 100 μ l are taken from the outlet tank, placed in a 96-well plate and analyzed for fluorescence.

Figure 6

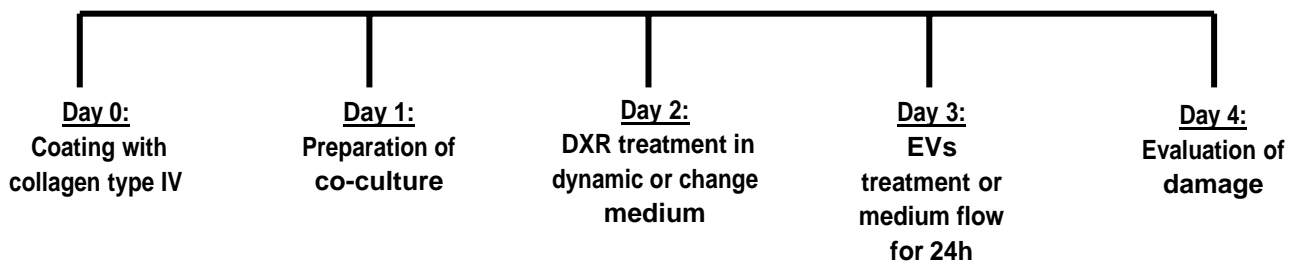


Figure 6. Timing of the experiment in dynamics. The first step is the coating of the bioreactor membrane with type IV collagen, both sides (day 0). The sowing of h-GECs and h-PODs (day 1) and the eventual treatment with DXR (day 2) follow. After 24h in medium poor in FBS or EVs treatment (day 3) the damage is assessed (day 4).

Apoptosis

Cytofluorimetric evaluation of apoptotic cells was performed using the Muse™ Annexin V & Dead Cell Kit (Merck-Millipore), according to the manufacturer's recommendations. Briefly, after dynamic treatment, cells were detached from membranes and resuspended in Muse™ Annexin V & Dead Cell Kit, and the percentage of apoptotic cells (Annexin V +) was detected. The assay utilizes Annexin V to detect phosphatidylserine on the external membrane of apoptotic cells. A dead cell marker (7-AAD) is also used as an indicator of cell membrane structural integrity.

Immunofluorescence studies

Immunofluorescence was performed on cells co-cultured on membranes. After treatment in dynamic conditions, the membranes are removed from the support rings and sectioned. Cells were fixed in 4% paraformaldehyde for 20 minutes at room temperature and permeabilized with 0.1% Triton X100 (Sigma-Aldrich)/PBS for 10 minutes at 4°C. Aspecific sites were blocked with 1.5% Bovine Serum Albumine/PBS for 20 minutes at room temperature, followed by incubation with primary antibodies for 1h at room temperature and 3 washes with PBS 1x-BSA 0.1%. Secondary antibodies and Phalloidin (1: 1000) are then put together for 1 h at room temperature. Finally, an 8 minutes treatment with DAPI (1: 10000) ensures the nuclear staining. After the final washing, coverslips were mounted with Fluoromount on cover glasses. In some cases, to obtain cross-sections of the cell-covered membrane, the membranes were included in OCT gel and stored at -80 ° C. After a few days we proceeded with the IF staining. Imaging was performed using a Leica TCS SP5 confocal system (LEICA Microsystems S.r.l.) equipped with 405 nm diode and an argon ion lasers. Samples were imaged using a 40X PlanApo/1.4 NA oil immersion objectives. Series of x-y-z images (typically 0.19*0.19*0.5 μm³ voxel size) were collected along the z-axis at 0.5 μm intervals throughout the

sample depth (36 μm). Adjusting of colours and 3D reconstruction was performed using tools of Imagej.

Extracellular vesicles

Extraction of EVs

Isolation of EVs was performed as described. Confluent MSC were cultured in serum-free RPMI for about 18 h. Post culture, the medium was centrifuged for 30 min at 3,000g to remove cell debris and apoptotic bodies. After which, the supernatant was ultracentrifuged for 2 h at 100,000g, 4 °C using the Beckman Coulter Optima L-100 K Ultracentrifuge with the rotor type 70 Ti 38,000 rpm. The pellet of EVs obtained was resuspended in RPMI supplemented with 1% DMSO. Suspension of MSC-EVs was then stored at -80 °C until further use. EVs were analyzed using NTA analysis using the NanoSight NS300 system (Malvern Instruments, Ltd), mean size of EVs evaluated by electron microscopy was 90 nm (± 20).

Tests of Serum-EVs uptake by podocytes were made. In this case, serum EVs were obtained from healthy people. The serum was centrifuged for 5 minutes at 3000 rpm at room temperature, to eliminate any debris present. The supernatant is then subjected to another 30-minute centrifuge at 3000 rpm. To recover the EVs, the supernatant is subjected to ultracentrifuge, as already described.

EVs treatment

After DXR treatment, the cells in the bioreactor are washed with PBS and the media in the tanks are changed. The input tank entering the endothelial compartment is filled with complete EndoGRO (without FBS) enriched with 4×10^9 MSC-EVs (20.000 EVs per cell), while in the upper part DMEM

HG without FBS flows. The configuration of the dynamic system is that of fluid recirculation both in the lower and upper part as shown in figure 4a, for 24h at 37°C, fluid flow of 80 µl/min.

Staining of EVs

The staining of the MSC-EVs or serum-EVs was achieved by staining the cells in suspension with Vybrant™ Cell-labeling Solution (thermo Fisher Scientific). Briefly, MSCs were cleaved with trypsin for 5 min at 37°C and resuspended at a density of 1×10^6 /mL in serum-free medium. After adding 5 µl per ml of cell labeling solution, the suspension was incubated for 20 min at 37 ° C. Three washes were then made by adding warm medium and centrifuging at 1500 rpm for 5 min. After 10 minutes of recovery the cells were plated and the produced EVs collected [20].

Electroporation of EVs with MiRNA 39 of C.el. and use in dynamic model

To verify the entry of the EVs into the podocytes, a part of the collected MSC-EVs were electroporated to allow the encapsulation of an exogenous MiRNA, Mir39 of the organism *C.El.*, as described below. A suspension of about 200 µl was prepared containing 6×10^{10} EVs, 5 µl of miRNA 39 (20 µM) and the reaction solution of the kit (NEON™, Invitrogen). After an incubation of 30 min at 37 ° C, electroporation is carried out. The suspension is poured into a cuvette with 3 ml of the reagent E2, as indicated, and 10 discharges of 20 ms at 750 volts are performed. Then the suspension is placed at 4 ° C overnight. The following day an ultracentrifuge is made (2h, 4°C, 38,000 rpm), The EVs are resuspended in medium without FBS with the addition of 1% DMSO and stored at -80 ° C.

The electroporated EVs are then inserted into the system, inside the tanks whose contents are directed towards the endothelial compartment. the configuration used is the one in recirculation of fluid

described in image 4a. after 24h of treatment the h-PODs are detached from the membrane and placed in Trizol reagent (thermoFisher) until the extraction of the mRNA.

PCR analysis

Total RNA was isolated from different cell preparations using Trizol reagent (Ambion, ThermoFischer) according to manufacturer's protocol. RNA was quantified spectrophotometrically (Nanodrop ND-1000, Wilmington, DE). First-strand cDNA was produced from 200 ng of total RNA using the High Capacity cDNA Reverse Transcription Kit (Applied Biosystems, ThermoFischer). For gene expression analysis, quantitative real-time PCR (qRT-PCR) was performed in 20- μ l reaction mixtures containing 5 ng of cDNA template, the sequence-specific oligonucleotide primers (purchased from MWG-Biotech, Eurofins Scientific, Bruxelles, Belgium) and the Power SYBR Green PCR Master Mix (Applied Biosystems). GAPDH mRNA was used as housekeeping normalizer. Fold change expression respect to control was calculated for all samples.

To confirm the presence of miRNA 39 of *C. El.* inside the cells that had undergone dynamic treatment with electroporated EVs, qRT-PCR was also used. Briefly, 200 ng of input RNA from all samples were reverse transcribed with the miScript Reverse Transcription Kit and the cDNA was then used to detect and quantify miRNA 39, using the miScript SYBR Green PCR Kit (all from Qiagen). All samples were run in triplicate using 3 ng of cDNA for each reaction as described by the manufacturer's protocol (Qiagen). Relative expression data were then normalized using the mean expression value, calculated on the overall miRNA expression in each array, according to a Ct detection cut-off of 35 PCR cycles. In this case, RNAU6B mRNA was used as housekeeping normalizer.

All reactions were performed using an Applied Biosystems 7900HT real-time PCR instrument equipped with a 96-well reaction plate.

Statistical analysis

Data are showed as mean \pm standard deviation (SD). At least three triplicates were performed for each experiment. Unpaired t test was used for analysis when two groups of data were compared, while 2way ANOVA with Dunnett's multiple comparison test was applied when comparing more than two groups of data. All statistical analyses were done with GraphPad Prism software version 8.0 (GraphPad Software, Inc.). P values of < 0.05 were considered significant.

5.4 Results

Setup of a glomerular millifluidic model

A glomerular millifluidic model was obtained by assembling a tri-layer formed by a transparent membrane coated with type IV collagen and human glomerular cells. The membrane in PET, a material widely used in the medical field, allows for the microscopic evaluation of cellular changes according to the different treatments. The presence of collagen IV is important because it is a fundamental element for GFB, allowing the adhesion and maintenance of the cellular phenotype [21,22] and results to be more efficient than using type I collagen, which is not specific for the glomerulus [23]. The cells used are human and have been obtained from primary lines.

Figure 1

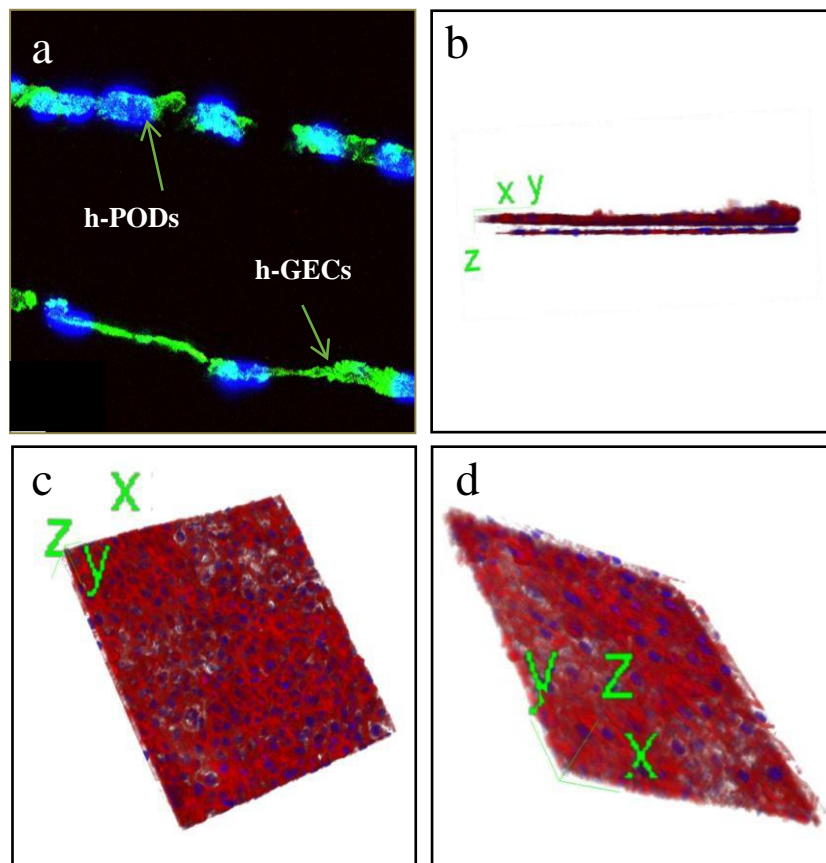


Figure 1. Co-culture assembly on bioreactor membranes. a) after being subjected to 24h of flow, the membrane of the bioreactor on which the glomerular cells are present was fixed to highlight the two cell types, visible thanks to the IF staining. Actin in green in *a* image and in red in *b*, *c* and *d*.; nuclei in blue. a) The membrane was included in OCT, preserved in nitrogen and subsequently cut in the cryotome to obtain a cross section. b) Using the 3D reconstruction tool available on Imagej it was possible to transversally highlight the presence of the 2 monolayers on the sides of the membrane (h-PODs at the top and h-GECs at the bottom). In *c*) the podocytic cell monolayer is represented, while in *d*) the endothelial monolayer. The membrane examined in *b*, *c* and *d* is the same.

Assembly of co-cultures in the bioreactors

The co-culture assembly protocol was optimized, and then following steps were developed. During the first phase, the membrane is covered on both sides with a 25% solution of type IV collagen, diluted in 70% ethanol (EtOH). The membrane is then rebalanced overnight in a culture medium and the next day it is possible to proceed with the seeding of the cells. The endothelial layer is set up in the lower part of the membrane, which will be upside down in the bioreactor, and after 4-5h the chamber is assembled and sown directly inside the h-PODs, in the upper compartment. The cell density is the same, 1×10^5 cells per cell type. The *in vitro* glomerulus thus formed is placed in an incubator until the next day when it can be inserted into the dynamic circuit. Once the cells are adhered, the chamber is attached to the peristaltic pump which allows the passage of fluid at the rate of 80 $\mu\text{l}/\text{min}$ (Figure 1). During perfusion, cells in the chamber have been subjected to a shear stress of $\sim 6,4 \times 10^{-5} \text{ dyn}/\text{cm}^2$. To calculate roughly this value, we used the following equation: $\tau = 6\mu Q/bh^2$, where μ is the medium viscosity ($\text{gm}/\text{cm}/\text{s}$), Q is the volumetric flow rate (cm^3/s), b is the channel width, and h is the channel height [24–26]. Haemodynamic forces influence the functional properties of vascular endothelium. Endothelial cells have a variety of receptors, which sense flow and transmit mechanical signals through mechanosensitive signalling pathways to recipient molecules that lead to phenotypic and functional changes [27,28]. The importance of blood flow for the maintenance of glomerular endothelial cells is certainly one of the causes of the loss of the phenotype in traditional *in vitro* cultures. Already after 24h of perfusion, the h-GECs show an ordered and distended cytoskeleton, the actin is oriented in the direction of flow (Figure 2), in a similar way to what happens physiologically. Maintaining the integrity of the barrier also requires the production of laminin. Total absence of laminin is known to cause GBM to rupture and glomerular vascularization to fail, resulting in proteinuria, hematuria, and ultimately death [29]. As shown in figure 3c, the production of laminin increases considerably after only 24 hours of flow.

Figure 2

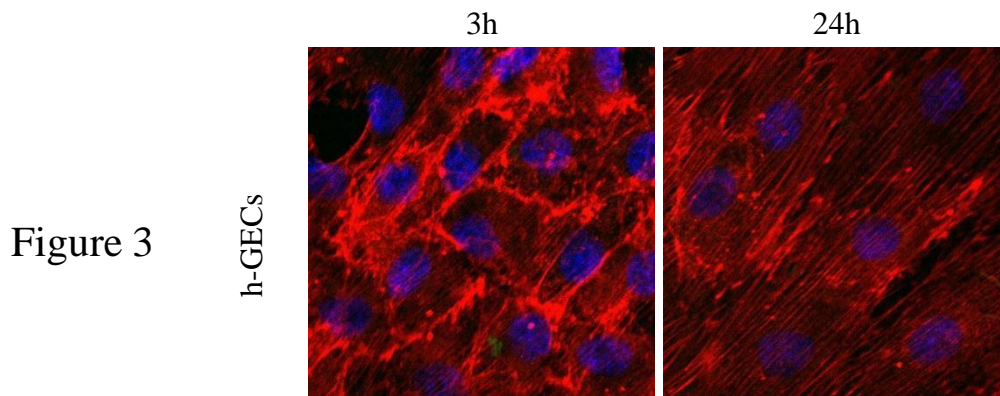


Figure 2. Morphological changes of h-GECs in co-culture subjected to 3h or 24h of perfusion (actin in red and nuclei in blue). Actin clearly appears more orderly and tidier in the direction of flow. The images were acquired with a Leica SP5 confocal microscope, 40x objective.

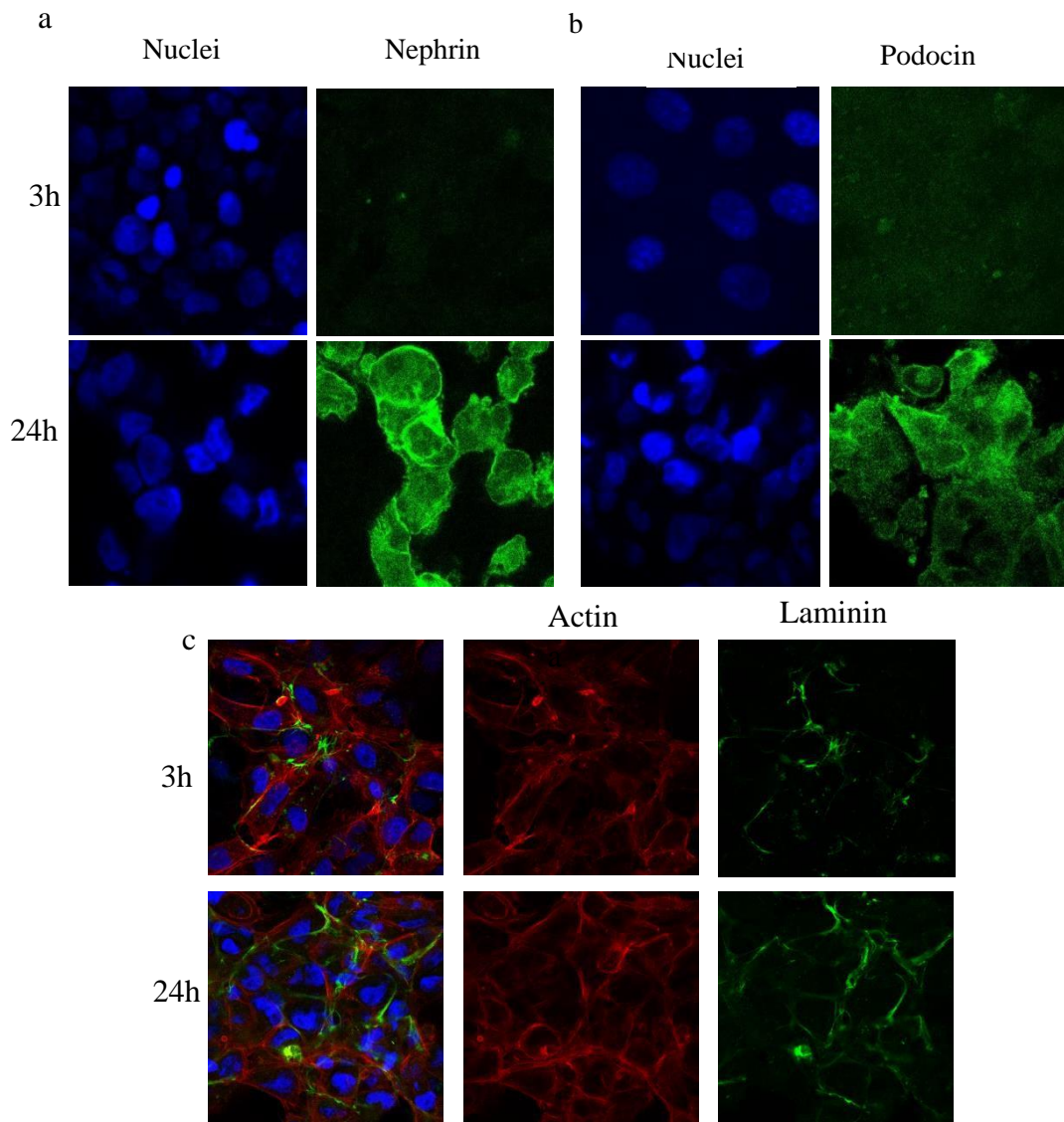


Figure 3. The effect of flow in the dynamic model. h-Pod/h-GEC co-cultures subject to perfusion for 3h and 24h. After treatment the cells on the membranes were fixed and stained (nuclei in blue, actin in red, laminin, nephrin and podocin in green). the difference in expression of two of the major podocytic markers in the different times (a and b) is evident. Furthermore, the laminin secreted by the bilayers, which guides the formation of the extracellular matrix, is much more evident after 24h (c). The images were acquired with a Leica SP5 confocal microscope, 40x objective.

The podocytes, more loosely attached to the matrix, are particularly sensitive to shear stress. Conceptually, the slit diaphragm can be thought of as being composed of signal receptors (nephrin, podocin) that connect to signal integrators or adapters which then associate to the actin cytoskeleton. These markers that play a fundamental role in the dynamics of the actin cytoskeleton of podocytes result to be increased in a time-dependent manner in case of perfusion [25] (Figure 3a and 3b).

Validation of the model through the permeability test

Since proteinuria is the index of renal damage, a filtration test based on the use of BSA-FITC was adopted to evaluate the integrity of the barrier. Already shown in previous works in static conditions, it has however been adapted to the dynamic system [19,30]. In the dynamic circuit, the tanks whose fluid is directed towards the endothelial compartment are filled with DMEM HG enriched with BSA-FITC 1mg / ml, while simple DMEM HG is directed towards the h-PODs. The medium enriched with BSA-FITC proceeds in recirculation in the circuit, while the medium is collected in an outlet bottle. The medium coming out from the upper part of the chamber (podocytic compartment), will therefore be enriched by a certain amount of BSA-FITC and the measurement of fluorescence as a percentage is taken as an index of barrier integrity. In basal conditions, the presence of the complete glomerular tri-layer (the 2 cell types and the coated membrane), appears to oppose the greatest resistance to the passage of albumin.

From figure 4 the great contribution to barrier permeability of h-GECs is clear, their morphological and charge characteristics are thought to be fundamental in maintaining glomerular physiology. The presence of podocytes alone is less effective in avoiding the passage of serum protein, it is comparable to the contribution of the membrane coated with type IV collagen; the uncoated membrane filters significantly more than the other conditions analyzed.

Figure 4

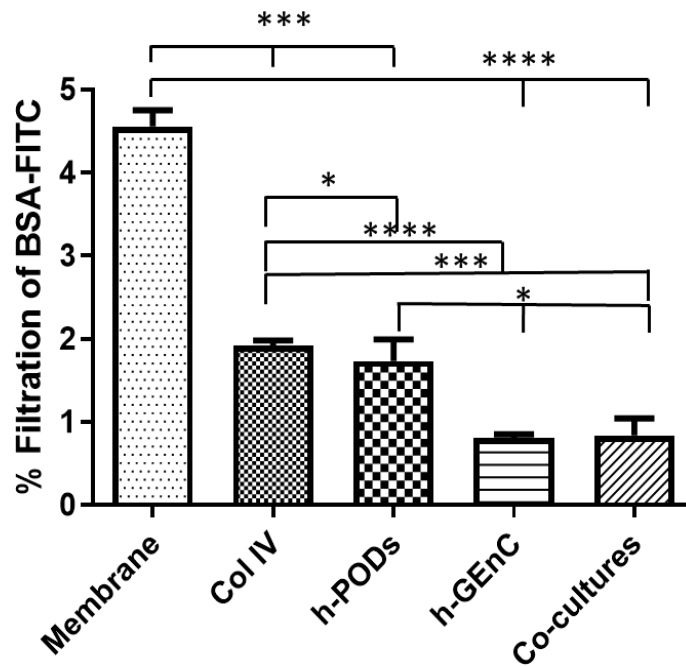


Figure 4. Evaluation of filtration with permeability test. The passage of BSA-FITC through the GFB in the dynamic model was evaluated, in 5 different conditions: membranes free of col IV and cells (membrane), membranes coated with Col IV (Col IV), and membranes coated with COL.IV in presence of cells (only h-PODs , only h-GeCs and both cell types in co-cultures). The co-cultures were perfused for 3h, at 37 ° C. At the end of 3h the fluid exiting from h-POD compartment contained in the outlet tank was analyzed.

EVs are internalized by podocytes in the dynamic model

The cellular uptake mechanisms of EVs have been extensively debated in the literature. Certainly, one of the basic requirements for their use as therapeutics is to demonstrate that they can be internalized by target cells. The hypothesized mechanisms for cellular internalization include practically all known cellular uptake methods, from the most frequent to cell-specific mechanisms, not yet fully understood. The differences could concern both the type of vesicles and the cells being treated [31].

Figure 5

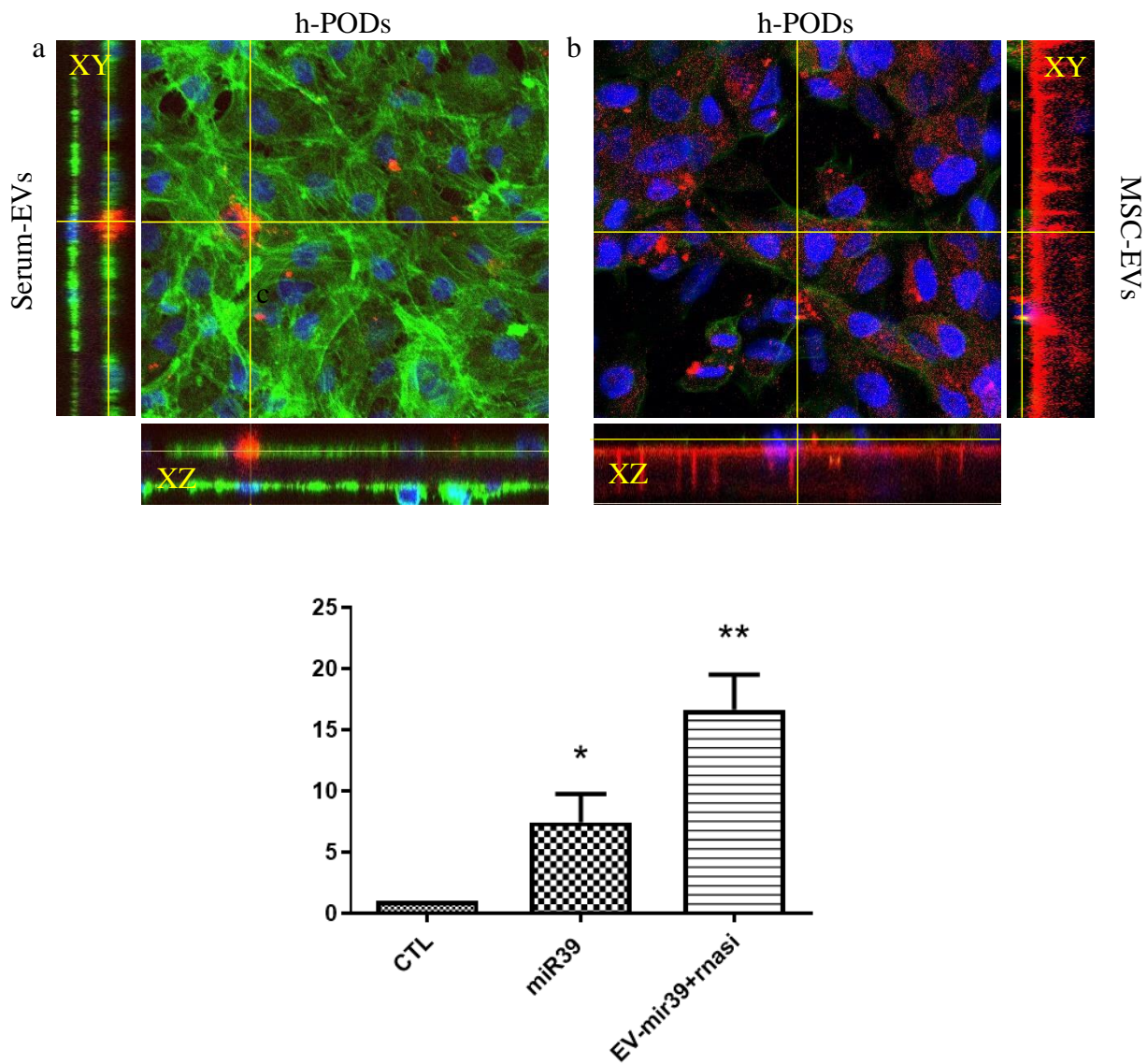


Figure 5. Internalization MSC-EVs by h-PODs in the dynamic model. Co-cultures in bioreactors were subjected to a dynamic experiment for 24h with DII stained EVs from serum (a) and from MSC-EVs (b). c) The co-cultures in the bioreactors were subjected to a dynamic experiment for 24h in 3 different conditions: 24h of perfusion with culture medium (CTL), 24h of perfusion with Mir39 of free Cel (mir39), 24h of perfusion with EVs electro-pored with Mir39 and subjected to subsequent treatment with RNase (EV-mir39 + RNase). For both conditions, both free miR39 and electroperated EVs were inserted into the tanks for the endothelial compartment, and the presence of Mir39 internalized by podocytes was then analyzed. The images were made with leica SP5 confocal, 40X objective, while the orthogonal sections with the Imagej software.

In the millifluidic system, the co-cultures were infused with 4×10^9 serum-derived EVs (figure 5a), or MSC-derived EVs, for 24h (figure 5b). Orthogonal view highlights a plane inside the cell. EVs previously stained in DII are clearly visible within the cell body. The advantage of using the millifluidic system is the ability to clearly focus on what is happening in the glomerular cell layers. A quick microscopic and possibly molecular analysis is possible. Finally, to eliminate any doubt about internalization, we electroperated MSC-EVs with an exogenous miRNA (miRNA39

from the organism *C. Elegans*). The co-cultures in the bioreactor were perfused for 24h with medium enriched with the exogenous miRNA, introduced into the circuit from the endothelial part. At the end of the perfusion, the podocytes were isolated and analyzed for the presence of the miRNA (Figure 5c).

From the results obtained, the internalization of miRNA39 is more effective if carried through the EVs, than if the miRNA is free in the culture medium.

Mimicking a pharmacological acute kidney injury

To demonstrate the capability of our millifluidic device, we used it to study the pathophysiology of drug-induced acute kidney injury (AKI) and to assess podocyte toxicity. We used doxorubicin (DXR) as model drug. A solution of DMEM HG-DXR (0.5 μ l/mL) was circulated in the endothelial part of the chamber, while the simple medium flowed in the upper podocyte part. After 3h the noxious stimulus was removed and culture medium with 2% FBS was added, for 24h. After treatment, the podocytes were detached from the upper part of the chamber and their morphology and vitality (Figure 8a) was evaluated. Figure 6 shows a co-culture after treatment with DXR, fixed and subjected to IF staining, while figure 7 shows the mRNA expression of some podocyte markers after don DXR treatment, in comparison with co-cultured podocytes subjected to flow for 24h. The mRNA expression of damage markers caspase 3, 7 (CASP3 and CASP7) and metalloproteinase 9 (MMP9), as expected, are significantly increased. However, it is interesting to note that synaptopodin (SYN) and podocalixin (PDX) expression also increases after pharmacological treatment.

Figure 6

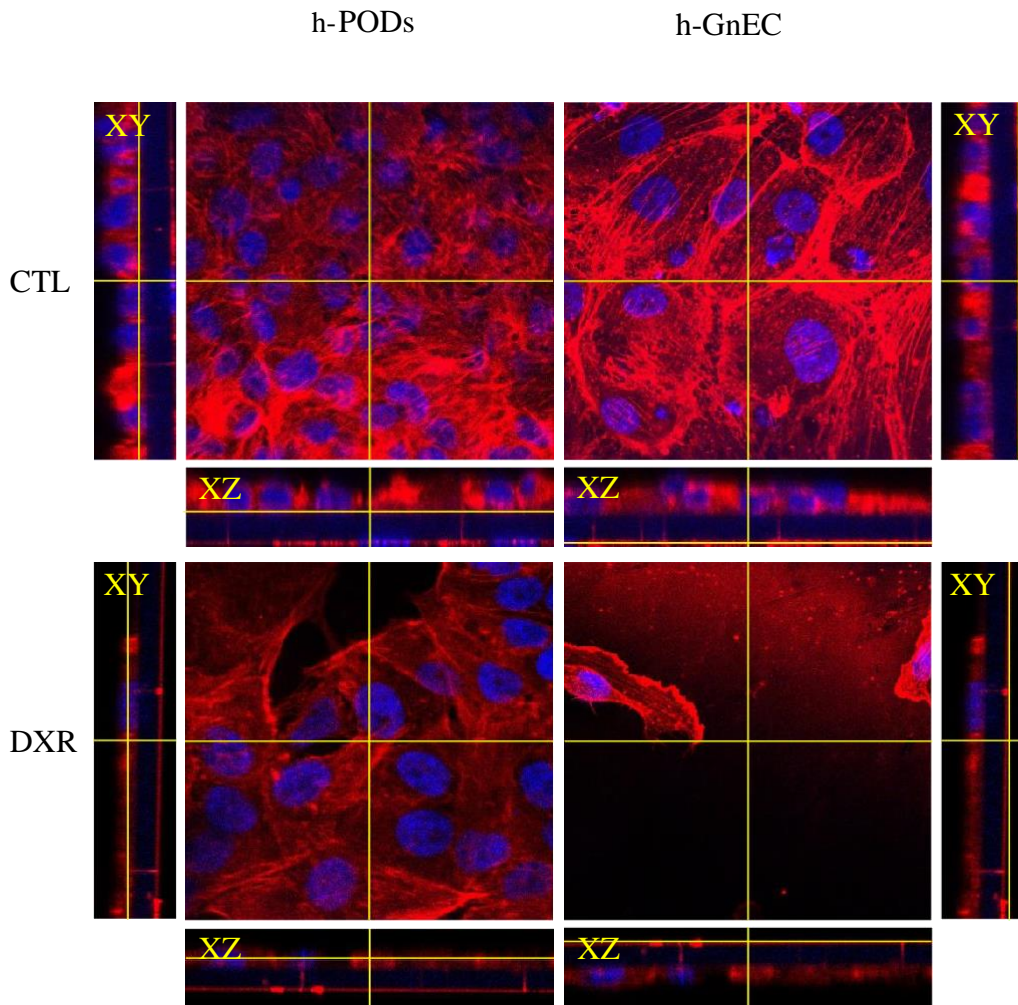


Figure 6. The effect of DXR treatment in the dynamic model. h-Pod/h-GEC co-cultures in orthogonal sections: the two cell types were plated on bioreactors and subjected to reperfusion. In the case of co-cultures treated with doxorubicin (DXR), the cells were first perfused for 3h with DXR enriched medium, then for 24h with canonical medium. In the case of the control co-cultures, after 24h of continuous perfusion with culture medium, the cells were fixed. They were then stained with DAPI to highlight the nuclei (in blue), and with phalloidin-texas red to highlight the actin (in red). The images were acquired with a Leica SP5 confocal microscope, 40x objective.

Figure 7

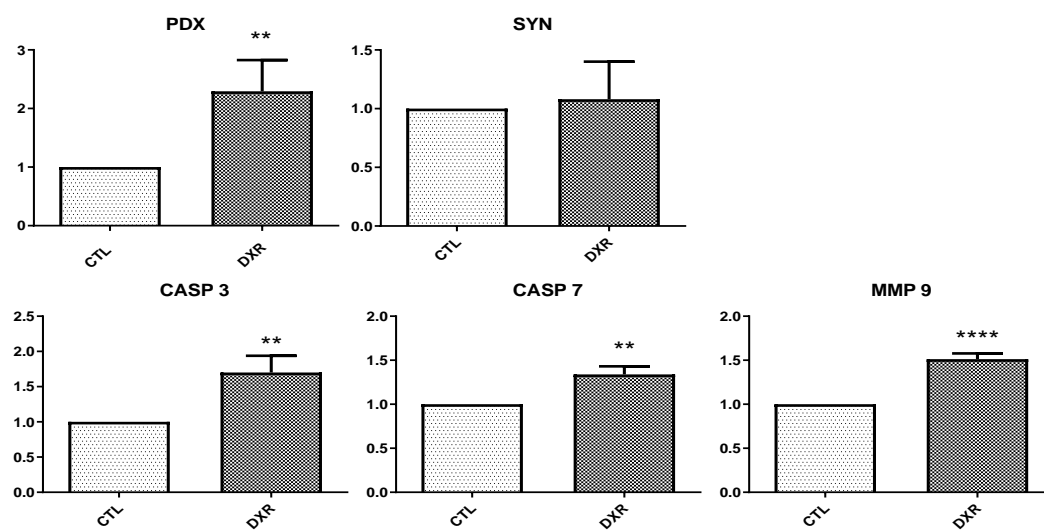


Figure 7. mRNA relative expression of h-PODs damage markers. CTLs are h-PODs in co-cultures undergoing 3h of perfusion, while DXRs are h-PODs in cocultures undergoing 3h of DXR treatment, followed by 24 of perfusion with medium without FBS. Cell damage markers increase, as do some of the major podocyte markers responsive to cell damage. The results obtained were made comparable by setting the controls equal to 1.

Some evidence, in fact, correlate the increased levels of morphological markers, especially PDX, with the increase in proteinuria, probably due to the activation of pathways in response to the stimulus of reorganization of the cytoskeleton [32].

MSC-EVs penetrate podocytes under dynamic conditions and improve cell viability

We preliminarily tested the effectiveness of EVs isolated from MSCs on our "glomerulus *in vitro*" previously subjected to DXR treatment. The dynamic model has been used for 24h in conditions of fluid recirculation both in the upper and lower part of the chamber, with the difference that in the endothelial compartment there was medium, but with the addition of 4×10^9 MSC-EVs. At the end of the reperfusion, it was possible to analyze the cells on the membrane.

Figure 7

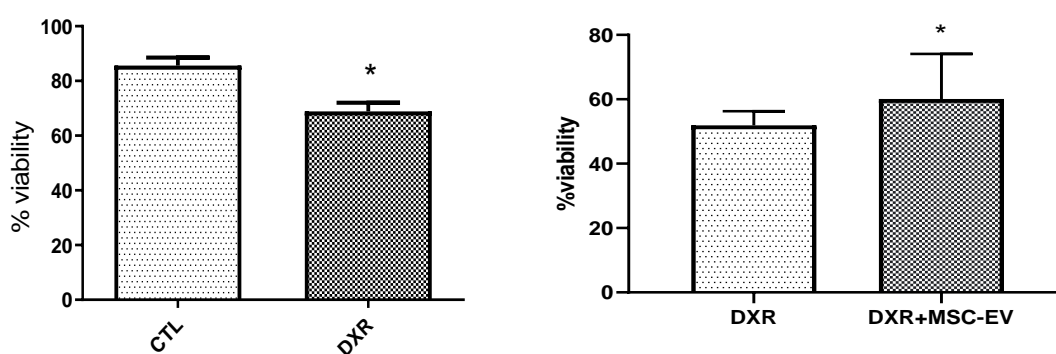


Figure 7. Viability analysis of h-PODs after dynamic experiments. a) The bioreactors containing the co-cultures were subjected to 3h of treatment with DXR, followed by 24h of dynamic treatment with low-serum medium, while the CTLs were subjected to 24h of constant perfusion. b) In comparison h-PODs coming from DXR treatment, and h-PODs in co-cultures treated for 24h with MSC-EVs after treatment with DXR. In both cases, after treatments the podocytes were detached, and a cell viability analysis was performed.

From the study of cell viability (Figure 7) a positive response to 24h therapy with MSC-EVs emerges, compared to cells that had only undergone treatment with DXR.

5.5 Discussion

Fluidic 3D models represent the future for pre-clinical *in vitro* experimentation. This is especially true for organs physiologically very affected by hemodynamics, such as liver, heart, kidney.

We propose a simplified human glomerulus *in vitro*, which reproduces all the most important characteristics: the 3-layer structure, the presence of human endothelial cells and podocytes, the continuous perfusion of fluid that mimics hemodynamics.

Glomerular hemodynamics are dependent upon integrated mechanical forces (including filtration pressure, flow, shear force, and traction force) which act by modifying cells and extracellular structures and which are fundamental for signaling and cell communication pathways. Changes in ultrafiltrate flow underlie the pathogenesis of many kidney diseases [33,34]. The flow of fluid acting on the glomerulus applies tangential forces and increased shear stress on the podocyte at 2 different sites: the foot processes, while the ultrafiltrate flows through the filter slots and the body surface of the podocyte, while the ultrafiltrate makes its way within Bowman's space [35]. The podocyte body is stretched, foot processes are deformed, and cell body thinned, with bulging into the urinary space. It has been suggested that the mild to moderate foot process effacement that develops is an adaptive phenomenon improving podocyte adhesion and hindering its detachment [36]. These changes lead to podocyte detachment, extensive denudation of the GBM, adherence of the capillary wall to Bowman's capsule, synechia and finally segmental sclerosis. These forces, and consequently these cellular responses, are not visible in traditional two-dimensional cultures and this does not make them optimal for the study of renal pathophysiology.

The use of type IV collagen for membrane lining is important for the preservation of podocyte properties and the formation of endothelial monolayers. IV collagen is the physiological collagen present in the glomerular basement membrane to which both podocytes and endothelial cells adhere *in vivo* [37]. The extracellular matrix, which includes basement membranes, is known to regulate both

tissue architecture and cell phenotype through matrix receptors, such as integrins, cells are able to detect matrix changes, which induce intracellular signals that regulate multiple cellular events, influencing their survival, differentiation and gene expression [38].

Fundamental feature of our model is also the use of human cell lines. It has in fact been determined that both the response to renal damage [39] and the murine cellular characteristics [40] are different from human conditions. Kidney toxicity is one major cause of drug attrition and failure. Only 2% of drug development failures are screened in the preclinical stage, and serious adverse effects in 420% of new medicines are discovered only after the clinical stages. In the study of renal toxicity, the currently most used pre-clinical models cannot be effective in predicting. Organ-on-a-chip technology may be the optimal solution, which has minimal functional units that use primary human cells, rather than animal cells, like a real human organ. The ideal methods will not only use human cells, but will also mimic the 3D architecture and flow conditions within real human organs [1], with our system we have set ourselves this goal. Moreover, our Glomerulus-on-a-chip could be used in the future in a multi-organ curcuito, able for example to predict the metabolism of a drug [41].

Another interesting feature that distinguishes our model from most organ-on-a-chip models is the volume of fluid capable of flowing inside the circuit, not in the order of microliters, but in the order of milliliters. This fact, on the one hand, limits the number of repetitions of a given experiment that can be done at one time, but on the other hand it facilitates the execution and the possibility of reusing the cells after the dynamics. For example, one of the major problems of using micro-fluidic systems is the formation of bubbles, that arise because of the small size. Before or during the perfusion of fluid, bubbles can form easily in the channels of devices but are difficult to remove [42]. Cells in the device are very susceptible to detachment and injury from such bubbles, although in some cases, such air – liquid interface – mediated injury itself can be physiologically relevant such as mimic lung injury. In most cases, researchers should carefully avoid bubbles or dust. Using our system, the bubbles formed at the beginning of perfusion in the bioreactor can be easily removed by placing the

bioreactor in a vertical position, with the output tubes facing upwards and connected to the collection tanks. After disconnecting the bioreactors from the pumping system, the cells can be analyzed both microscopically (the analysable surface is large and the membranes can be sectioned), as well as for gene or protein analysis. The PET membranes used are completely transparent, allowing the visualization of the cells during the experiment and afterwards.

In order to evaluate the barrier functionality, we thought of an assay that was significant from the pathophysiological point of view and also simple to perform. Taking a cue from what had already been reported in literature, but adapting it to our needs, we examined the passage through the barrier of BSA-FITC. The passage of serum albumin from the endothelial lumen to the urinary lumen is universally recognized as an index of renal damage. After examining different timing and flow rates, we decided for the minimum time that allowed us to have an appreciable difference in filtration percentage (3h) and for the maximum speed that guaranteed cell adhesion (80 μ l/min). The multiple differences between the volumes, surfaces, cell density, flow rate, shear stress of the different fluidic systems proposed so far, however, makes a comparison difficult. A comparison with what happens at the glomerulus level in the human organism is even more difficult. These are systems that approximate the glomerular cell response in a more physiological way than traditional culture models. It must be considered as a further step towards a more detailed investigation of the cellular and molecular processes that characterize GFB.

To test the reliability of the dynamic model, we used Doxorubicin (DXR), the most effective anticancer drug available today. Despite this, DXR induces induced renal toxicity that overshadows its anticancer effects. Organ toxicity after doxorubicin infusion is a major cause for discontinuation of treatment [43]. Moreover, DXR has been widely used as a rodent model of proteinuric nephropathy leading to renal fibrosis [44]. We perfused the co-cultures with DXR for 3h and after 24h of perfusion with simple culture medium we examined them, verifying an effective decrease in renal viability and

an increase in cell damage markers. the concentration (0.5 ug / ml) was chosen in such a way as to produce acute but potentially reversible kidney damage.

One of the greatest potential of this model is also the possibility of testing therapeutic molecules, as a tool to optimize subsequent animal experimentation. Extracellular vesicles (EVs), membrane vesicles that are secreted by a variety of mammalian cell types, have been shown to play an important role in intercellular communication. The contents of EVs, including proteins, microRNAs, and mRNAs, vary according to the cell type that secreted them. Accordingly, researchers have demonstrated that EVs derived from various cell types play different roles in biological phenomena. Considering the ubiquitous presence of mesenchymal stem cells (MSCs) in the body, MSC-derived EVs may take part in a wide range of events. In particular, MSCs have recently attracted much attention due to the therapeutic effects of their secretory factors. MSC-derived EVs may therefore provide novel therapeutic approaches [45]. In the last few years, several groups have investigated the therapeutic potential of MSC-derived EVs. Their therapeutic effects have been observed in several different types of diseases, including kidney injury, cardiac injury, and brain injury. These findings strongly support the idea that MSC-derived EVs imitate the phenotype of parent MSCs and hold therapeutic potential for a wide range of diseases. Since the recovery capacity of MSCs has been attributed to their secretory activity, extracellular vesicles originating from these cells have been tested on the kidney, due to the evidence showing the nephron's ability to repopulate after injury. As a part of the paracrine effect, Camussi's group demonstrated that BM-MSC-derived EVs protected acute kidney injury (AKI), using a model mouse induced with glycerol [46]. The effect of EVs on the recovery of AKI was similar to that of MSCs. EVs induced proliferation and resistance to apoptosis in tubular epithelial cells. This effect was also confirmed using a lethal version of cisplatin induced AKI [18]. Furthermore, the same group showed that a single administration of MSC-derived EVs immediately after ischemia-reperfusion injury protected against the development of both acute and chronic kidney injury [17]. The 24h administration of MSC-EVs to the co-cultures through the

dynamic system tries to mimic the blood passage of vesicles inside the blood lumen through the barrier, after a pharmacological acute glomerular injury. After several tests, we found the minimum effective dose to be 2×10^4 EVs per cell. At this concentration we obtained a significant decrease in cell mortality, justified by the effective penetration of the vesicles within the cell types present in the glomerulus *in vitro*, in particular within the podocytes. Also evaluation of miRNA content of podocytes treated in the dynamic model with vesicles electroporated with miRNA 39 of *C.El.*, gave a positive result. Finally, the observation of the internalization of the EVs obtained from serum is also very important. This in fact could be the basis for the use of autologous EVs of the patient, suitably engineered according to the therapeutic needs. The use of serum-EVs could speed up the purification times of the vesicles and not generate doubts about the immune-compatibility, being autologous.

References

1. Kim, S.; Takayama, S. Organ-on-a-chip and the kidney. *Kidney Res. Clin. Pract.* **2015**, *34*, 165–9.
2. Ashammakhi, N.; Wesseling-Perry, K.; Hasan, A.; Elkhammas, E.; Zhang, Y.S. Kidney-on-a-chip: untapped opportunities. *Kidney Int.* **2018**, *94*, 1073–1086.
3. Hruby, Z.; Lowry, R.P. Growth *in vitro* of cells from renal glomerulus difficulties in establishing long-term cultures of rat glomerular endothelium. *Int. Urol. Nephrol.* **1989**, *21*, 105–112.
4. Haraldsson, B.; Nyström, J. The glomerular endothelium. *Curr. Opin. Nephrol. Hypertens.* **2012**, *21*, 258–263.
5. Naylor, R.W.; Morais, M.R.P.T.; Lennon, R. Complexities of the glomerular basement membrane. *Nat. Rev. Nephrol.* **2020**, 1–16.
6. Reiser, J.; Altintas, M.M. Podocytes. *F1000Research* **2016**, *5*.
7. Richard Kitching, A.; Hutton, H.L. The players: Cells involved in glomerular disease. *Clin. J. Am. Soc. Nephrol.* **2016**, *11*, 1664–1674.
8. Leung, N.; Drosou, M.E.; Nasr, S.H. Dysproteinemias and glomerular disease. *Clin. J. Am. Soc. Nephrol.* **2018**, *13*, 128–139.
9. Henne, W.M.; Buchkovich, N.J.; Emr, S.D. The ESCRT Pathway. *Dev. Cell* **2011**, *21*, 77–91.
10. Ranghino, A.; Bruno, S.; Bussolati, B.; Moggio, A.; Dimuccio, V.; Tapparo, M.; Biancone, L.; Gontero, P.; Frea, B.; Camussi, G. The effects of glomerular and tubular renal progenitors and derived extracellular vesicles on recovery from acute kidney injury. *Stem Cell Res. Ther.* **2017**, *8*, 1–15.
11. Choi, H.Y.; Moon, S.J.; Ratliff, B.B.; Ahn, S.H.; Jung, A.; Lee, M.; Lee, S.; Lim, B.J.; Kim, B.S.; Plotkin, M.D.; et al. Microparticles from kidney-derived mesenchymal stem cells act as carriers of proangiogenic signals and contribute to recovery from acute kidney injury. *PLoS One* **2014**, *9*.
12. Jiang, Z.Z.; Liu, Y.M.; Niu, X.; Yin, J.Y.; Hu, B.; Guo, S.C.; Fan, Y.; Wang, Y.; Wang, N.S. Exosomes secreted by human urine-derived stem cells could prevent kidney complications from type i diabetes in rats. *Stem Cell Res. Ther.* **2016**, *7*.
13. Nagaishi, K.; Mizue, Y.; Chikenji, T.; Otani, M.; Nakano, M.; Konari, N.; Fujimiya, M. Mesenchymal stem cell therapy ameliorates diabetic nephropathy via the paracrine effect of renal trophic factors including exosomes. *Sci. Rep.* **2016**, *6*.
14. Conaldi, P.G.; Bottelli, A.; Baj, A.; Serra, C.; Fiore, L.; Federico, G.; Bussolati, B.; Camussi, G. Human immunodeficiency virus-1 Tat induces hyperproliferation and dysregulation of renal glomerular epithelial cells. *Am. J. Pathol.* **2002**, *161*, 53–61.
15. Conaldi, P.G.; Biancone, L.; Bottelli, A.; De Martino, A.; Camussi, G.; Toniolo, A. Distinct

pathogenic effects of group B coxsackieviruses on human glomerular and tubular kidney cells. *J. Virol.* **1997**, *71*, 9180–9187.

16. Saleem, M.A.; O'Hare, M.J.; Reiser, J.; Coward, R.J.; Inward, C.D.; Farren, T.; Xing, C.Y.; Ni, L.; Mathieson, P.W.; Mundel, P. A Conditionally Immortalized Human Podocyte Cell Line Demonstrating Nephrin and Podocin Expression. *J. Am. Soc. Nephrol.* **2002**, *13*.
17. Gatti, S.; Bruno, S.; Deregibus, M.C.; Sordi, A.; Cantaluppi, V.; Tetta, C.; Camussi, G. Microvesicles derived from human adult mesenchymal stem cells protect against ischaemia-reperfusion-induced acute and chronic kidney injury. *Nephrol. Dial. Transplant.* **2011**, *26*, 1474–1483.
18. Bruno, S.; Grange, C.; Collino, F.; Deregibus, M.C.; Cantaluppi, V.; Biancone, L.; Tetta, C.; Camussi, G. Microvesicles Derived from Mesenchymal Stem Cells Enhance Survival in a Lethal Model of Acute Kidney Injury. *PLoS One* **2012**, *7*, e33115.
19. Zhou, M.; Zhang, X.; Wen, X.; Wu, T.; Wang, W.; Yang, M.; Wang, J.; Fang, M.; Lin, B.; Lin, H. Development of a Functional Glomerulus at the Organ Level on a Chip to Mimic Hypertensive Nephropathy. *Sci. Rep.* **2016**, *6*, 31771.
20. Pomatto, M.A.C.; Bussolati, B.; D'Antico, S.; Ghiotto, S.; Tetta, C.; Brizzi, M.F.; Camussi, G. Improved Loading of Plasma-Derived Extracellular Vesicles to Encapsulate Antitumor miRNAs. *Mol. Ther. - Methods Clin. Dev.* **2019**, *13*, 133–144.
21. Borza, C.M.; Borza, D.B.; Pedchenko, V.; Saleem, M.A.; Mathieson, P.W.; Sado, Y.; Hudson, H.M.; Pozzi, A.; Saus, J.; Abrahamson, D.R.; et al. Human podocytes adhere to the KRGDS motif of the $\alpha 3\alpha 4\alpha 5$ collagen IV network. *J. Am. Soc. Nephrol.* **2008**, *19*, 677–684.
22. Musah, S.; Dimitrakakis, N.; Camacho, D.M.; Church, G.M.; Ingber, D.E. Directed differentiation of human induced pluripotent stem cells into mature kidney podocytes and establishment of a Glomerulus Chip. *Nat. Protoc.* **2018**, *13*, 1662–1685.
23. Li, M.; Corbelli, A.; Watanabe, S.; Armelloni, S.; Ikehata, M.; Parazzi, V.; Pignatari, C.; Giardino, L.; Mattinzoli, D.; Lazzari, L.; et al. Three-dimensional podocyte–endothelial cell co-cultures: Assembly, validation, and application to drug testing and intercellular signaling studies. *Eur. J. Pharm. Sci.* **2016**, *86*, 1–12.
24. Sureshbabu, A.; Okajima, H.; Yamanaka, D.; Shastri, S.; Tonner, E.; Rae, C.; Szymanowska, M.; Shand, J.H.; Takahashi, S.I.; Beattle, J.; et al. IGFBP-5 induces epithelial and fibroblast responses consistent with the fibrotic response. In Proceedings of the Biochemical Society Transactions; Biochem Soc Trans, 2009; Vol. 37, pp. 882–885.
25. Asanuma, K.; Yanagida-Asanuma, E.; Faul, C.; Tomino, Y.; Kim, K.; Mundel, P. Synaptopodin orchestrates actin organization and cell motility via regulation of RhoA signalling. *Nat. Cell Biol.* **2006**, *8*, 485–491.
26. Lausecker, F.; Tian, X.; Inoue, K.; Wang, Z.; Pedigo, C.E.; Hassan, H.; Liu, C.; Zimmer, M.; Jinno, S.; Huckle, A.L.; et al. Vinculin is required to maintain glomerular barrier integrity. *Kidney Int.* **2018**, *93*, 643–655.
27. Chistiakov, D.A.; Orekhov, A.N.; Bobryshev, Y. V. Effects of shear stress on endothelial

cells: go with the flow. *Acta Physiol.* 2017, 219, 382–408.

28. Kutikhin, A.G.; Sinitsky, M.Y.; Yuzhalin, A.E.; Velikanova, E.A. Shear stress: An essential driver of endothelial progenitor cells. *J. Mol. Cell. Cardiol.* 2018, 118, 46–69.
29. Goldberg, S.; Adair-Kirk, T.L.; Senior, R.M.; Miner, J.H. Maintenance of glomerular filtration barrier integrity requires laminin $\alpha 5$. *J. Am. Soc. Nephrol.* **2010**, 21, 579–586.
30. Iampietro, C.; Bellucci, L.; Arcolino, F.O.; Arigoni, M.; Alessandri, L.; Gomez, Y.; Papadimitriou, E.; Calogero, R.A.; Cocchi, E.; Van Den Heuvel, L.; et al. Molecular and functional characterization of urine-derived podocytes from patients with Alport syndrome. *J. Pathol.* **2020**, 252, 88–100.
31. Mulcahy, L.A.; Pink, R.C.; Carter, D.R.F. Routes and mechanisms of extracellular vesicle uptake. *J. Extracell. Vesicles* 2014, 3.
32. Shoji, M.; Kobayashi, K.; Takemoto, M.; Sato, Y.; Yokote, K. Urinary podocalyxin levels were associated with urinary albumin levels among patients with diabetes. *Biomarkers* **2016**, 21, 164–167.
33. Chagnac, A.; Zingerman, B.; Rozen-Zvi, B.; Herman-Edelstein, M. Consequences of Glomerular Hyperfiltration: The Role of Physical Forces in the Pathogenesis of Chronic Kidney Disease in Diabetes and Obesity. *Nephron* **2019**, 143, 38–42.
34. Blantz, R.C.; Gabbai, F.B.; Blantz, R.C. Glomerular hemodynamics in pathophysiologic conditions. *Am. J. Hypertens.* **1989**, 2, 208S-212S.
35. Kriz, W.; Lemley, K. V. A potential role for mechanical forces in the detachment of podocytes and the progression of CKD. *J. Am. Soc. Nephrol.* 2015, 26, 258–269.
36. Srivastava, T.; Celsi, G.E.; Sharma, M.; Dai, H.; McCarthy, E.T.; Ruiz, M.; Cudmore, P.A.; Alon, U.S.; Sharma, R.; Savin, V.A. Fluid flow shear stress over podocytes is increased in the solitary kidney. *Nephrol. Dial. Transplant.* **2014**, 29, 65–72.
37. Miner, J.H. Glomerular basement membrane composition and the filtration barrier. In *Proceedings of the Pediatric Nephrology*; Springer, 2011; Vol. 26, pp. 1413–1417.
38. Schwartz, M.A. Integrin signaling revisited. *Trends Cell Biol.* **2001**, 11, 466–70.
39. Si, H.; Banga, R.S.; Kapitsinou, P.; Ramaiah, M.; Lawrence, J.; Kambhampati, G.; Gruenwald, A.; Bottinger, E.; Glicklich, D.; Tellis, V.; et al. Human and Murine Kidneys Show Gender- and Species-Specific Gene Expression Differences in Response to Injury. *PLoS One* **2009**, 4, e4802.
40. Chittiprol, S.; Chen, P.; Petrovic-Djergovic, D.; Eichler, T.; Ransom, R.F. Marker expression, behaviors, and responses vary in different lines of conditionally immortalized cultured podocytes. *Am. J. Physiol. - Ren. Physiol.* **2011**, 301, F660.
41. Maschmeyer, I.; Lorenz, A.K.; Schimek, K.; Hasenberg, T.; Ramme, A.P.; Hübner, J.; Lindner, M.; Drewell, C.; Bauer, S.; Thomas, A.; et al. A four-organ-chip for interconnected long-term co-culture of human intestine, liver, skin and kidney equivalents. *Lab Chip* **2015**, 15, 2688–2699.

42. Huh, D.; Fujioka, H.; Tung, Y.-C.; Futai, N.; Paine, R.; Grotberg, J.B.; Takayama, S. Acoustically detectable cellular-level lung injury induced by fluid mechanical stresses in microfluidic airway systems. *Proc. Natl. Acad. Sci. U. S. A.* **2007**, *104*, 18886–91.
43. Hassan, M.H.; Ghobara, M.; Abd-Allah, G.M. Modulator Effects of Meloxicam against Doxorubicin-Induced Nephrotoxicity in Mice. *J. Biochem. Mol. Toxicol.* **2014**, *28*, 337–346.
44. Grant, M.K.O.; Seelig, D.M.; Sharkey, L.C.; Choi, W.S.V.; Abdelgawad, I.Y.; Zordoky, B.N. Sexual dimorphism of acute doxorubicin-induced nephrotoxicity in C57Bl/6 mice. *PLoS One* **2019**, *14*.
45. Yao, J.; Zheng, J.; Cai, J.; Zeng, K.; Zhou, C.; Zhang, J.; Li, S.; Li, H.; Chen, L.; He, L.; et al. Extracellular vesicles derived from human umbilical cord mesenchymal stem cells alleviate rat hepatic ischemia-reperfusion injury by suppressing oxidative stress and neutrophil inflammatory response. *FASEB J.* **2019**, *33*, 1695–1710.
46. Bruno, S.; Grange, C.; Deregibus, M.C.; Calogero, R.A.; Saviozzi, S.; Collino, F.; Morando, L.; Busca, A.; Falda, M.; Bussolati, B.; et al. Mesenchymal stem cell-derived microvesicles protect against acute tubular injury. *J. Am. Soc. Nephrol.* **2009**, *20*, 1053–67.

6. Application of millifluidic device in renal disease models


The glomerular dynamic model was created starting from a static model. This model, from which the cell plating and permeability evaluation protocol was translated, was necessary to carry out initial tests, as well as to have higher experimental numbers.

In the first work presented below, published in September 2020, both culture systems were used. C. Iampietro and colleagues isolated, characterized and immortalized podocytes from urine of patients with Alport Syndrome. In this congenital pathology, an incorrect assembly of type IV collagen, a fundamental component of the glomerular basement membrane, causes severe renal failure. In this context, the dynamic system was achieved by avoiding the coating with collagen, usually carried out before cell plating. In addition, podocytes derived from AS patients and human glomerular endothelial cells were plated in co-culture. The results showed that the presence of these podocytes within the glomerular filtration barrier causes greater proteinuria than controls with healthy cells.

In the second work presented Prof Levtchenko's research team had successfully immortalized for the first time a podocyte line having a mutation, G2, for Apolipoprotein 1 (APOL1). In the African population, the G1 and G2 variants are related to pathological renal conditions. After characterizing the cell line, a functional test was needed to demonstrate the correlation with the glomerular defect. In this case, podocytes G2 or CTL were used in monoculture, under dynamic conditions. APOL1 expression was induced by placing poly (I: C), a synthetic double-stranded RNA agonist of TLR3, directly into the dynamic system. After 16 hours, ie the drug's peak functioning, glomerular filtration was evaluated.

The result in this case was very significant: the mutated podocyte population stimulated with Poly (I: C) increases filtration by more than 50 times compared to control podocytes or unstimulated G2.

Molecular and functional characterization of urine-derived podocytes from patients with Alport syndrome

Corinne Iampietro¹, Linda Bellucci¹, Fanny O Arcolino², Maddalena Arigoni¹, Luca Alessandri¹, Yonathan Gomez¹, Elli Papadimitriou¹, Raffaele A Calogero¹, Enrico Cocchi^{3,4}, Lambertus Van Den Heuvel², Elena Levtchenko^{2,5} and Benedetta Bussolati^{1*} 

¹ Department of Molecular Biotechnology and Health Sciences, University of Torino, Torino, Italy

² Laboratory of Pediatric Nephrology, Department of Development & Regeneration, University of Leuven, Leuven, Belgium

³ Department of Pediatric Nephrology, University of Torino, Torino, Italy

⁴ Division of Nephrology and Center for Precision Medicine and Genomics, Department of Medicine, Columbia University, New York, NY, USA

⁵ Department of Pediatric Nephrology, University Hospitals Leuven, Leuven, Belgium

*Correspondence to: B Bussolati, Molecular Biotechnology Centre, University of Torino, via Nizza 52, 10126 Torino, Italy.

E-mail: benedetta.bussolati@unito.it

Abstract

Alport syndrome (AS) is a genetic disorder involving mutations in the genes encoding collagen IV $\alpha 3$, $\alpha 4$ or $\alpha 5$ chains, resulting in the impairment of glomerular basement membrane. Podocytes are responsible for production and correct assembly of collagen IV isoforms; however, data on the phenotypic characteristics of human AS podocytes and their functional alterations are currently limited. The evident loss of viable podocytes into the urine of patients with active glomerular disease enables their isolation in a non-invasive way. Here we isolated, immortalized, and subcloned podocytes from the urine of three different AS patients for molecular and functional characterization. AS podocytes expressed a typical podocyte signature and showed a collagen IV profile reflecting each patient's mutation. Furthermore, RNA-sequencing analysis revealed 348 genes differentially expressed in AS podocytes compared with control podocytes. Gene Ontology analysis underlined the enrichment in genes involved in cell motility, adhesion, survival, and angiogenesis. In parallel, AS podocytes displayed reduced motility. Finally, a functional permeability assay, using a podocyte–glomerular endothelial cell co-culture system, was established and AS podocyte co-cultures showed a significantly higher permeability of albumin compared to control podocyte co-cultures, in both static and dynamic conditions under continuous perfusion. In conclusion, our data provide a molecular characterization of immortalized AS podocytes, highlighting alterations in several biological processes related to extracellular matrix remodelling. Moreover, we have established an *in vitro* model to reproduce the altered podocyte permeability observed in patients with AS.

© 2020 The Authors. *The Journal of Pathology* published by John Wiley & Sons Ltd on behalf of Pathological Society of Great Britain and Ireland.

Keywords: Alport syndrome; genetic defects; collagen IV; urine-derived podocytes; glomerular endothelial cells; co-culture; permeability

Received 10 January 2020; Revised 25 May 2020; Accepted 22 June 2020

No conflicts of interest were declared.

Introduction

Alport syndrome (AS) is a genetic disorder that affects one in every 50 000 newborns. Around 80% of AS families have X-linked inheritance caused by mutations in the *COL4A5* gene, while the others have autosomal recessive, or less commonly autosomal dominant, disease, caused by mutations in *COL4A3* or *COL4A4* genes [1]. These genes encode for three of the six different collagen IV α -chains ($\alpha 1$ – $\alpha 6$), which are assembled in type IV collagen networks [2,3]. Collagen IV $\alpha 3\alpha 4\alpha 5$ heterotrimer is the main component of the basal membrane in glomeruli, as well as in the cochlea, lens capsule, and retina [4,5]. Mutations in any one of the three genes lead to

the absence of the collagen IV $\alpha 3\alpha 4\alpha 5$ network, resulting in typical AS clinical features: kidney disease, hearing loss, and eye abnormalities [1].

In particular, the absence of a correct collagen IV $\alpha 3\alpha 4\alpha 5$ network impairs the functional properties of the glomerular filtration barrier [6]. During nephron maturation, podocytes express, assemble, and secrete collagen IV $\alpha 3\alpha 4\alpha 5$ proteins that replace the initial embryonic collagen IV $\alpha 1\alpha 1\alpha 2$ network in the glomerular basal membrane (GBM) [7]. After this developmental switch, the resulting mature GBM is a highly organized 300–400 nm thick collagen IV network [8]. In AS patients, alterations of the GBM, presenting as lamellation of the lamina densa, affect the function of podocytes, which appear to be the first altered cell type.

AS podocytes demonstrate foot process effacement, resulting in impaired filtration of blood and passage of blood and/or proteins into the urine [9,10]. Likewise, in murine models of AS disease (*Col4a3^{+/-}* and *Col4a3^{-/-}* mice), podocytes appear with specific morphological alterations characterized by long filamentous and round shaped projections as compared to the podocytes of wild-type mice [11].

Since in glomeruli, the production of the collagen IV $\alpha3\alpha4\alpha5$ heterotrimer is restricted to podocytes [12], their involvement in AS pathogenesis is of great interest. Recently, the analysis of kidney biopsies of AS patients clearly showed that podocyte loss starts as early as birth and results in the progressive reduction of podocyte number per glomerulus with time, correlating with overall renal damage [13]. In particular, podocyte number per glomerulus and podocyte nuclear density are significantly reduced in AS patients [14]. However, data on the phenotypic characteristics of human AS podocytes and their functional alterations are currently limited.

Several studies demonstrated that podocyte excretion is a natural phenomenon which precedes proteinuria [15,16] and that it might be a sensitive marker of glomerular damage [16–19]. Importantly, this phenomenon could also offer the possibility to isolate podocytes from normal subjects and patients with glomerular disorders [16]. Recently, podocytes isolated from the urine of AS patients have been used for genetic characterization of mutations [20]. However, the restricted cell doubling of primary AS podocytes limits their use as an *in vitro* model necessary for the characterization of their morphological, molecular, and functional profile.

The goal of our study was to set up a novel human *in vitro* model to evaluate possible functional and molecular alterations in human AS podocytes. Urine-derived podocytes from AS patients were isolated, immortalized, and cloned, and their gene expression profile was characterized by RNA sequencing, in comparison with normal urine-derived podocytes. Moreover, a three-dimensional system of podocyte–glomerular endothelial cell (GEC) co-culture was established to analyse the selective filtration of AS podocytes, compared with control podocytes. Permeability was measured in both static

and dynamic co-culture conditions, confirming the defective filtration observed in patients with AS.

Materials and methods

Patients

A total of three patients diagnosed with AS were recruited in this study. All parents of the AS patients provided informed signed consent for urine collection and subsequent experiments, and the Ethics Committee of the University Hospital Leuven approved the research protocol (S54695). The diagnosis was based on measuring creatinine levels and estimated glomerular filtration rate (eGFR) and was confirmed by the characterization of the mutated Alport syndrome genes (Table 1). Patient 1 had decreased eGFR [chronic kidney disease (CKD) stage 2], while patients 2 and 3 showed normal kidney function. All patients had proteinuria and were treated with enalapril. Patients 1 and 3 had perceptive hearing loss; patient 2 had normal hearing. Urine-derived podocytes were also isolated from a young healthy donor (Table 1).

Generation of podocyte cell lines

Freshly collected urine was centrifuged at $200 \times g$ for 10 min and the pellet was resuspended in DMEM/F-12 (Life Technologies, Carlsbad, CA, USA) supplemented with 10% FCS (Invitrogen, Carlsbad, CA, USA), 50 IU/ml penicillin, 50 g/ml streptomycin, 5 mM glutamine, 5 g/ml insulin, 5 g/ml transferrin, and 5 mg/ml selenium (all from Sigma-Aldrich, St Louis, MO, USA). Cells (AS and control podocytes) were immortalized and subcloned using a temperature-sensitive Simian virus 40 large T (SV40T) and human telomerase reverse transcriptase vectors, as described previously [21]. AB kidney-derived podocytes, immortalized using the same protocol and kindly gifted by MA Saleem, were used as an additional control [21].

Control and AS podocytes were grown at 33 °C and transferred to 37 °C for 10–14 days to obtain fully differentiated podocytes. Details are provided in

Table 1. Clinical features of control and AS patients.

Patient	Age (years)	Sex	Mutated gene	Mutation type	Mutation	Protein/creatinine (g/g)	eGFR (ml/min per 1.73 m ²)	Treatment
AS 1	14	F	COL4A3	Compound heterozygote	Maternal: p.(Glu647Argfs*45) c.1937dup Paternal: p.(Gly1602Alafs*13) c.4803del	0.47	71	Enalapril
AS 2	11	F	COL4A5	Heterozygote	p.(Gly926Alafs*70) c.2777del	0.6	135	Enalapril
AS 3	22	M	COL4A5	Hemizygote	p.Gly849Glu (c.2546G>A)	0.36	122	Enalapril
Control	11	F	–	–	–	Neg	–	–

eGFR: estimated glomerular filtration rate.

Normal protein/creatinine ratio: 0.2 g/g; normal eGFR: ≥ 90 ml/min per 1.73 m²; control: healthy urine donor.

supplementary material, Supplementary materials and methods.

Purification of glomerular endothelial cells (GECs)

Primary normal glomerular microvascular endothelial cells were previously obtained from cell outgrowths of human glomeruli and CD31 sorting, and characterized by morphology and expression of a panel of endothelial antigens [22] (see supplementary material, Supplementary materials and methods and Figure S1).

RNA extraction and RT-qPCR

RNA was extracted using Trizol (Life Technologies) according to the manufacturer's protocol. Aliquots of total RNA (200 ng) were reverse-transcribed using a High Capacity cDNA Reverse Transcription Kit (Applied Biosystems, Foster City, CA, USA). Levels of mRNA were assessed by qPCR, using a mix containing 5 ng of cDNA, 100 nM of each primer (see supplementary material, Supplementary materials and methods), and 1× SYBR Green PCR Master Mix (Applied Biosystems), and assembled into a 96-well StepOne Real Time System (Applied Biosystems). Negative cDNA controls were cycled in parallel in each run. Data are shown as relative quantification ($2^{-\Delta\Delta C_t}$). *GAPDH* expression was used to normalize cDNA inputs. Sample similarity plots were generated using Morpheus (<https://software.broadinstitute.org/morpheus/>).

Protein extraction and western blotting

Cell pellets were lysed at 4 °C for 15 min in RIPA buffer (Sigma) supplemented with protease and phosphatase inhibitors. Details are provided in supplementary material, Supplementary materials and methods.

ELISA assays

The concentrations of human VEGFA, Col4α3, and Col4α5 in protein lysate and supernatant of differentiated podocytes were measured using ELISA kits according to the manufacturer's instructions ($n = 3$ experiments in duplicate). Details may be found in supplementary material, Supplementary materials and methods.

RNA sequencing and analysis

Details are presented in supplementary material, Supplementary materials and methods. RNA-seq data have been deposited in the GEO database (<http://www.ncbi.nlm.nih.gov/projects/geo/>) under the GEO accession number GSE134011.

Single-cell tracking assay

For each condition, 2000 differentiated cells per well were seeded in a polystyrene, transparent 96-well plate, 6 h prior to the assay, in triplicate, as described

previously [23]. For 12 h, each well was imaged every 5 min at the same coordinates using 10× magnification. Live imaging was performed on a Zeiss LSM 880 Airyscan microscope (Carl Zeiss Microscopy GmbH, Oberkochen, Germany). Microscopy images were further processed and analysed using Zeiss ZEN imaging software (Carl Zeiss, Jena, Germany) and Fiji/ImageJ free software. In brief, ten cells were tracked per well, yielding 30 tracked cells per cell line. The total distance travelled and the speed of the individual cells were recorded.

Immunofluorescence

Immunostaining was performed on cells co-cultured for 48 h on an insert, fixed in 4% paraformaldehyde. Imaging was performed using a Leica TCS SP5 confocal system (Leica Microsystems S.r.l., Wetzlar, Germany). Details are provided in supplementary material, Supplementary materials and methods.

Three-dimensional co-culture assembly

For all co-culture experiments, GECs were seeded first on the lower PET membrane side at a density of 8×10^4 cells per 12-well insert (static co-culture: 3 μm pore size, Falcon-Corning, Glendale, AZ, USA; dynamic co-culture: 0.45 μm pore size, ipCELLCULTURE™ Track Etched Membrane, it4ip S.A., Louvain-la-Neuve, Belgium) and, after 6 h, podocytes were seeded on the upper side at the same density. Each cell type was cultured in its growth medium for 48 h before the permeability assay and medium were changed once the day after cell plating.

Millifluidic system

For dynamic experiments, we used a millifluidic device, fabricated by IVTech Srl (Lucca, Italy), consisting of two independent circuits that work in parallel. During permeability tests, the medium was maintained with a flow rate of 100 μl/min and cells in the chamber were subjected to a shear stress of 8×10^{-5} dyn/cm². To roughly calculate this value, the following equation was used: $\tau = 6\mu Q/bh^2$, where μ is the medium viscosity (g/cm per s), Q is the volumetric flow rate (cm³/s), b is the channel width, and h is the channel height [24–26].

Permeability assays

Permeability assays were performed after 48 h of co-culture by measuring BSA filtration. Complete medium (1 ml) containing or not FITC-BSA (1 mg/ml, Sigma) was placed in the lower endothelial and upper podocyte compartments, respectively. To measure the podocyte filtration ability in basal to apical direction, 100 μl of medium was taken after 6 h from the podocyte compartment and the passage of FITC-BSA was determined by fluorimetry in triplicate. For the dynamic system, podocyte medium enriched with FITC-BSA (1 mg/ml) was circulated into the endothelial compartment, while normal culture medium circulated into the upper

compartment. After 3 h of perfusion, the passage of BSA-FITC across the barrier was determined by sampling of fluid from the upper channel. FITC signal was measured in triplicates using a fluorimeter.

Statistics

Data are shown as mean \pm SD. At least three replicates were performed for each experiment. Two-tailed Student's *t*-tests were used for analysis when two groups of data were compared, while two-way ANOVA with Dunnett's multiple comparison test was applied when comparing more than two groups of data. All statistical analyses were performed using GraphPad Prism software version 6.0 (GraphPad Software, Inc, San Diego, CA, USA). $p < 0.05$ was considered significant.

Results

Generation of conditionally immortalized podocyte lines from urine of patients with AS

We generated conditionally immortalized podocytes from the urine of three different patients with AS (aged 16.5 \pm 5.5 years) and from a normal subject (aged 11 years). AS patient 1 showed compound heterozygous mutations in the *COL4A3* gene, while AS patients 2 and 3 had mutations in the *COL4A5* gene in heterozygosity and in hemizyosity, respectively (Table 1). All AS patients were characterized by an altered protein/creatinine ratio (0.48 \pm 0.12 g/g), but only patient 1 presented a mildly reduced eGFR (Table 1).

Primary urine-derived podocytes were immortalized by inducing the expression of temperature-sensitive SV40T and telomerase reverse transcriptase allowing growth at 33 °C and differentiation at 37 °C [21]. Nine clones were picked for each patient and were subsequently grown as separate cell lines. Conditionally immortalized podocytes previously obtained from a normal renal biopsy and characterized [21] were used as an additional control. At the permissive temperature of 33 °C, AS podocytes proliferate in a comparable way to normal urine-derived and kidney-derived podocytes, used as controls (Figure 1A). After 10–14 days at 37 °C, differentiated cells showed an irregular and enlarged cell body with formation of protrusions very similar to controls (Figure 1A).

Podocyte marker expression in differentiated AS podocytes

To confirm the podocyte feature of AS podocytes, three clones for each AS patient were analysed for the expression of the specific podocyte markers synaptopodin, podocalyxin, nephrin, podocin, WT1, and VEGFA. All markers were expressed by AS podocytes, although a reduction in some adhesion molecules in relation to urinary and tissue control podocytes was observed, in line with previous reports [27]. In particular, levels of

nephrin and podocin were reduced in AS podocytes compared with controls (Figure 1B), while synaptopodin showed only a trend for reduction. No differences were observed in WT1 expression. Increased expression of VEGFA was also found in AS patients 2 and 3 (Figure 1C). *VEGFA* transcript levels were also significantly increased in AS patient 2 compared with controls. AS podocytes also expressed lower levels of *SYNPO* mRNA, but not of *PODXL* (Figure 1D). Glomerular endothelial cells were used as a negative control (Figure 1D). The expression of podocyte markers in AS podocytes was significantly increased after 10–14 days of differentiation at 37 °C, in relation to proliferating cells at 33 °C (Figure 1E), as reported for control kidney-derived podocytes [21].

Taken together, these results indicate that AS podocytes express most of the typical podocyte markers, with a specific reduction of glomerular slit diaphragm proteins.

Collagen IV isoform expression in differentiated AS podocytes

In order to better evaluate the collagen IV characteristics in the three different AS patients of our study, we created 3D models of the protein secondary structure of the C-terminal C4 domains, the terminal portion predictable by 3D modelling (see supplementary material, Supplementary materials and methods). The models of Col4 α 3 and Col4 α 5 represent the normal 3D aspect of the protein C4 terminal domains. AS patient 1 presented frameshift mutations in *COL4A3* leading to a truncated amino-acid sequence at residues 690 (maternal allele) and 1613 (paternal allele), resulting in alterations of the conformation of C-terminal C4 residues as shown in Figure 2A. Similarly, frameshift mutation of *COL4A5* in AS patient 2 resulted in a truncated amino-acid sequence at residue 994, causing the protein to be truncated and unfolded (Figure 2A) from one of the two X chromosomes. In AS patient 3, a single nucleotide variant of *COL4A5* was present, leading to minor differences from the reference sequence, as shown in Figure 2A.

We subsequently analysed the expression of collagen IV isoforms in three clones for each patient. At protein level, *COL4A3* gene-mutated podocytes from AS patient 1 showed a significant reduction of COL4 α 3 protein in both the cell lysate and the supernatant compared with control (Figure 2B). In addition, COL4 α 5 protein was also reduced (Figure 2B). In parallel, podocytes from AS patients 2 and 3, mutated in the *COL4A5* gene, showed a significant reduction of Col4 α 5 protein compared with control both in cell lysates and in the supernatant (Figure 2C). A reduction in Col4 α 5 protein was confirmed in AS patient 3 by confocal microscopy (see supplementary material, Figure S2). COL4 α 3 protein was also reduced in the cell lysate, but not in the supernatant (Figure 2C), of AS patients 2 and 3, as confirmed at mRNA level in AS patient 2 (see supplementary material, Figure S3).

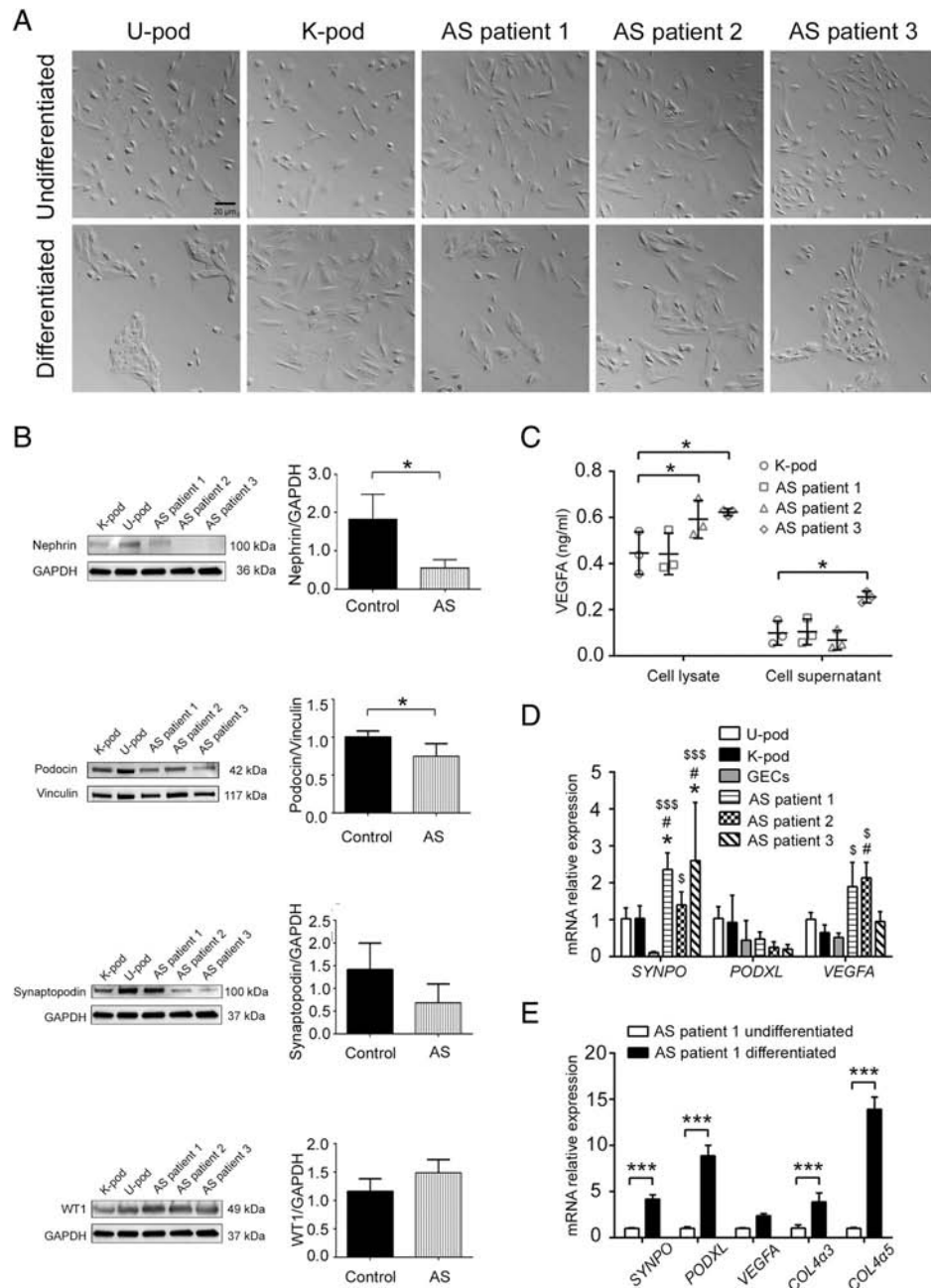


Figure 1. Morphology and marker expression of cultured AS podocytes. (A) Representative light microscopy images of undifferentiated (upper panels) and differentiated (lower panels) podocytes from normal urine (U-pod), normal kidney (K-pod), and AS patient urine. Original magnification: $\times 20$; scale bar: 20 μm . (B) Western blot analysis (representative images and quantification) of nephrin, podocin, synaptopodin, and WT1 of differentiated control (U-pod and K-pod) and AS podocytes. Data are expressed as mean \pm SD of band intensity normalized to vinculin or GAPDH of three different experiments. $*p < 0.05$. (C) VEGFA ELISA performed on cell lysates and cell supernatants obtained from differentiated AS podocytes, compared with control (K-pod). Data are mean \pm SD of three different experiments. $*p < 0.05$. (D) RT-qPCR for synaptopodin (*SYNPO*), podocalyxin (*PODXL*), and *VEGFA* transcripts. Data are shown as relative quantification, normalized to *GAPDH* and to control podocytes (U-pod). Three clones for each AS patient were used and data are expressed as mean \pm SD of three different experiments. GECs were used as a negative control. $*p < 0.05$ AS patient podocytes versus U-pod; $^{\#}p < 0.05$ AS patient podocytes versus kidney-derived podocytes (K-pod); $^{\$}p < 0.05$ and $^{\$ \$ \$}p < 0.0001$ AS patient podocytes versus GECs (negative control). (E) RT-qPCR for podocyte marker transcripts (*SYNPO*, *PODXL*, *VEGFA*) and collagen IV isoforms (*COL4A3*, *COL4A5*) of AS patient 1 podocytes before and after differentiation. Data shown as relative quantification, normalized to *GAPDH* and to undifferentiated AS patient 1 podocytes, expressed as mean \pm SD. $^{***}p < 0.0001$.

COL4A1 and *COL4A2* transcript levels appeared significantly increased in AS patient 1 compared with control podocytes (Figure 2D). These analyses confirm the alterations in collagen IV expression by AS podocyte lines, reflecting disease mutations.

RNA-sequencing analysis of differentiated AS podocytes

RNA sequencing was performed on podocytes isolated from urine of the three AS patients to investigate the characteristics of the AS transcriptome, using urine-

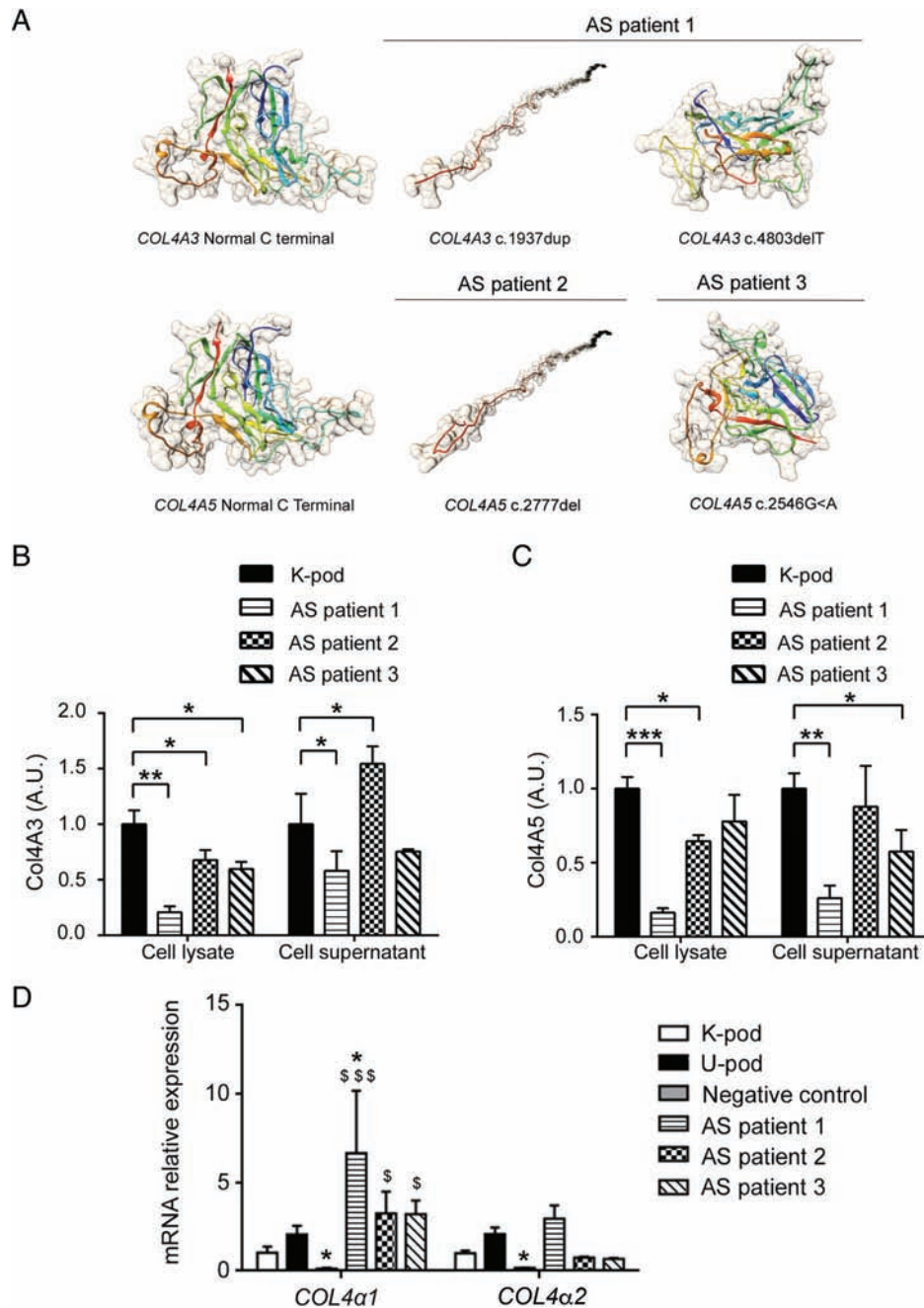


Figure 2. Collagen IV isoform expression in AS podocytes. (A) 3D models of the C-terminal C4 domains for Col4α3 and Col4α5 in AS patients were generated using *Phyre2* software, as described in supplementary material, Supplementary materials and methods. Images show the structural modifications of COL4α3 and COL4α5 chains predicted on the basis of the different mutations, compared with normal. In patients AS1 and AS2, frameshift mutations cause the protein to be truncated and with predicted alteration in folding (c.1937dup and c.2777del), or conformation (c.4803del). In patient AS3, a single nucleotide variant (c.2546G>A) leads to minor differences in protein folding. (B) COL4α3 ELISA performed on cell lysates and cell supernatants of differentiated AS podocytes and control kidney-derived podocytes (K-pod). (C) COL4α5 ELISA performed on cell lysates and cell supernatants of differentiated AS podocytes compared with control kidney-derived podocytes (K-pod). ELISA data are expressed as arbitrary units (A.U.) and are the mean ± SD of three different experiments normalized to control (referred to as 1). **p* < 0.05; ***p* < 0.001; ****p* < 0.0001. (D) RT-qPCR for *COL4A1* and *COL4A2* genes. Data are shown as relative quantification, normalized to *GAPDH* and to control kidney-derived podocytes (K-pod). Three clones for each AS patient were analysed and data are expressed as mean ± SD. GECs were used as a negative control. \$*p* < 0.05 and \$\$\$*p* < 0.0001 versus K-pod; **p* < 0.05 versus U-pod.

derived podocytes as a control. A specific signature composed of 68 podocyte-typical genes, previously described by Lu *et al* [28], was investigated. AS podocyte lines did not reveal significant differences from the control (Figure 3A,B), confirming the podocyte phenotype of all AS cell lines (three clones per patient).

To identify altered gene expression profiles specific for AS podocytes, we analysed the differential expression analysis of the three different AS podocyte lines (three clones per patient) with respect to control podocytes and detected a total of 348 deregulated genes (1 log₂ fold-change ≥ 0.8, adjusted *p* ≤ 0.1) out of 17 948

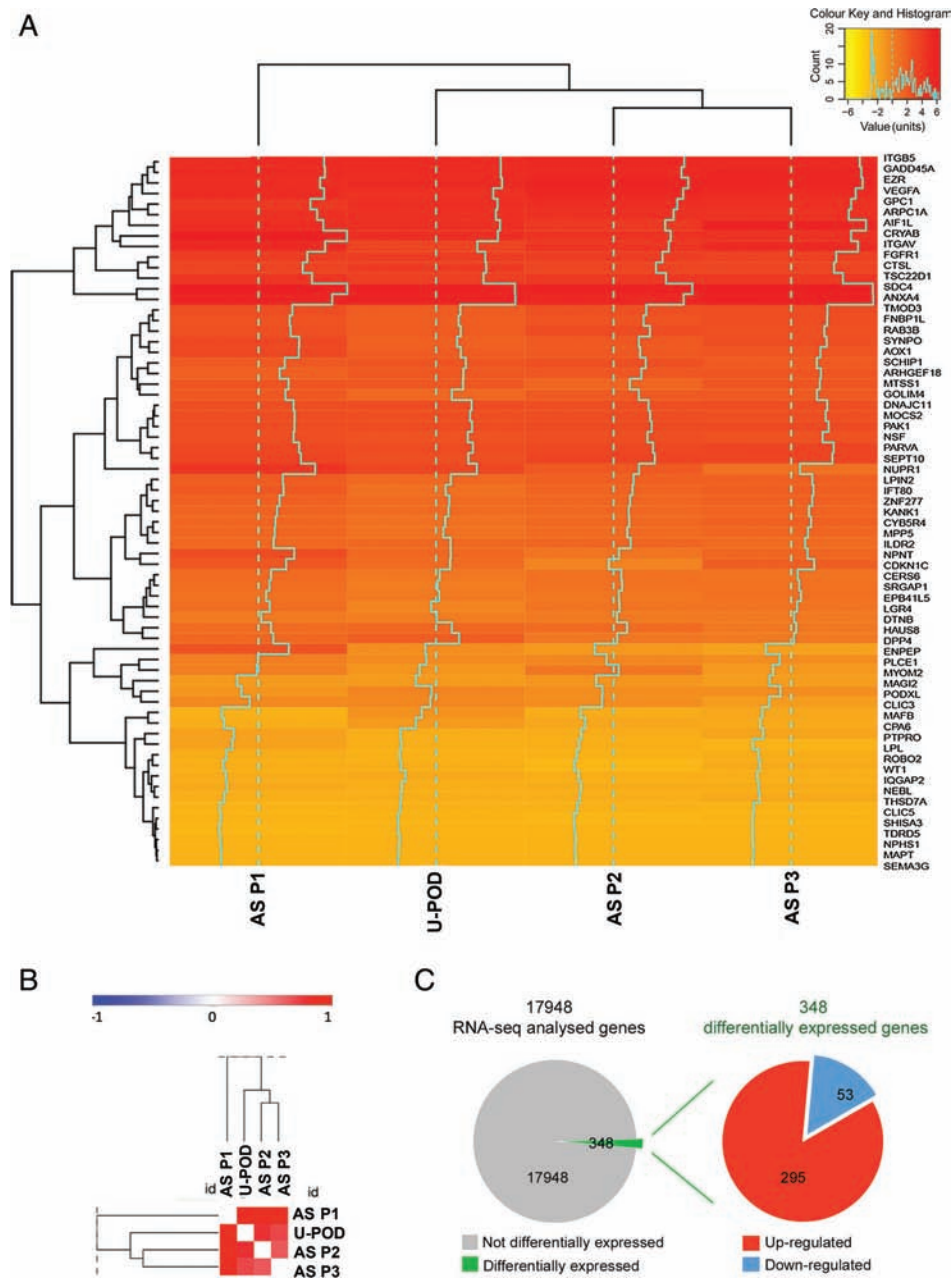


Figure 3. RNA-seq analysis of AS patients. (A) Heatmap of podocyte signatures showing similar levels of expression of podocyte genes in AS podocytes (three clones per patient) and in control podocytes (U-pod). (B) Pearson similarity plot of podocyte signature showing similar levels of expression of podocyte genes in AS podocytes (three clones per patient) and in control podocytes (U-pod). (C) Pie chart representation of up-regulated (red) and down-regulated (blue) differentially expressed transcripts in AS patient- compared with control urine-derived podocytes. RNA-seq was performed on three AS patients (AS P1, P2, P3), including three clones for each patient, and urine-derived podocytes (U-pod) as a control.

(Figure 3C). Specifically, 295 genes were up-regulated, while 53 were down-regulated. To functionally characterize the differentially expressed genes, Gene Ontology (GO) enrichment analysis was performed. GO enrichment analysis of biological processes highlighted the presence of genes involved in morphogenesis and development of a branching epithelium, extracellular matrix and structure organization, cell adhesion, and cellular response to endogenous stimulus (Table 2). Moreover, the GO cellular components confirmed the role of extracellular matrix and adhesion components (Table 2).

Using Ingenuity Pathways Analysis (IPA), we observed a high level of connectivity among a large subset of differentially expressed genes in AS podocytes (supplementary material, Figure S4). The differential expression, identified by RNA sequencing, of collagen molecules (*COL6A1*, *COL6A2*, *COL8A1*), *MMP2*, extracellular matrix–actin interactors (*LAMA5*, *TALIN2*, *RHOD*), and adhesion molecules (*SEMA5A*, *SEMA6A*) was confirmed by RT-qPCR analysis (Figure 4A). Moreover, players of the WNT signalling pathway (*WNT2B*, *WNT10A*) and molecules involved in cell

Table 2. Gene Ontology (GO) analysis of differentially expressed genes.

GO biological process	ID	Name	P value
1	GO:0060429	Epithelium development	3.618E-9
2	GO:0035295	Tube development	1.375E-8
3	GO:0061138	Morphogenesis of a branching epithelium	2.574E-8
4	GO:0002009	Morphogenesis of an epithelium	2.688E-8
5	GO:0007155	Cell adhesion	2.980E-8
6	GO:2000026	Regulation of multicellular organismal development	3.537E-8
7	GO:0030198	Extracellular matrix organization	3.907E-8
8	GO:0022610	Biological adhesion	3.931E-8
9	GO:0071495	Cellular response to endogenous stimulus	4.120E-8
10	GO:0043062	Extracellular structure organization	4.122E-8
GO cellular component	ID	Name	P value
1	GO:0031012	Extracellular matrix organization	1.062E-8
2	GO:0070161	Anchoring junction	1.614E-5
3	GO:0045178	Basal part of cell	1.905E-5
4	GO:0005912	Adherens junction	2.586E-5
5	GO:0030054	Cell junction	1.335E-4
6	GO:0005604	Basement membrane	1.600E-4
7	GO:0044420	Extracellular matrix component	2.458E-4
8	GO:0005615	Extracellular space	1.487E-4
9	GO:0005925	Focal adhesion	3.051E-4
10	GO:0005815	Microtubule organization centre	3.052E-4

This table (in two parts) shows the Gene Ontology (GO) analysis of differentially expressed genes in AS patients compared with control urine-derived podocytes: biological process and cellular component. In each table, the identification (ID) number, the name, and the *P* value associated with the GO are given.

survival (*IGFBP5*, *NGFR*) and angiogenesis (*THBS1*, *SERPINE1*) were also confirmed as differentially expressed in AS podocytes by RT-qPCR (Figure 4A).

Taken together, these data highlight differential expression in AS podocytes of genes involved in cell adhesion, motility, and survival, with alteration in extracellular matrix and cell junction component biosynthesis, including collagen molecules. We therefore analysed the possible impact of the altered podocyte phenotype on their ability to migrate. As shown in Figure 4B,C, AS podocytes showed reduced motility in terms of speed and distance with respect to controls.

Static permeability analysis of GEC–podocyte co-cultures

To study the functionality of AS podocytes *in vitro*, a co-culture system that mimics the interaction between GECs and podocytes was assembled. GECs were seeded on the bottom side of PET inserts, and differentiated kidney-derived or AS podocytes were seeded on the upper side (Figure 5A). The co-culture obtained consisted of two homogeneous confluent layers of cells separated by a porous PET membrane, as shown by immunofluorescence (Figure 5B,C). The orthogonal view of co-culture slides shows a single thick layer of differentiated podocytes with typical protrusions, separated by the thin membrane from a single flat layer of GECs (Figure 5B). The 3D reconstruction allowed the inspection, in all three dimensions, of the co-culture assembly (Figure 5C and supplementary material, Video S1).

A filtration assay was performed by measuring the transit of FITC-BSA from the lower GEC compartment to the upper podocyte compartment in different experimental conditions (Figure 5D,E). Albumin permeability

was significantly reduced when GECs or/and control podocytes were plated on the insert after 6 h of incubation ($p < 0.0001$). In particular, podocytes alone showed a higher resistance to albumin transit through the membrane than GECs alone. Interestingly, the presence of AS podocytes alone significantly increased albumin permeability after 6 h, compared with control podocytes alone ($p < 0.0001$). Finally, the same significantly increased permeability was obtained when GEC–AS podocyte co-cultures were compared with GEC–control podocyte co-cultures ($p < 0.0001$), reproducing the defective permeability typical in AS patients. Cell counts of the plated cells showed no significant difference between control and AS podocytes, excluding that the altered filtration of AS podocytes was due to an increased cell detachment.

Dynamic permeability analysis of GEC–podocyte co-cultures

To analyse the permeability of AS podocytes in dynamic conditions, we adopted a millifluidic system that allows continuous perfusion in co-culture under 8×10^{-5} dyn/cm² shear stress (Figure 6A). Cells plated on the PET membrane were maintained in the bioreactor for 48 h before starting the permeability assay (Figure 6B). The albumin filtration rate 3 h after GEC–AS podocyte co-culture was significantly higher than that in the GEC–control kidney-derived podocyte co-culture (Figure 6C, $p = 0.0012$), confirming the increased permeability in AS conditions. The permeability assays were therefore able to recapitulate the AS alterations and confirm from a functional point of view the altered podocyte phenotype demonstrated by molecular analysis.

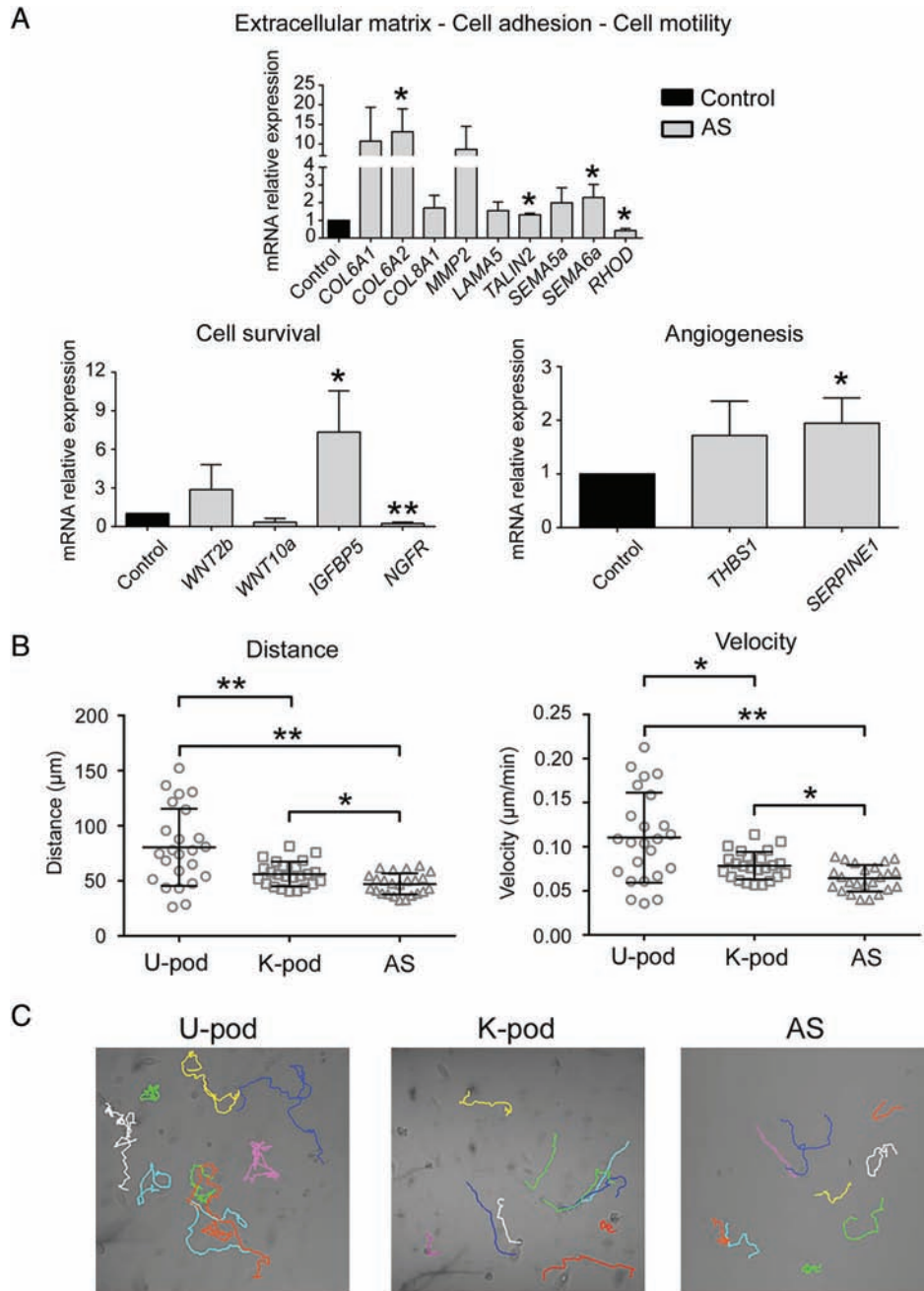


Figure 4. Validation of differentially expressed genes in AS. (A) mRNA expression of genes differentially expressed in AS related to cell motility, survival, and angiogenesis was evaluated by RT-qPCR. Data are shown as relative quantification, normalized to *GAPDH* and to control kidney-derived podocytes (K-pod). One clone for each AS patient was analysed and the results are expressed as mean \pm SD of the three AS patients. (B) Single-cell tracking assay showing reduced motility in AS podocytes compared with urine-derived podocytes (U-pod) and kidney-derived podocytes (K-pod). Three independent experiments were performed. * $p < 0.05$; ** $p < 0.001$. (C) Representative images of the cell motility of control podocytes and AS podocytes.

Discussion

Increasing evidence indicates that AS podocytes possess an altered phenotype, beyond their altered collagen IV synthesis, which can be involved in the pathogenesis and progression of the disease. In the present study, we isolated and characterized podocytes derived from the urine of three patients with AS, with genetic alterations of either *COL4A3* or *COL4A5*, to assess common pathological features due to collagen IV mutations. AS

podocytes showed specific changes in the transcript levels of genes involved in cell motility, adhesion, proliferation, and angiogenesis, with related alterations in their functional properties. In order to study their permeability *in vitro*, we set up a co-culture system that reproduced the functional aberrations typical of AS.

The availability of human AS podocytes in culture is at present limited. Podocyte-like cells have been recently obtained from induced pluripotent stem cells (iPS) of AS patients [29,30] and may represent a promising

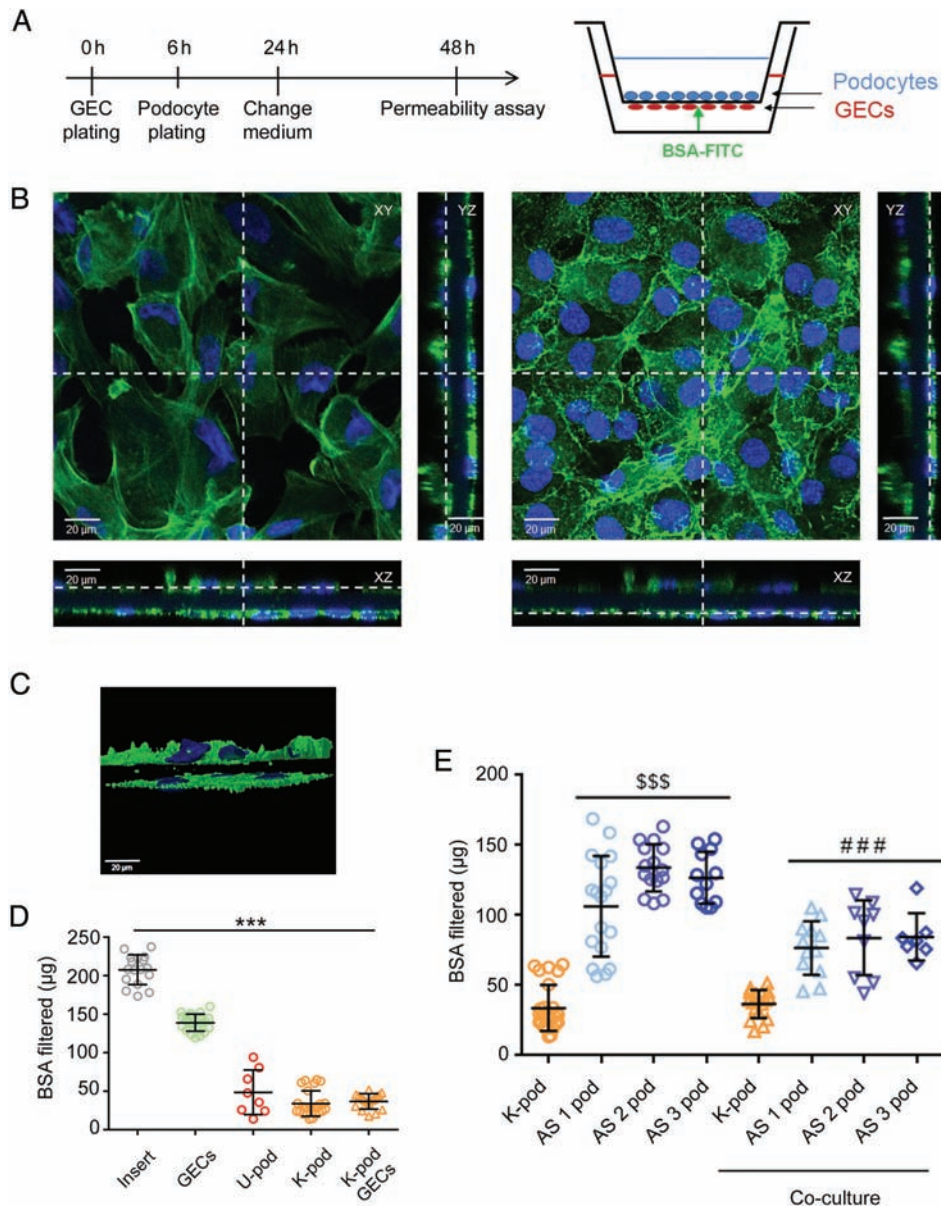


Figure 5. Static permeability assay in podocyte–GEC co-cultures. (A) Schematic representation of co-culture and experimental set-up: podocytes and GECs were co-cultured for 48 h before the permeability assay was performed, as described in the Materials and methods section. (B) Immunofluorescence of co-cultures showing the entire field and cross-sections (XZ and YZ) of both the upper podocyte layer (left) and the lower GEC layer (right). Cells were stained with phalloidin (green) and nuclear staining was performed with Hoechst dye 33342. Original magnification: $\times 400$. (C) Snapshot of a perspective view of 3D reconstruction of the co-culture system (see supplementary material, Video S1). (D, E) FITC-BSA permeability indicating albumin passage from the GEC compartment to the podocyte compartment was measured over 6 h. AS podocytes alone or in co-culture showed significantly increased filtration compared with control podocytes alone or in co-culture. Data are expressed as the mean amount of filtered BSA–FITC of four different experiments using at least three inserts for each condition in each experiment. $***p < 0.0001$ insert versus all conditions; $$$$p < 0.0001$ AS podocytes versus K-pod; $###p < 0.0001$ AS podocyte co-culture versus K-pod co-culture. U-pod: urine-derived podocytes; K-pod: kidney-derived podocytes; AS 1–2–3 pod: AS 1–2–3 patient podocytes.

approach. However, it might be difficult to obtain a pure population for podocyte characterization, as differentiated iPS cultures contained only 30–50% cells with podocyte-like morphology [29]. Human urine, both from patients and from healthy subjects, has been used previously as a non-invasive valuable source of podocytes [16]. In patients with active glomerular disease, podocytes are shed from the glomerulus as a response to local environmental factors. Urine-derived podocytes from both patient and healthy subjects appear positive

for podocyte markers, viable, and able to grow in culture [16]. For instance, urine-derived AS podocytes have been recently obtained and used for genetic studies [20]. In the present study, by exploiting the accelerated podocyte loss in patients with AS [13,14], we successfully isolated AS podocytes from the urine of three young patients with different collagen IV mutations; conditionally immortalized the primary cells; and generated clonal lines in order to avoid the presence of contaminating non-podocytic cell types [16]. A similar

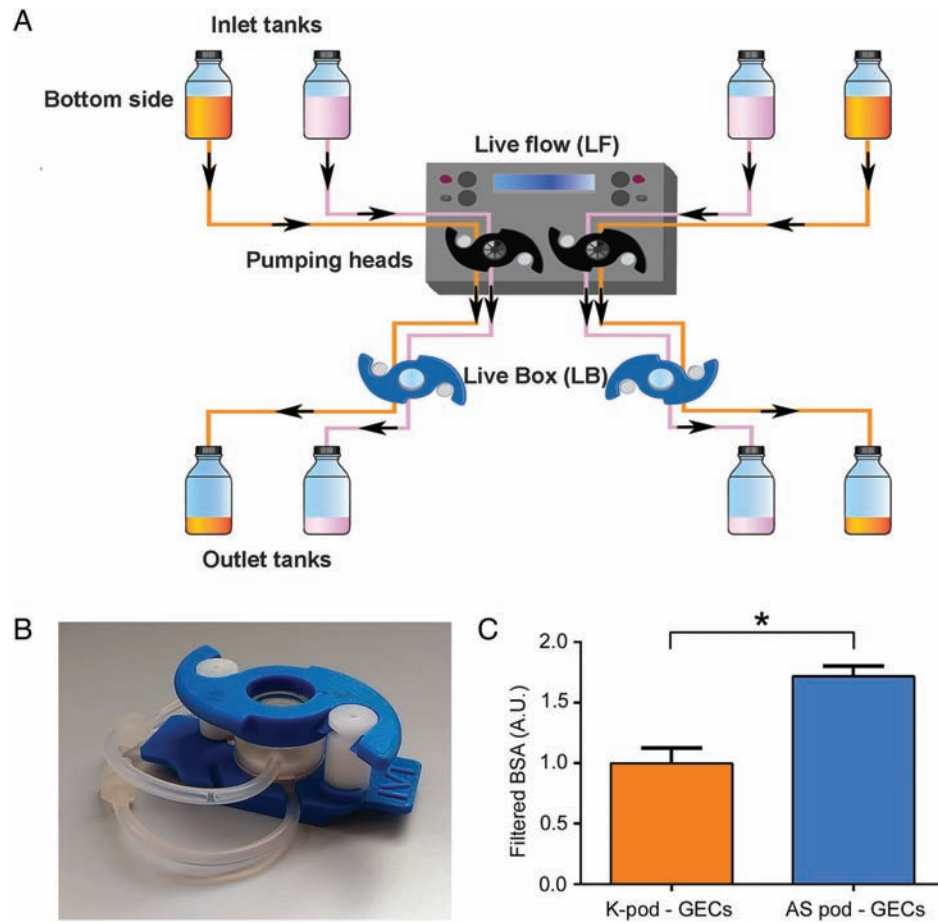


Figure 6. Millifluidic system and permeability assay in podocyte–GEC co-cultures. (A) Schematic representation of the millifluidic system, as described in the Materials and methods section. Cells seeded in the LiveBox (LB) were perfused with fluids circulated by peristaltic pumps at 100 $\mu\text{l}/\text{min}$ in two independent circuits. (B) Representative image of a chamber of LiveBox. (C) After 48 h of podocyte/GEC co-culture, the passage of FITC-BSA from the lower to the upper compartment was measured in the dynamic system over 3 h. The permeability in AS co-cultures was significantly higher than that in control kidney-derived co-cultures. Data are expressed as mean \pm SD of three different experiments performed in parallel in control and AS podocytes. * $p < 0.05$. K-pod: kidney-derived podocytes.

procedure has been described for urine-derived podocytes from patients with focal and segmental glomerulosclerosis [27].

The evaluation of a podocyte signature, using a panel of 68 previously described genes [28], demonstrated the podocyte nature of our clonal cell lines. Interestingly, we found down-regulation of nephrin, podocin, and synaptopodin in AS podocytes, confirming an observation already described in AS kidney biopsies [31]. The relevance of nephrin and synaptopodin levels was previously underlined by their negative correlation with the degree of proteinuria in AS patients [31]. Moreover, we confirmed in each AS podocyte line the alterations in the expression of the mutated collagen IV isoform, confirming that these AS lines are useful for investigating the defective collagen IV protein network and the related podocyte alterations.

Literature data describing the AS podocyte phenotype are quite scarce. Reduced podocyte number per glomerulus and podocyte nuclear density [14] are commonly described in human AS biopsies; however, podocyte hypertrophy is the only cell feature reported [32]. In a murine model of AS, electron microscopy analysis showed the presence of altered podocyte cell bodies with

disorganized primary processes and protrusions [11,33]. From a molecular point of view, the glomerular gene expression profile in a mouse model of AS highlighted induction of MMP-10 and of the matrix protein mindin, suggesting the involvement of matrix factors in progression [34]. Our study provides evidence of an altered phenotype of AS podocytes, in comparison with control podocytes, common to the three different collagen IV mutations, reflected into altered functions, namely decrease in cell motility and increase in permeability. By gene profiling, we identified restricted and specific alteration of pathways related to basal membrane adhesion, cytoskeleton modulation, and angiogenesis. These data clearly indicate that AS podocytes display altered features related to their interaction with the matrix. We identified 295 up-regulated and 53 down-regulated genes as compared to control urine-derived podocytes. Among differentially expressed genes, we found *MMP2*, whose altered expression was previously described in an AS canine model [35], and *LAMA5*, whose mRNA and protein up-regulation were shown in AS-mouse glomeruli [36]. Among the identified genes and pathways differentially expressed in AS podocytes, dysregulated activation of the WNT pathway has been

related to podocytopathies and proteinuria [37,38], while *IGFBP5* has been described as a promoter of epithelial and fibroblast responses in fibrosis [39].

Taken together, the data indicate a general alteration in AS podocytes of matrix interaction and cytoskeletal organization, both necessary to prevent podocyte effacement and maintain permeability control. For instance, reduction of synaptopodin, which in turn controls RhoA activity [40], as well as of cytoskeletal proteins such as vinculin, known to maintain an intact glomerular filtration barrier [41], may induce impairment of cell motility and increase permeability. Further investigation of small GTPase activities in urinary AS podocyte would be important to support the findings.

The observed alterations were reflected by altered podocyte functions, mainly related to cell motility and adhesion. Furthermore, we could reproduce the *in vivo* AS permeability alteration by assembling a co-culture system of AS podocytes and GECs. In our co-culture model, we preferred to avoid the addition of an exogenous collagen IV coating, as this GBM component is defective in AS [42]. In this system, we measured the passage of BSA-FITC from the lower (GEC compartment) to the upper (podocyte compartment) side, which is driven by osmotic forces and is halted by the presence of cellular elements [42,43]. Similar to the defective glomerular permeability in AS patients [1], AS podocyte–GEC co-cultures showed significantly increased filtration of albumin compared with the control co-cultures. To mimic the physiological haemodynamic component, we switched from a static to a dynamic model using a millifluidic device. Also in this dynamic system the permeability in AS podocyte–GEC co-culture was significantly increased. We are, however, aware that this model does not fully mimic the glomerular alterations observed in AS patients, due to the lack of a glomerular basal membrane. Moreover, the isolation of urinary AS podocytes detached by the glomerular basal membrane in a disease state may introduce a selection bias.

In conclusion, we describe here a new human *in vitro* model that molecularly and functionally reproduces the defective AS podocytes. Using urine-derived AS podocyte cell lines, we characterized molecular and morphological defects common to collagen IV mutation and related to cell adhesion, motility, survival, and angiogenesis. Moreover, altered permeability measured in AS podocyte–GEC co-culture underlines the potentiality of this model. In fact, this *in vitro* model could also be used for the screening of pharmacological compounds, which might restore functional properties to AS podocytes.

Acknowledgements

We thank Dr Moin Saleem for providing tissue-derived control podocytes. We thank Sandra Van Aerschot of the University of Leuven for performing cell culture and immortalization experiments, Marta Gai, and the Open Lab of Advanced Microscopy (OLMA) at the

Molecular Biotechnology Center (MBC) for support with confocal microscopy. This study was supported by the Ministry of Education, Universities and Research (MIUR), ex-60% (to BB).

Author contributions statement

CI performed characterization and functional experiments, statistical analysis, interpretation of results, and prepared the manuscript and all the figures. EC performed the 3D modelling. LB, FA, YG and EP performed *in vitro* experiments. MA, LA and RC performed RNA sequencing and data analysis. FA, LVDH and EL generated immortalized podocytes and contributed to the study design. BB contributed to the study design, study coordination, and interpretation of the data. All the authors were involved in writing the paper and had final approval of the submitted and published versions.

Data availability statement

RNA-seq data have been deposited in the GEO database under the GEO accession number GSE134011 (<https://www.ncbi.nlm.nih.gov/geo/query/acc.cgi?acc=GSE134011>).

References

1. Watson S, Padala SA, Bush JS. Alport Syndrome. In *StatPearls*. StatPearls Publishing: Treasure Island, FL, 2020.
2. Timpl R, Brown JC. Supramolecular assembly of basement membranes. *Bioessays* 1996; **18**: 123–132.
3. Sundaramoorthy M, Meiyappan M, Todd P, *et al*. Crystal structure of NC1 domains. Structural basis for type IV collagen assembly in basement membranes. *J Biol Chem* 2002; **277**: 31142–31153.
4. Sado Y, Kagawa M, Naito I, *et al*. Organization and expression of basement membrane collagen IV genes and their roles in human disorders. *J Biochem* 1998; **123**: 767–776.
5. Hudson BG. The molecular basis of Goodpasture and Alport syndromes: beacons for the discovery of the collagen IV family. *J Am Soc Nephrol* 2004; **15**: 2514–2527.
6. Kalluri R, Shield CF, Todd P, *et al*. Isoform switching of type IV collagen is developmentally arrested in X-linked Alport syndrome leading to increased susceptibility of renal basement membranes to endoproteolysis. *J Clin Invest* 1997; **99**: 2470–2478.
7. Abrahamson DR, Hudson BG, Stroganova L, *et al*. Cellular origins of type IV collagen networks in developing glomeruli. *J Am Soc Nephrol* 2009; **20**: 1471–1479.
8. Miner JH. Glomerular basement membrane composition and the filtration barrier. *Pediatr Nephrol* 2011; **26**: 1413–1417.
9. Cosgrove D, Liu S. Collagen IV diseases: a focus on the glomerular basement membrane in Alport syndrome. *Matrix Biol* 2017; **57–58**: 45–54.
10. Kruegel J, Rubel D, Gross O. Alport syndrome – insights from basic and clinical research. *Nat Rev Nephrol* 2013; **9**: 170–178.
11. Tsuji K, Suleiman H, Miner JH, *et al*. Ultrastructural characterization of the glomerulopathy in Alport mice by helium ion scanning microscopy (HIM). *Sci Rep* 2017; **7**: 11696.

12. Kuroda N, Yoshikawa N, Nakanishi K, et al. Expression of type IV collagen in the developing human kidney. *Pediatr Nephrol* 1998; **12**: 554–558.
13. Ding F, Wickman L, Wang SQ, et al. Accelerated podocyte detachment and progressive podocyte loss from glomeruli with age in Alport syndrome. *Kidney Int* 2017; **92**: 1515–1525.
14. Wickman L, Hodgin JB, Wang SQ, et al. Podocyte depletion in thin GBM and Alport syndrome. *PLoS One* 2016; **11**: e0155255.
15. Trimarchi H, Canzonieri R, Muryan A, et al. Podocyuria: a clue for the rational use of amiloride in Alport renal disease. *Case Rep Nephrol* 2016; **2016**: 1492743.
16. Vogelmann SU, Nelson WJ, Myers BD, et al. Urinary excretion of viable podocytes in health and renal disease. *Am J Physiol Renal Physiol* 2003; **285**: F40–F48.
17. Hara M, Yanagihara T, Kihara I. Cumulative excretion of urinary podocytes reflects disease progression in IgA nephropathy and Schönlein–Henoch purpura nephritis. *Clin J Am Soc Nephrol* 2007; **2**: 231–238.
18. Nakamura T, Ushiyama C, Suzuki S, et al. Urinary excretion of podocytes in patients with diabetic nephropathy. *Nephrol Dial Transplant* 2000; **15**: 1379–1383.
19. Yu D, Petermann A, Kunter U, et al. Urinary podocyte loss is a more specific marker of ongoing glomerular damage than proteinuria. *J Am Soc Nephrol* 2005; **16**: 1733–1741.
20. Daga S, Baldassarri M, Lo Rizzo C, et al. Urine-derived podocytes-lineage cells: a promising tool for precision medicine in Alport syndrome. *Hum Mutat* 2018; **39**: 302–314.
21. Saleem MA, O'Hare MJ, Reiser J, et al. A conditionally immortalized human podocyte cell line demonstrating nephrin and podocin expression. *J Am Soc Nephrol* 2002; **13**: 630–638.
22. Collino F, Bussolati B, Gerbaudo E, et al. Preeclamptic sera induce nephrin shedding from podocytes through endothelin-1 release by endothelial glomerular cells. *Am J Physiol Renal Physiol* 2008; **294**: F1185–F1194.
23. Ivanova EA, Arcolino FO, Elmonem MA, et al. Cystinosis deficiency causes podocyte damage and loss associated with increased cell motility. *Kidney Int* 2016; **89**: 1037–1048.
24. Jang KJ, Suh KY. A multi-layer microfluidic device for efficient culture and analysis of renal tubular cells. *Lab Chip* 2010; **10**: 36–42.
25. Duan Y, Gotoh N, Yan Q, et al. Shear-induced reorganization of renal proximal tubule cell actin cytoskeleton and apical junctional complexes. *Proc Natl Acad Sci U S A* 2008; **105**: 11418–11423.
26. Kim S, LeshnerPerez SC, Kim BC, et al. Pharmacokinetic profile that reduces nephrotoxicity of gentamicin in a perfused kidney-on-a-chip. *Biofabrication* 2016; **8**: 015021.
27. Sakairi T, Abe Y, Kajiyama H, et al. Conditionally immortalized human podocyte cell lines established from urine. *Am J Physiol Renal Physiol* 2010; **298**: F557–F567.
28. Lu Y, Ye Y, Bao W, et al. Genome-wide identification of genes essential for podocyte cytoskeletons based on single-cell RNA sequencing. *Kidney Int* 2017; **92**: 1119–1129.
29. Musah S, Dimitrakakis N, Camacho DM, et al. Directed differentiation of human induced pluripotent stem cells into mature kidney podocytes and establishment of a Glomerulus Chip. *Nat Protoc* 2018; **13**: 1662–1685.
30. Haynes JM, Selby JN, Vandekolk TH, et al. Induced pluripotent stem cell-derived podocyte-like cells as models for assessing mechanisms underlying heritable disease phenotype: initial studies using two Alport syndrome patient lines indicate impaired potassium channel activity. *J Pharmacol Exp Ther* 2018; **367**: 335–347.
31. Wang H, Yue Z, Wu J, et al. The accumulation of VEGFA in the glomerular basement membrane and its relationship with podocyte injury and proteinuria in Alport syndrome. *PLoS One* 2015; **10**: e0135648.
32. Heidet L, Gubler MC. The renal lesions of Alport syndrome. *J Am Soc Nephrol* 2009; **20**: 1210–1215.
33. Randles MJ, Collinson S, Starborg T, et al. Three-dimensional electron microscopy reveals the evolution of glomerular barrier injury. *Sci Rep* 2016; **6**: 35068.
34. Naudin C, Smith B, Bond DR, et al. Characterization of the early molecular changes in the glomeruli of *Cd151*^{-/-} mice highlights induction of mindin and MMP-10. *Sci Rep* 2017; **7**: 15987.
35. Rao VH, Lees GE, Kashtan CE, et al. Increased expression of MMP-2, MMP-9 (type IV collagenases/gelatinases), and MT1-MMP in canine X-linked Alport syndrome (XLAS). *Kidney Int* 2003; **63**: 1736–1748.
36. Abrahamson DR, Isom K, Roach E, et al. Laminin compensation in collagen $\alpha3(IV)$ knockout (Alport) glomeruli contributes to permeability defects. *J Am Soc Nephrol* 2007; **18**: 2465–2472.
37. Zhou L, Liu Y. Wnt/ β -catenin signalling and podocyte dysfunction in proteinuric kidney disease. *Nat Rev Nephrol* 2015; **11**: 535–545.
38. Chen L, Chen DQ, Wang M, et al. Role of RAS/Wnt/ β -catenin axis activation in the pathogenesis of podocyte injury and tubulo-interstitial nephropathy. *Chem Biol Interact* 2017; **273**: 56–72.
39. Sureshbabu A, Okajima H, Yamanaka D, et al. IGFBP-5 induces epithelial and fibroblast responses consistent with the fibrotic response. *Biochem Soc Trans* 2009; **37**: 882–885.
40. Asanuma K, Yanagida-Asanuma E, Faul C, et al. Synaptopodin orchestrates actin organization and cell motility via regulation of RhoA signalling. *Nat Cell Biol* 2006; **8**: 485–491.
41. Lausecker F, Tian X, Inoue K, et al. Vinculin is required to maintain glomerular barrier integrity. *Kidney Int* 2018; **93**: 643–655.
42. Li M, Corbelli A, Watanabe S, et al. Three-dimensional podocyte–endothelial cell co-cultures: assembly, validation, and application to drug testing and intercellular signaling studies. *Eur J Pharm Sci* 2016; **86**: 1–12.
43. Delézy O, He Z, Hodin S, et al. Glomerular filtration drug injury: *in vitro* evaluation of functional and morphological podocyte perturbations. *Exp Cell Res* 2017; **361**: 300–307.
44. Ryan MJ, Johnson G, Kirk J, et al. HK-2: an immortalized proximal tubule epithelial cell line from normal adult human kidney. *Kidney Int* 1994; **45**: 48–57.

Reference 44 is cited only in the supplementary material.

SUPPLEMENTARY MATERIAL ONLINE

Supplementary materials and methods

Figure S1. Glomerular endothelial cell (GEC) characterization

Figure S2. Immunofluorescence microscopy for COL4 α 5 protein

Figure S3. RT-PCR for *COL4A3* and *COL4A5* transcripts

Figure S4. Connectome of differentially expressed genes in AS podocytes

Video S1. 3D reconstruction of a podocyte–GEC co-culture

6. 2 Novel podocyte cell model from human apol1 high risk genotype

Abstract

APOL1 variants, G1 and G2, increase the risk of various nondiabetic kidney diseases in African population. To date, the precise mechanisms by which APOL1 risk variants induce injury on podocytes and other kidney cells remains unclear. Trying to unravel these mechanisms, most of *in vitro* studies used animal or cell models created by gene editing. In the present study, we have successfully generated for the first time APOL1 G2/G2 podocyte cell lines isolated from urine of a human donor carrying APOL1 high-risk genotype (HRG). Upon induction of APOL1 overexpression by polyinosinic-polycytidylic acid (poly(I:C)), G2/G2 podocyte cell lines exhibited altered features, including downregulation of synaptopodin, alteration of cytoskeleton, reduction of autophagic flux and increased permeability in an *in vitro* model. The human G2/G2 podocyte cell model is a powerful tool for unravelling the mechanisms of APOL1-induced podocyte injury and the cellular function of APOL1.

Introduction

APOL1 risk variants (RVs), G1 and G2, significantly influence the risk of various forms of chronic kidney diseases (CKD) among individuals of sub-Saharan African descent [1,2]. Prior to establishing its role in kidney diseases, APOL1 was known to protect against certain trypanosomes in humans and some primates [3]. APOL1 circulates in blood as part of a high-density lipoprotein (HDL) complex that also contains apolipoprotein A1 (APOA1) and haptoglobin related protein (HPR). This complex named trypanosome lytic factor (TLF) confers innate protection against subspecies of *Trypanosoma brucei* (T.b.) [4,5]. T.b. rhodesiense and T.b. gambiense have evolved a mechanism to evade the TLF lysis. T.b. rhodesiense evades lysis by expressing serum resistance associated (SRA) protein that binds to the C-terminus domain of the APOL1, in the process neutralizing its lytic activity leading to infection of the host and the development of sleeping sickness [3,6]. In turn, T.b. gambiense resists TLF via a multifactorial defence mechanism. APOL1 risk variants G1 and G2 restored the lytic activity of human serum, providing selective advantage to carriers against sleeping sickness caused by T.b. rhodesiense but not gambiense [7,8].

APOL1 is expressed in various tissues such as lung, placenta, pancreas, liver and kidney. In the kidney, different cell types express APOL1, including extra glomerular vascular endothelial cells, podocytes and proximal tubular cells [5,6]. However to date, reported data on the features of kidney disease related to APOL1 RVs have been mostly limited to podocytes [7].

APOL1 RVs confer susceptibility to podocyte and/or microvascular injury, so that individuals with two APOL1 risk alleles exposed to additional cellular stressors are more likely to develop cell dysfunction, injury and loss [8]. A better understanding of APOL1-induced podocyte injury is required in order to devise more effective therapies [8]. As such, cell and animal models overexpressing APOL1 G1 and G2 variants showed increased cytotoxicity by apoptosis, necrosis or inflammatory cell death (pyroptosis) [7-10], disrupted autophagic flux [8,11,12], altered

mitochondrial function, increased potassium efflux and enhanced stress response pathways [13,14].

In most of these studies, polyinosinic-polycytidylic acid (poly(I:C)), a synthetic double-stranded RNA, TLR3 agonist, was used for the activation of APOL1 driven by upregulation of IFNs.

In most *in vitro* mechanistic studies of APOL1 variants, cell models were created using gene editing techniques such as viral vector transductions or CRISPR-cas9 technology [8,10-14]. Therefore, due to the artificial modifications, the outcomes might not completely represent the actual cell phenotype found in patients and, in addition, it is still unknown to which extent these mechanisms affect humans [15]. In this study, we generated for the first time a podocyte cell model derived directly from a human carrying APOL1 high-risk genotype (HRG) G2/G2. Using this model, we demonstrate dysfunction of APOL1 G2/G2 podocyte in comparison with the reference podocyte carrying APOL1 allele G0.

Results

1. Generation and identification of novel podocyte model from human APOL1 high-risk genotype

APOL1 genotyping and culture of cells harvested from APOL1 HRG carriers

The study population was recruited among African community living in Belgium and APOL1 sequencing analysis was performed. Out of 89 recruited participants, six (6.7%) carried HRG, being G1/G1 (n=1), G2/G2 (n=1), and G1/G2 (n=4) (Table 1). The low risk genotype (LRG) frequencies were 55.0%, 23.5% and 14.6% for G0/G0, G1/G0 and G2/G0, respectively. After collection of urine samples from the six participants carrying APOL1 HRG, only cells harvested from G2/G2 carrier proliferated successfully and twelve conditionally immortalized clones were generated. Interestingly, from four participants who carried HRG G1/G2, no growing cells were observed despite three consecutive urine collections from each donor. On the other hand, from the participant carrying APOL1 HRG G1/G1, cells were isolated and cultured, but they did not survive the antibiotic selection upon immortalization in three consecutive attempts.

Participant	Age (years)	Gender	Country	Medical history	eGFR (mL/min/1.73 m ²)	P/C ratio (mg/mg)	APOL1 Genotype
1	6	M	Ghana	Kidney injury post neonatal asphyxia	28	0.15	G2/G2
2	28	F	Cameroon	Normal	NA	NA	G1/G2
3	37	M	DRC	Hypertension	98	0.25	G1/G1
4	38	F	DRC	Normal	104	0.18	G1/G2
5	40	M	DRC	Normal	NA	NA	G1/G2
6	43	F	DRC	Sickle cell trait	112	0.12	G1/G2

eGFR, estimated glomerular filtration rate; P/C ratio, protein to creatinine ratio; NA, data not available; DRC, Democratic Republic of Congo. M, male; F, female.

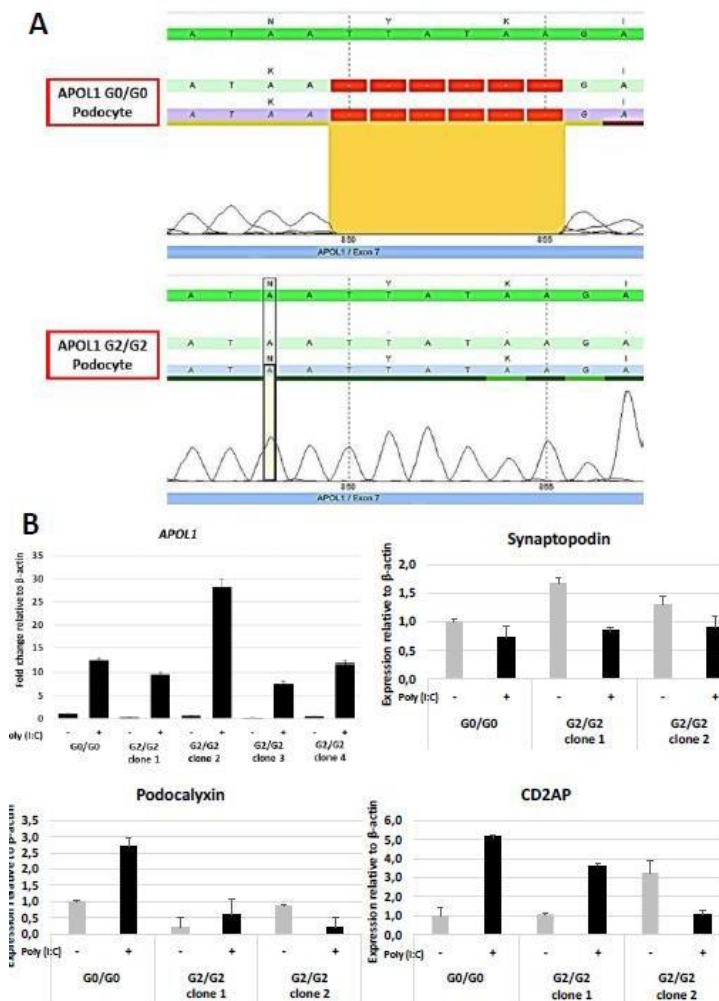
Table 1. Baseline characteristics of participants carrying *APOL1* HRG

APOL1 G2/G2 podocyte cell model characterization

We amplified and sequenced the targeted exon 7 (883 bp) of APOL1 for the variant G2 from gDNA isolated from the APOL1 G2/G2 clones and a podocyte control cell line (APOL1 G0/G0) (Figure 1a).

Then, we evaluated the expression of specific podocyte genes synaptopodin, CD2AP and podocalyxin in the two most proliferative clones isolated from APOL1 G2/G2 carrier in comparison with APOL1 G0/G0 podocytes (Figure 1b, grey bars). In general, all podocyte genes were expressed in APOL1 G2/G2 podocytes as well as the podocyte-specific proteins synaptopodin, podocalyxin and podocin (Figure 1c) confirming the podocyte phenotype. These two clones were further assessed for functionality.

Figure 1



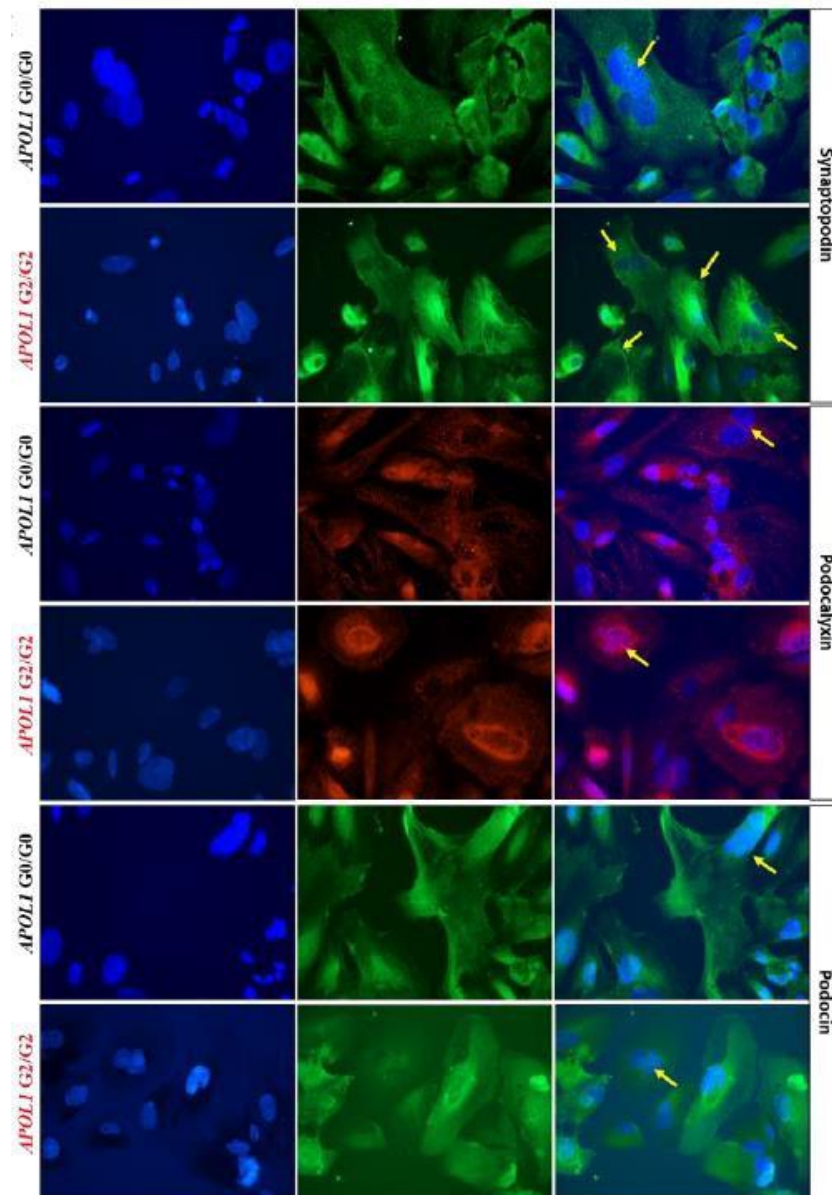


Figure 1. Characterization of human podocytes obtained from urine of the donor carrying *APOLI G2/G2*: **a.** Genotyping of *APOLI G0/G0* and *APOLI G2/G2* podocytes upon amplification of exon 7. *APOLI G2/G2* clonal cell line presents a six-base pair deletion (TTATAA) as expected for the specific variant *APOLI G2*. **b.** quantitative polymerase chain reaction (qPCR) analysis of expression of *APOLI* and podocyte-specific markers synaptopodin; CD2-associated protein gene (CD2AP) and podocalyxin in *APOLI G2/G2* podocytes normalized to *G0/G0* expression before and after exposure to poly(I:C). Each bar represents mean \pm SD of a representative experiment with three technical replicates; three independent experiments were performed. **c.** Immunofluorescence staining of cultured podocytes for podocyte-specific proteins synaptopodin (green), podocin (green), podocalyxin (red) and the nuclear marker 4',6-diamidino-2-phenylindole (DAPI) (blue), arrows point to bi-nucleated cells or arborized structure which are characteristic to podocytes. Magnification: 400x.

2. Functional features of APOL1-induced podocyte dysfunction in human APOL1 G2/G2 podocyte model

Overexpression of APOL1-G1 and -G2 variants has been proposed as a mechanism of APOL1-associated kidney diseases mainly by affecting podocytes [1-3]. We performed various cell biological assays and assessed podocyte specific functions, which have been suggested as APOL1 HRG driven dysfunctions to validate our podocytes cell lines as a model to study mechanisms of APOL1-associated kidney disease. Overexpression of APOL1 was induced by incubation of podocytes with polyI:C for 24h in all assays. Results showed that poly(I:C) significantly induced APOL1 overexpression independently of the presence of G2 risk variant (Figure 1b). Interestingly, upon APOL1 induction by poly:IC, podocyte specific genes were also differentially regulated (Figure 1b-black bars), drawing attention to the downregulation of synaptopodin.

APOL1-induced cytotoxicity

Normal podocyte density (number of cells per glomerular tuft volume) is necessary to maintain glomerular filtration. Reduction of podocyte density, caused by increased glomerular volume and/or reduced podocyte number is associated with proteinuria, glomerulosclerosis and end stage kidney disease in various progressive glomerular diseases. It was recently proposed in a mouse model of HIV-associated nephropathy, that APOL1-G0 expression in podocytes have a protective function against podocyte loss or injury when exposed to an environmental stressor. This protective function was absent in mice carrying Apol1-G2 variant [16]. We analysed podocyte detachment in culture upon overexpression of APOL1 induced by poly(I:C) in APOL1 G2/G2 versus APOL1 G0/G0 cell lines. The results showed high percentage of detached cells, but no significant difference in podocyte detachment related to the APOL1 variant (Figure 2a).

Figure 2

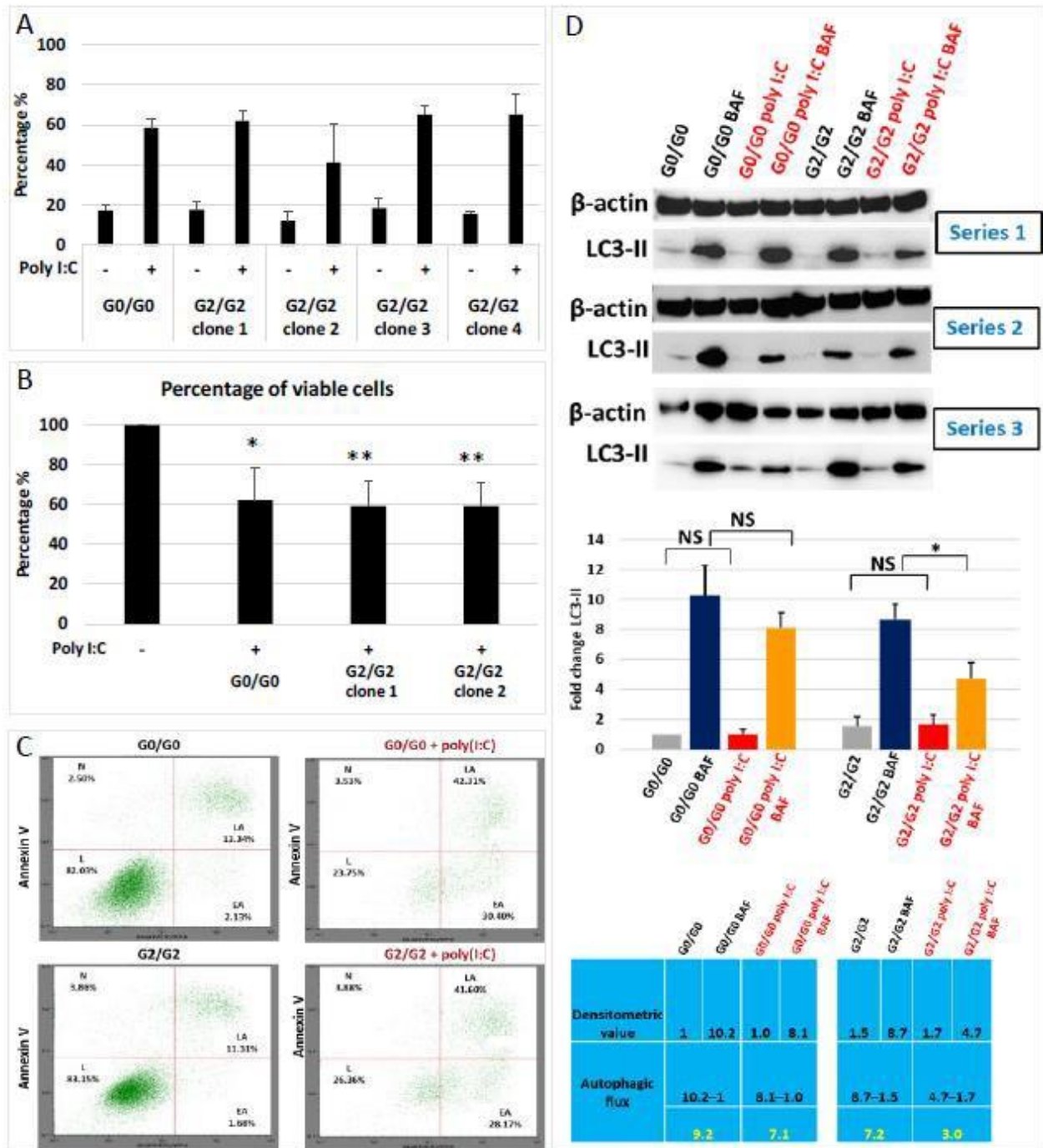


Figure 2: APOLI-induced cell toxicity: **a.** Proportion of detached podocytes *APOLI* G0/G0 and *APOLI* G2/G2 by the total number of cells before and after 24 hours of incubation with poly(I:C). Each bar represents mean \pm SD of a representative experiment; three independent experiments with three technical replicates for each cell line were performed. **b.** The WST-1 assay with two clones of G2/G2 and one G0/G0 podocyte cell lines after incubation with poly(I:C) (50 μ g/ml) demonstrated similar cytotoxicity of *APOLI* upregulation in all cell lines. Each bar represents mean \pm SD of three independent experiments with three technical replicates for each cell line. * $p < 0.05$; ** $p < 0.01$. **c.** *APOLI* G2/G2 podocyte with or without poly(I:C) (lower panels) and control cells (upper panels) were analysed by flow cytometry after FITC-annexinV/PI staining. The spot plots show the percentage of cells in each quadrant (L, live; EA, early apoptotic; LA, late apoptotic; N, necrotic) from a representative replicate of two independent experiments. **d.** Western blot analysis of three independent experiments in G0/G0 and G2/G2 podocyte cell lines in: basal level (G0/G0; G2/G2); after treatment with bafilomycin A (Baf, 100 nM) to induce an autophagic block; after 24-hour incubation with poly(I:C) (50 ng/ml) to induce upregulation of *APOLI*; and combined induction with poly(I:C) and treatment with bafilomycin A (poly I:C+Baf) (top left blot figure). Quantification of the protein abundance of LC3II and β -actin after immunoblotting in each cell line condition (top right figure). Assessment of autophagic flux using densitometric analysis of the LC3-II band (below table).

Moreover, upregulation of APOL1 in G0, G1 and G2 variants was shown to cause cell death in mammalian cell lines or model organisms [10,11,14,17]. Therefore, we investigated whether our human APOL1 G2/G2 podocytes could model cytotoxicity upon APOL1 upregulation induced by poly(I:C). The results showed that indeed the proportion of viable cells was significantly reduced in APOL1 G2/G2 podocyte clones (from 100% to 59.17% +/- 12.2% in clone 1 and to 59.01% +/- 11.9% in clone 2) as well as the control APOL1 G0/G0 podocytes (from 100% to 61.93% +/- 16.2%) (Figure 2b).

Enhanced apoptosis rate has been reported among various pathways of kidney cell damage associated with APOL1 RVs [13]. To evaluate the cell death effect of APOL1 overexpression in the human G2/G2 podocyte model we analysed apoptosis and necrosis by flow cytometry before and after incubation of cells with poly(I:C) for 24h. The results showed increased apoptosis rate rather than necrosis in APOL1 podocyte cell lines regardless of the genotype, suggesting that increased apoptosis owing to APOL1 induction is again variant-independent (Figure 2c).

Additionally, APOL1 overexpression has been associated with autophagic cell death [18,19], therefore we evaluated the effect of APOL1 upregulation on autophagy in APOL1 G2/G2 podocyte clones and in APOL1 G0/G0 podocyte as control.

Autophagy is a dynamic process, involving the generation as well as the degradation of autophagosomes. Therefore, the determination of autophagic flux (accumulation of LC3-II) is essential to assess and differentiate between the induction or suppression of autophagy. Accumulation of LC3-II indicates either the induction of autophagy or the inhibition of lysosomal function and/or fusion of autophagosomes with lysosomes [20]. Blockage of autophagic degradation by lysosomal inhibitor Bafilomycin (Baf) A1 allowed the evaluation of autophagic flux in podocytes.

After exposure to poly(I:C) in the presence of Baf A1, LC3-II accumulation was lower in both APOL1-G0 and -G2 podocytes, however, the expression was significantly reduced in G2/G2

podocytes (Figure 3d), indicating reduced generation of autophagosomes, which was not present in control podocytes. Densitometric analysis suggested an overall reduction in autophagic flux of APOL1 G2/G2 podocytes compared with G0/G0 (9.2 vs 7.1 without and with Baf A1 respectively in G0/G0 and 7.2 vs 3.0 in G2/G2), likely due to autophagic degradation induced by poly(I:C) (Figure 2d, table).

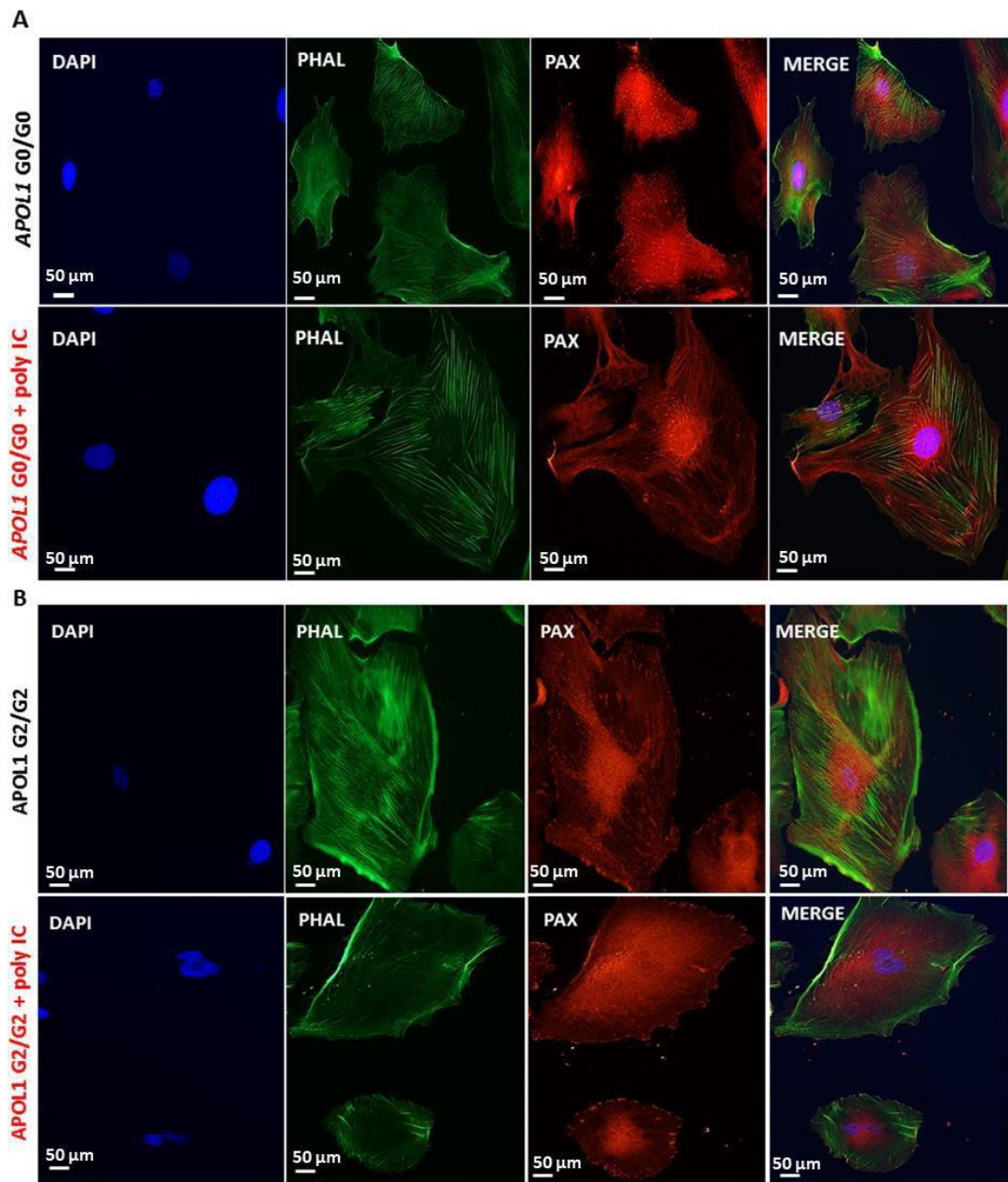
APOL1-induced podocytopathy

Podocytes exhibit a unique cytoskeletal architecture, which is linked to their function in maintaining the kidney filtration barrier [21]. Normally, loss of F-actin stress fibres and changes in lamellipodia mimic podocyte foot process effacement *in vivo*. We analysed podocyte cytoskeleton and distribution of adhesion sites in G2/G2 podocytes compared with G0/G0 in basal conditions and exposed to poly(I:C). Actin filaments were significantly reduced and disorganized in G2/G2 podocytes, but not in G0/G0 podocytes. Furthermore, after APOL1 induction, G2/G2 podocytes exhibited less adhesion sites than observed in basal conditions and when compared with G0/G0 podocytes (Figure 3a).

Impairments of the podocyte cytoskeletal apparatus by genetic mutations result in proteinuria, dysfunctional glomerular filtration and consequent glomerular disease [21]. We have used a permeability assay to model *in vitro* the glomerular permeability, assessing the passage of albumin across a barrier formed by APOL1 G2/G2 podocytes before and after incubation with poly(I:C) for 24h. In fact, our results showed that the *in vitro* glomerular barrier formed by APOL1 G2/G2 podocytes treated with poly(I:C) exhibited significant higher permeability to albumin compared to podocytes at basal conditions (Figure 3b).

Taken together, these data indicate that APOL1 G2/G2 human podocyte model can mirror *in vitro* the renal cytopathology observed in patients carrying APOL1 high-risk genotype, representing a novel tool to support the investigation of APOL1-related kidney diseases and to test new therapies.

Figure 3



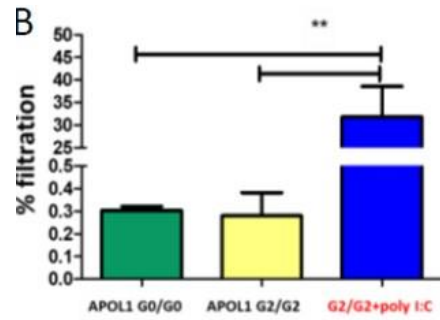


Figure 3: *APOL1*-induced cytoskeleton abnormalities: a. Staining for actin filaments using phalloidin (phal) (green) and focal adhesion molecules using paxillin (pax) (red) and DAPI (blue) in *APOL1* G0/G0 control cells and in *APOL1* G2/G2 podocytes in basal conditions and after *APOL1* induction by poly(I:C). b. Perfusion assay on GMVEC membrane with *APOL1* G2/G2 and G0/G0 podocyte cell lines using BSA-FITC. Each bar represents mean \pm SD of three independent experiments with three technical replicates for each cell line.

Discussion

The strong association between APOL1 gene expression with several nondiabetic chronic kidney diseases and its mechanisms have been widely investigated using animal or cell models created by gene editing [8,10-14]. Our group is acclaimed by the establishment of methodology to generate stable podocyte lines from cells exfoliated into urine of healthy subjects and patients [22-24]. Using the same approach, we successfully generated APOL1 G2/G2 podocyte cell model from urine of a human donor carrying APOL1 HRG (G2/G2). The obtained podocyte cell lines were characterized by the expression of podocyte genes and proteins and presented functional features of APOL1-induced injury when treated with poly(I:C). To our knowledge, this is the first G2/G2 human podocyte cell model derived from a patient carrying this genotype and it can be of great interest for researchers investigating cellular functions of APOL1.

It has been suggested that African Americans carrying HRG have an increased urinary loss of podocytes resulting in an inadequate number of glomerular podocytes, owing to the interference of HRG with apoptosis and autophagic cell death pathways [11,25]. We attempted to isolate and expand these podocytes lost in urine; however, we only succeeded to develop podocyte lines from the only individual bearing kidney disease (Table 1, patient #1). Nonetheless, the intriguing absence of isolated and growing cells from urine of healthy APOL1 HRG carriers raises the question on the relationship between each of the three variants and the urinary podocytes loss.

Anyhow, the association between APOL1 genotype and glomerular disease is factual. Using the new G2/G2 cell model, we confirmed several cellular phenotypes demonstrated in previous studies, indicating the auxiliary value of our model for unravelling molecular pathways of APOL1 related kidney cell damage.

The endogenous expression of APOL1 is induced under inflammatory conditions, such as viral infections, primarily activating the Toll-like receptor 3 (TLR3) via increased type 1 interferons, which

is mimicked *in vitro* by cell incubation with poly(I:C) [10,26]. As expected, our G2/G2 podocytes, upregulated APOL1 expression after incubation with poly(I:C) regardless of the APOL1 genotype. Therefore, we examined the risk variant dependent cytotoxicity induced by the upregulation of APOL1 in G2/G2 podocytes compared with control cells. We found that APOL1 overexpression induced podocytes detachment, decreased cells viability and increased apoptosis rate in G0/G0 and G2/G2 podocytes at similar levels. Using a tetracycline-regulated system in human embryonic kidney 293 (HEK293) cells, O'Toole et al. also suggested that ApoL1 overexpression drives variant-independent cytotoxicity [18]. In contrast, several other reports using HEK293 cells [9,12-14,17] or transduced human podocytes [11] but different methods of APOL1 induction, showed APOL1 variant-dependent cytotoxicity.

Poly(I:C) treatment induces a tremendous overexpression of APOL1 in all podocyte genotypes, which might be too harsh for the cells, hiding the specific toxicity due to variant-dependent APOL1 overexpression. Therefore, the direct induction of APOL1 with IFNs [10] could be an alternative to induce a weaker, but more similar physiological activation of APOL1.

Nonetheless, our podocyte cell model showed an overall reduction in the autophagic flux in G2/G2 compared with G0/G0 podocytes in basal conditions, which was enhanced after treatment with poly(I:C). Several studies reported that overexpression of APOL1 led to autophagic cell death in different cell types [19,27]. Using TRE-APOL1 constructs in HEK293 cells, a lower degree of autophagic flux in cells transfected with a risk allele (as compared to G0-allele-expressing cells) was demonstrated. Further analysis confirmed that risk-allele-transfected cells contained a greater amount of autophagic vacuoles, but fewer autolysosomes compared with cells transfected with the reference allele, indicating a blockage in autophagic flux [12]. The relevance of these findings were shown in human APOL1 HRG G1/G2 podocytes and now confirmed by our model of G2/G2 podocytes. Interestingly, in contrast to the aforementioned results, using HEK293 cell model, O'Toole et al. examined autophagy in three clones of each genotype (G0, G1, G2), 8 and 16 hours

after tetracycline induction. Investigators found that APOL1 overexpression did not affect autophagy at these two time points and that the autophagic flux was not altered by the expression of APOL1-G0, -G1, or -G2 [18].

Again, it becomes clear that the differences in cell type and protocols used for induction of APOL1 overexpression highlight the heterogeneous nature of explanations of the proposed mechanisms linking APOL1 expression and altered autophagy.

Usually, mechanisms underpinning acquired glomerular pathologies converge on abnormal podocytes cytoskeleton, suggesting that this subcellular structure could be targeted for therapeutic purposes [21]. Differences in podocyte cytoskeleton and its consequences were the most striking findings in our study. It has been suggested that APOL1 RVs promoted podocyte dedifferentiation with decreased expression of podocyte-specific genes [28,29]. Interestingly, we observed a downregulation of synaptopodin in podocytes after treatment with poly(I:C) (Figure 2b). Synaptopodin is an actin-associated protein of differentiated podocytes. It plays a role in modulating actin-based shape and motility of podocyte foot processes. Thus, a reduced expression of synaptopodin leads to an alteration of the podocyte cytoskeleton. We analysed the actin filaments of G2/G2 podocytes in comparison with G0/G0 before and after APOL1 overexpression. Our results showed that podocyte cytoskeleton was differentially arranged and actin filaments appeared to be disorganized in poly(I:C) induced APOL1 G2/G2 podocytes compared with the treated control cells. Furthermore, induced G2/G2 podocytes showed a lower number and distribution of adhesion sites than controls. These results suggest alteration of podocyte cytoskeleton driven by APOL1 upregulation.

Using lentivirus transduced human podocyte cell model, Lan et al. reported that overexpression of APOL1 -G1 and -G2 dramatically increased lysosomal membrane permeability and the leakage of lysosomal components into the cytosol, which was accompanied by APOL1-induced F-actin degradation and necrotic cell death in podocytes [11]. As a possible mechanism of disorganized actin

cytoskeleton in podocytes carrying RVs, Kuma et al. reported using transduced human podocyte cells, that APOL1-miR193a preserves the integrity of actin cytoskeleton in differentiated podocytes through the stabilization of the adherence complex, while disruption of APOL1-miR193a axis in podocytes expressing APOL1 risk alleles induces loss of this function. More specifically, their data showed that overexpression of APOL1 in G0 podocytes downregulated the expression of miR193a indicating an intact actin cytoskeleton, while the expression of APOL1 in G1 and G2 podocytes was associated with upregulation of miR193a resulting in a disorganized actin cytoskeleton [28].

Further studies should be performed to elucidate the functional significance of these findings. Still, it is well accepted that abnormal podocyte cytoskeleton and adhesion sites result in proteinuria and glomerulosclerosis [21]. In an assay to mimic the glomerular filtration *in vitro*, our APOL1 G2/G2 podocytes treated with poly(I:C) showed increased permeability to albumin compared with baseline.

In conclusion, we succeeded to generate APOL1 HRG (G2/G2) podocyte cell lines from a human donor, which represents a robust and powerful tool to unravel the mechanisms of APOL1 induced kidney injuries.

Materials and methods

Ethics

This study was approved by the Ethical Committee of the University Hospital/KU Leuven (S61246). The participants were recruited from the African community living in Belgium after signing an informed consent form.

Reagents and antibodies

All reagents were of analytical grade or used as specified. The antibodies used in this study include anti-synaptopodin (65294, Progen Biotechnik), anti-podocin (EB 12149, Everest Biotech), anti-paxillin (610569, BD Transduction laboratories), anti-podocalyxin (MAB 430, Millipore), anti-APOL1 (HPA018885, Sigma-Aldrich), anti-LC3-II (5F10, Nanotools), anti- β -Actin (Cell Signaling Technology), polyclonal Goat Anti-mouse IgG-HRP (DAKO), polyclonal Goat Anti-rabbit IgG-HRP (DAKO). Alexa Fluor-488-conjugated phalloidin was from Life Technologies, as well as Alexa-546-conjugated secondary antibodies. Poly (I:C) was purchased from Invivogen (San Diego, USA) and used in a concentration of 50 μ g/mL. Radioimmunoprecipitation assay (RIPA) buffer containing 10mM sodium phosphate, 150 mM NaCl, 1.5 mM MgCl₂, 0.5mM Dithiothreitol (DTT), 1% Triton X-100, complete EDTA-free protease inhibitor tablets (Roche Applied Science) was used to prepare protein lysate. Fluorescein isothiocyanate (FITC)-Annexin V/Propidium Iodide (PI) for flow cytometry (Invitrogen) were used for apoptosis assay. WST-1 (11644807001, Roche) was used for cytotoxicity assay.

Participants and APOL1 genotyping

Since the podocyte isolation requires fresh urine, participants were recruited among African community living in Belgium (n=89). From the whole blood samples collected, DNA was extracted using QIAGEN kit following the manufacturer's instructions (QIAamp® DNA Mini kit; QIAGEN, Venlo, Netherlands) in the laboratory of Pediatric Nephrology, KU Leuven. APOL1 genotyping was performed for two renal risk alleles (G1 and G2). APOL1 high risk genotype (HRG) was defined by the presence of two risk variants (G1/G1, G2/G2 or G1/G2) while low-risk genotype (LRG) if zero or one risk variant were present.

Blood and urine samples were collected from those who were identified carrying HRG to assess kidney function (eGFR) and urinary protein excretion. Serum creatinine and random spot urine protein/creatinine (P/C) ratio were measured according to standard laboratory protocols. Estimated glomerular filtration rate (eGFR) was calculated using the Schwartz formula [30] for participants aged less than 18 years and the Cockcroft-Gault (C-G) equation [31] for those aged above 18 years.

Isolation and culture of podocytes exfoliated into urine

From the participants in whom APOL1 HRG has been detected (6 out of 89), freshly voided urine was collected and exfoliated cells were cultured as previously described [22]. In brief, urine was centrifuged at 200g for 5 minutes, the pellet was washed in PBS and re-suspended in DMEM-HAM's F-12 (Lonza, Basel, Switzerland) with 10% fetal bovine serum (Gibco), 50 IU/mL penicillin and 50 mg/mL streptomycin (Lonza), 5 µg/ml insulin, 5 µg/ml transferrin, 5 ng/ml selenium (Sigma) (podocyte medium). Cells were immortalized and sub-cloned using a temperature-sensitive SV40-TERT viral system. Cells grew at permissive temperature of 33°C and, prior to the experiments, they were incubated at 37°C for 10 days to ensure growth arrest and differentiation. APOL1 WT (G0/G0)

podocytes used as control were already available and previously generated from a Caucasian donor [32].

Quantitative polymerase chain reaction (qPCR)

The expression of the specific podocyte markers synaptopodin, podocalyxin and Cluster of Differentiation 2-Associated Protein (CD2AP) was analysed by qPCR in the clonal cell lines isolated from G2/G2 carrier and compared with APOL1 G0/G0 podocytes. qPCR was also used to analyse the expression of APOL1 in cell clones before and after 24 hours of incubation with Poly I:C (50 µg/mL). Beta-actin was used as housekeeping gene. RNA was isolated using RNeasy Micro Kit (Qiagen GmbH, Hilden, Germany) according to the manufacturer's instructions. 500 ng of RNA was used to synthesize cDNA using a mix of Oligo (dT) 12-18 Primer (Invitrogen: 1206193), random hexamer primers (Invitrogen: 1208582), dNTP mix (100 mM Invitrogen: AM8228G) and SuperScript® III, plus 5x first-strand reaction mix (Invitrogen). qPCRs were performed in triplicate using a CFX96 Real-Time detection system (Bio-Rad) with Platinum SyberGreen qPCR Supermix (Invitrogen, 11733-046), 10 µM of primers and 1.5 µl of cDNA. Results were analyzed using CFX Manager™ software.

Immunofluorescence staining

The immunofluorescence staining was performed for the podocyte specific proteins synaptopodin, podocalyxin and podocin, as well as for analysing the podocyte cytoskeleton (phalloidin staining) and adhesion site (paxillin staining), as previously described [23]. Briefly, cells grown on glass coverslips were fixed with 4% paraformaldehyde for 10 min at room temperature and washed once in PBS. They were permeabilized with 0.1% Triton X-100 (Sigma –Aldrich) for 5 min on ice and washed twice with PBS. Blocking solution (0.5% BSA, 0.2% gelatin, 0.5% FBS in PBS) was added

to cells for 1 hour. Cells were incubated with primary antibodies overnight at 4°C and further with AlexaFluor secondary antibodies for 1 hour in dark at room temperature. 4', 6-diamidino-2-phenylindole (DAPI) was diluted to 1:1000 in mounting medium (DAKO, S3023) for nuclear staining. The cells were washed 5 times with PBS between steps. Samples were examined with a fluorescence microscope (Olympus BX41, Olympus Belgium NV). Image processing and analysis were performed using Image J.

Detachment assay

To analyse detachment of cells in culture upon upregulation of APOL1 induced by poly(I:C), 20,000 APOL1 HRG podocytes and control podocytes were seeded in a 6-well plate. After 7 days at 37°C, cells were incubated with poly(I:C) (50µg/mL) for 24 hours. The supernatant was collected and detached cells were counted using the TC20™ Automated Cell Counter (Bio-Rad), which estimates the number of live and dead cells in the cells' suspension. Percentage of detachment was represented as (number of detached cells) / (number of detached + attached cells). Three independent experiments were performed with three technical replicates in each.

Cytotoxicity assay

APOL1-mediated cytotoxicity in G2/G2 podocyte cell lines and in control cells was measured using a Water Soluble Tetrazolium salt (WST-1) cytotoxicity assay (11644807001, Roche®) according to manufacturer instructions. WST-1 is reduced in metabolically active cells to produce a blue precipitate, formazan. The detection of formazan level in the cells allows quantifying the number of viable cells. Briefly, cells were grown in culture, trypsinized and seeded at a density of 20'000 cells

per well in a 96-well plate. Cells were incubated overnight in 33°C to allow attachment, and then transferred to 37° for 10 days. Poly(I:C) (50 µg/mL) was added for APOL1 induction. After at least 16 hours of incubation, 10 µl of WST-1 was added in 100µl of medium per well and cells were incubated further for 2 hours at 37°C. Absorbance was then measured at 450 nm versus a 620 nm reference by using an ELISA reader. Three independent experiments were performed with three technical replicates in each.

FITC-Annexin V / PI staining for apoptosis assay

To analyse the APOL1-induced apoptotic cell death pathway, human HRG podocyte cell lines and controls treated or not with poly(I:C) were stained using the FITC-AnnexinV apoptosis detection kit and PI kit according to the manufacturer's instructions. Samples were analysed by Fluorescence-activated cell sorting (FACS) within 30 min. The analysis allowed to obtain the proportion of live, early apoptotic, late apoptotic and necrotic cells contained in each sample. Two independent experiments were performed.

Western blot for autophagy analysis

Western Blotting was used to investigate the expression and possible modifications of LC3-II involved in autophagy. Immunodetection of LC3-II was performed in basal conditions and after 24 hours of incubation with poly(I:C) in G0/G0 and G2/G2 podocytes. However, detection of LC3-II only shows a snapshot of protein levels in the cell without reproducing the dynamic information of the autophagic process, so-called autophagic flux. As autophagy is a continuously ongoing process, an increased level of LC3-II may result from either increased production or a decreased degradation of autophagosomes. To assess autophagic flux, cells were treated with 100nM Bafilomycin A1 (Baf

A1) (LC Laboratories) or dimethylsulfoxide (DMSO) as vehicle for 3 hours before collecting pellet, as previously described [33]. Baf A1 is a lysosomal inhibitor and autophagic flux blocker. It blocks the fusion of autophagosomes and lysosomes leading to an accumulation of the autophagosomal marker LC3-II. As such, in the presence of Baf A1, information is gathered only about LC3-II (and autophagosome) production. For the blotting, cells were lysed with 50-100 μ l of RIPA buffer. The protein concentration was determined using BCA protein assay kit (Thermo Fisher). Equivalent amounts of protein were separated on a NuPAGETM 4-12% Bis-Tris Protein Gel (Invitrogen) and followed by blotting on polyvinylidene difluoride (PVDF) membrane. Primary and secondary antibodies were used according to the manufacturer's instructions. Blots were developed using HRP-conjugated secondary antibodies and analysed using Image J software. Three independent experiments were performed.

Perfusion assay for glomerular membrane permeability assessment using G2/G2 podocytes

To perform the filtration assay, a dynamic millifluidic culture system (IVtech Srl) was used. The differentiated podocytes (80.000) were plated on the PET porous membrane (ipCELLCULTURETM) embedded in the central part of a small (2,5 mL of volume capacity) bioreactor. The membrane divides the cell-chamber into 2 compartments, each with an inlet and outlet channel, to allow, once connected the circuit, the continuous flow of fluid in one direction only. In case of administration of drug, the day after the setup of culture in the bioreactor, podocyte-medium were changed with medium plus 50 μ g/mL Poly I:C, otherwise a normal change of medium was made. After 16 hours of drug incubation, or 2 days after setting the culture, the perfusion assay was performed. Firstly, in an incubator the bioreactor was connected to the main body of the system, capable of delivering liquid at a certain flow rate (in this case, 100 μ L/min), directly into bioreactor. During the filtration assay, in each circuit a peristaltic pump allows the entry of medium with 1 mg/mL Albumin-fluorescein

isothiocyanate conjugate (Sigma-Aldrich) in the lower part of the bioreactor, and in the upper part instead of normal medium. After 3 hours of perfusion, the liquids coming out of the two compartments of the bioreactor are separately collected and their fluorescence is measured, in triplicate. A higher fluorescence indicates lower podocitary integrity.

Statistical analysis

Statistical analysis was performed using Microsoft Excel® and GraphPad Prism® software. Data from at least three independent experiments were analysed for each condition, unless stated in methods. Immunofluorescence images were obtained from randomly selected cells from three independent experiments, and the images shown are representative of the majority of cells. Statistical significance was evaluated using Student's t-test and considered as significance when $p < 0.05$ (* $p < 0.05$; ** $p < 0.01$; *** $p < 0.001$; **** $p < 0.0001$).

References

- 1 Genovese, G. et al. Association of trypanolytic ApoL1 variants with kidney disease in African Americans. *Science* 329, 841-845, doi:10.1126/science.1193032 (2010).
- 2 Kopp, J. B. et al. APOL1 genetic variants in focal segmental glomerulosclerosis and HIV-associated nephropathy. *J Am Soc Nephrol* 22, 2129-2137, doi:10.1681/ASN.2011040388 (2011).
- 3 Kasembeli, A. N. et al. APOL1 Risk Variants Are Strongly Associated with HIV-Associated Nephropathy in Black South Africans. *J Am Soc Nephrol* 26, 2882-2890, doi:10.1681/ASN.2014050469 (2015).
- 4 Thomson, R. et al. Evolution of the primate trypanolytic factor APOL1. *Proc Natl Acad Sci U S A* 111, E2130-2139, doi:10.1073/pnas.1400699111 (2014).
- 5 Friedman, D. J. & Pollak, M. R. Apolipoprotein L1 and Kidney Disease in African Americans. *Trends Endocrinol Metab* 27, 204-215, doi:10.1016/j.tem.2016.02.002 (2016).
- 6 Madhavan, S. M. & O'Toole, J. F. The biology of APOL1 with insights into the association between APOL1 variants and chronic kidney disease. *Clin Exp Nephrol* 18, 238-242, doi:10.1007/s10157-013-0907-4 (2014).
- 7 Freedman, B. I., Limou, S., Ma, L. & Kopp, J. B. APOL1-Associated Nephropathy: A Key Contributor to Racial Disparities in CKD. *Am J Kidney Dis* 72, S8-S16, doi:10.1053/j.ajkd.2018.06.020 (2018).
- 8 Heymann, J., Winkler, C. A., Hoek, M., Susztak, K. & Kopp, J. B. Therapeutics for APOL1 nephropathies: putting out the fire in the podocyte. *Nephrol Dial Transplant* 32, i65-i70, doi:10.1093/ndt/gfw402 (2017).
- 9 Nichols, B. et al. Innate immunity pathways regulate the nephropathy gene Apolipoprotein L1. *Kidney Int* 87, 332-342, doi:10.1038/ki.2014.270 (2015).
- 10 Uzureau, S. et al. Apolipoproteins L control cell death triggered by TLR3/TRIF signaling in dendritic cells. *Eur J Immunol* 46, 1854-1866, doi:10.1002/eji.201546252 (2016).
- 11 Lan, X. et al. APOL1 risk variants enhance podocyte necrosis through compromising lysosomal membrane permeability. *Am J Physiol Renal Physiol* 307, F326-336, doi:10.1152/ajprenal.00647.2013 (2014).
- 12 Beckerman, P. et al. Transgenic expression of human APOL1 risk variants in podocytes induces kidney disease in mice. *Nat Med* 23, 429-438, doi:10.1038/nm.4287 (2017).
- 13 Ma, L., Divers, J. & Freedman, B. I. Mechanisms of Injury in APOL1-associated Kidney Disease. *Transplantation* 103, 487-492, doi:10.1097/TP.0000000000002509 (2019).

- 14 Olabisi, O. A. et al. APOL1 kidney disease risk variants cause cytotoxicity by depleting cellular potassium and inducing stress-activated protein kinases. *Proc Natl Acad Sci U S A* 113, 830-837, doi:10.1073/pnas.1522913113 (2016).
- 15 Ekulu, P. M. et al. APOL1 Risk Genotypes Are Associated With Early Kidney Damage in Children in Sub-Saharan Africa. *Kidney Int Rep* 4, 930-938, doi:10.1016/j.ekir.2019.04.002 (2019).
- 16 Bruggeman, L. A. et al. APOL1-G0 protects podocytes in a mouse model of HIV-associated nephropathy. *PLoS One* 14, e0224408, doi:10.1371/journal.pone.0224408 (2019).
- 17 Granado, D. et al. Intracellular APOL1 Risk Variants Cause Cytotoxicity Accompanied by Energy Depletion. *J Am Soc Nephrol* 28, 3227-3238, doi:10.1681/ASN.2016111220 (2017).
- 18 O'Toole, J. F. et al. ApoL1 Overexpression Drives Variant-Independent Cytotoxicity. *J Am Soc Nephrol* 29, 869-879, doi:10.1681/ASN.2016121322 (2018).
- 19 Zhaorigetu, S., Wan, G., Kaini, R., Jiang, Z. & Hu, C. A. ApoL1, a BH3-only lipid-binding protein, induces autophagic cell death. *Autophagy* 4, 1079-1082, doi:10.4161/auto.7066 (2008).
- 20 Ni, H. M. et al. Dissecting the dynamic turnover of GFP-LC3 in the autolysosome. *Autophagy* 7, 188-204, doi:10.4161/auto.7.2.14181 (2011).
- 21 Schell, C. & Huber, T. B. The Evolving Complexity of the Podocyte Cytoskeleton. *J Am Soc Nephrol* 28, 3166-3174, doi:10.1681/ASN.2017020143 (2017).
- 22 Ivanova, E. A. et al. Cystinosis deficiency causes podocyte damage and loss associated with increased cell motility. *Kidney Int* 89, 1037-1048, doi:10.1016/j.kint.2016.01.013 (2016).
- 23 Arcolino, F. O. et al. Urine of Preterm Neonates as a Novel Source of Kidney Progenitor Cells. *J Am Soc Nephrol* 27, 2762-2770, doi:10.1681/ASN.2015060664 (2016).
- 24 Oliveira Arcolino, F. et al. Human Urine as a Noninvasive Source of Kidney Cells. *Stem Cells Int* 2015, 362562, doi:10.1155/2015/362562 (2015).
- 25 Bruggeman, L. A. et al. APOL1-G0 or APOL1-G2 Transgenic Models Develop Preeclampsia but Not Kidney Disease. *J Am Soc Nephrol* 27, 3600-3610, doi:10.1681/ASN.2015111220 (2016).
- 26 Uzureau, S. et al. APOL1 C-Terminal Variants May Trigger Kidney Disease through Interference with APOL3 Control of Actomyosin. *Cell Rep* 30, 3821-3836 e3813, doi:10.1016/j.celrep.2020.02.064 (2020).
- 27 Heneghan, J. F. et al. BH3 domain-independent apolipoprotein L1 toxicity rescued by BCL2 prosurvival proteins. *Am J Physiol Cell Physiol* 309, C332-347, doi:10.1152/ajpcell.00142.2015 (2015).
- 28 Kumar, V. et al. Disruption of APOL1-miR193a Axis Induces Disorganization of Podocyte Actin Cytoskeleton. *Sci Rep* 9, 3582, doi:10.1038/s41598-019-39376-y (2019).

- 29 Kumar, V. et al. Disrupted apolipoprotein L1-miR193a axis dedifferentiates podocytes through autophagy blockade in an APOL1 risk milieu. *Am J Physiol Cell Physiol* 317, C209-C225, doi:10.1152/ajpcell.00538.2018 (2019).
- 30 Schwartz, G. J. et al. New equations to estimate GFR in children with CKD. *J Am Soc Nephrol* 20, 629-637, doi:10.1681/ASN.2008030287 (2009).
- 31 Cockcroft, D. W. & Gault, M. H. Prediction of creatinine clearance from serum creatinine. *Nephron* 16, 31-41, doi:10.1159/000180580 (1976).
- 32 Saleem, M. A. et al. A conditionally immortalized human podocyte cell line demonstrating nephrin and podocin expression. *J Am Soc Nephrol* 13, 630-638 (2002).
- 33 Mizushima, N. & Yoshimori, T. How to interpret LC3 immunoblotting. *Autophagy* 3, 542- 545, doi:10.4161/auto.4600 (2007).

Conclusions and directions for future research

In light of the results obtained, the following can be concluded:

- We have developed a 3D milli-fluidic glomerulus system, characterized by its key elements: a tri-layer formed by h-GECs, a membrane covered by type IV collagen and h-PODs.
- We developed an easy and simple to detect permeability assay, to evaluate the integrity of the filtration barrier. We validated the model through the evidence that the complete in-vitro glomerulus offers greater resistance to the passage of albumin.
- Through the infusion into the system of electroporated MSC-EVs with an exogenous miRNA, we confirmed the internalization of the vesicles in the podocytes. Microscopic analyzes confirmed this finding.
- We tried to create an AKI *in vitro* model, with the use of DXR directly in the dynamical system, describing a decrease in cell viability and an increase in the expression of damage markers in podocytes.
- To repair the acute pharmacological damage, MSC-EVs were used, perfused for 24h in the endothelial compartment of the circuit. this resulted in a decrease in cell mortality.
- We tried to mimic with success glomerular disorders, in particular AS, AKI and APOL1-mutated podocytes

Future implementations:

- The results with EVs need further investigation. Molecular and protein analyzes could be performed to understand the activated pathways.
- The role of glomerular endothelial cells in different damage patterns needs to be investigated.
- Multi-organ systems in series could be very useful in the study of toxicology.
- An interesting implication could be the use of these models in personalized medicine: using for example cells or extracellular vesicles taken from the patient's serum.

Acknowledgments

Foremost, I would like to express my sincere gratitude to my tutor Prof. Benedetta Bussolati and her lab group, for the continuous support of my PhD study and research, I have learned something from each of you that I'm sure I will need for my future career.

Thanks in particular to my special *Cricca*, Lola, Dorotea, and Sofia, for sharing the road with me, I could not have asked for better company. Thanks also to Andrea, Fabio, Sharad, Roberta, Sarah for the thousand tips, for the laughs, the work, and personal support.

My immense gratitude also goes to all my warm family, always ready to fight all my battles with me and to enjoy my achievements. Thanks to my closest friends, distance never really takes us away. Thanks to Stefano who I know is proud of me.

Thanks to Michele, for never stopped believing in me.